RESPONSE OF SOIL MINERAL WEATHERING TO ELEVATED CARBON DIOXIDE

Thesis by

Jennie Catherine Stephens

In Partial Fulfillment of the Requirements

for the Degree of

Doctor of Philosophy

California Institute of Technology

Pasadena, California

2002

(Defended April 25, 2002)

Acknowledgements

I am very thankful to my advisor, Janet Hering, for all that she has done in helping me with this research. Her insight and her thoroughness have taught me a lot; I have learned from her how to critically assess my own scientific work and the work of others. I would also like to express my appreciation to the other members of my thesis advisory committee: Mike Hoffmann, who was supportive of me since I first arrived on campus; Jim Randerson, who agreed to be on my committee shortly after he arrived on campus; and Jim Morgan, who has generously given of his time to offer advice.

I would also like to thank Professor Robert C. Graham of University of California, Riverside who was extremely helpful particularly at the beginning as I embarked on this soil mineralogy project without knowing much about soils or mineralogy. My thanks and appreciation go out to all the others who helped me with technical aspects of this project, including John Rogie at U.S.G.S, Chi Ma for help with XRD, Professor George Rossman and Ronit Kesselman for help with mineralogical analysis, Kathleen Treseder and Sasha Tsapin for their preliminary analysis of the mycorrhizal fungi and microbial populations, Carole Garland and Andrea Belz for help with TEM, Mike Vondrus for making my reaction vessels, Dianne Newman for letting us borrow her HPLC column, Peter Green, Nathan Dalleska, Yaniv Dubowksi and Bob Becker for analytical support, and Bill Balcerski for help with the IC. Thanks also to Johnny Lam, a SURF student.

For financial support of my graduate studies I want to acknowledge the EPA Star Graduate Fellowship program and the NSF graduate fellowship program. For additional

funds that helped defray childcare costs provided by the ARCS Foundation and the Caltech Graduate Office, I am also extremely grateful.

I want to take this opportunity to thank Linda Scott for her always positive, friendly, supportive manner. If Linda had not casually encouraged me to submit an application even though the deadline had passed five years ago, Dan and I would probably have stayed in Boston instead of coming to Pasadena. Thanks also to Fran who has helped and supported me in many ways over the years. Thanks also to Irene, Laurel, Elena and Belinda, for creating a friendly atmosphere in Keck. Thanks also to all past and present members of the Hering and Hoffmann research groups who have been friends as well as colleagues, including Penny Kneebone, Tatiana Piatina, Van Chiu, Dan Giammar, Tina Salmassi, Megan Knight, Melissa Kelly, Suvasis Dixit, Giehyeon Lee, Yael Dubowski, Tim Lesko, Bill Balcerski, Weng-ki Ching, Chris Boxe, Hugo Destaillats, Fok-yan Leung and A. J. Colussi. Special thanks to my former office mates, Mariu Hernandez and Anne Johansen, with whom I shared many special times.

For their immeasurable support and encouragement for as long as I can remember, I thank my parents, Sarah and Cahal Stephens. I also thank my siblings, Niall, Nora and Kate for always being around even if we live thousands of miles apart. For many much appreciated and necessary interruptions to my work, I thank Cecelia and Anna who make everything in life special and amazing. But most importantly and most significantly I thank Dan for being the most wonderful, generous, supportive, honest, genuine person; I am so lucky to be sharing my life with you.

Abstract

Understanding the rates of weathering of soil minerals and the factors that may either enhance or inhibit these rates is a crucial part of understanding many processes from the watershed to the global scale. One potentially important factor in mineral weathering that is not yet well understood is the effect of elevated CO_2 concentrations on weathering rates. Here, the direct and indirect effects of elevated soil CO_2 are examined in field and laboratory-based studies, and the incorporation of the relationship between CO_2 and mineral weathering in soil chemistry models is critically evaluated.

At Mammoth Mountain, California, volcanic ash soil is exposed to naturally occurring high levels of CO_2 from a magmatic source. Comparative analyses of chemical and mineralogical characteristics of exposed and control soils suggest that decade-long exposure to elevated CO_2 concentrations has altered soil dissolution rates. Indirect effects of elevated soil CO_2 at this site, including vegetation mortality and a decrease in pH, have significant potential to alter weathering rates. Laboratory dissolution studies on whole soils under varying conditions of pH, P_{CO2}, and concentrations of oxalate (chosen as a proxy for low-molecular-weight organic acids associated with vegetation in soils) were designed to assess both the direct and indirect effects of CO_2. The results of these experiments provide confirming evidence that CO_2 does not directly influence soil dissolution rates under acidic conditions. However, soil dissolution rates are sensitive to indirect effects of elevated CO_2, including changes in pH and organic acid concentration. The inclusion of a direct CO_2 dependence in a widely used soil chemistry model, PROFILE, may be perpetuating confusion on this issue. Erroneous conclusions in future

model applications could result if this relationship is not removed from the PROFILE model.

A significant and striking decrease in the specific surface area of the soil material was observed during all soil dissolution experiments. These observations call into question the informal convention of normalizing reported dissolution rates to the initial surface area. For effective comparison of weathering rates and identification of the factors influencing them, changes in surface area must be accounted for in reporting dissolution rates.

Contents

List of Figures

List of Tables

Chapter 1
INTRODUCTION

The soil is one of the most complex chemical systems known with unnumbered reactions occurring at any moment between mineral surfaces and the aqueous phase. Few soil chemical reactions go to completion and only through a quantitative understanding of the kinetics of competing reactions can we begin to predict the fate of any chemical species. (W. R. Gardner, President of Soil Science Society of America)

1.1 Motivation

Mineral weathering occurs when minerals that were formed deep within the Earth's crust at high temperatures and pressures are exposed to the atmosphere and react with water and its solutes. Understanding rates of soil mineral weathering and factors that may either enhance or inhibit soil weathering is a crucial part of understanding many watershed-scale processes as well as global-scale processes. On the watershed scale, rates of cation release from mineral dissolution affect nutrient availability in soils (Rogers et al., 1998), buffering capacity against acidification (Schnoor, 1990), and the chemistry of the soil, ground and surface waters within a watershed. On the global scale, mineral weathering regulates cation fluxes to the world's rivers and oceans (Gaillardet et al., 1999; Lasaga et al., 1994) and is the primary sink for atmospheric CO_2 over geologic time (Berner, 1995). Improving the understanding of factors affecting mineral weathering rates, therefore, will provide information useful for regional scale soil management and expand our ability to model global biogeochemical cycles.

One potentially important factor in mineral weathering that is not yet well understood is how elevated CO_2 concentrations affect weathering rates. The only effect of CO_2 currently incorporated into global models of weathering rates is the indirect effect of lowering pH (Berner, 1992), however several soil chemistry models assume a direct affect of CO_2 on weathering rates (Marshall et al., 1988; Sverdrup and Warfvinge, 1993; Volk, 1987). Laboratory experiments designed to assess a direct (i.e., independent of pH) effect of CO_2 on weathering rates have been somewhat contradictory; some researchers claim to have observed enhanced dissolution rates in the presence of elevated CO_2 (Lagache, 1965) while others report no effect (Brady and Carroll, 1994; Grandstaff, 1977) or an effect only under basic conditions where the carbonate ion is dominant (Berg, 1997; Berg and Banwart, 2000; Bruno et al., 1992; Osthols and Malmstrom, 1995).

The concentrations of CO_2, one of the main greenhouse gases responsible for regulating global climate, is increasing dramatically in the atmosphere primarily from the burning of fossil fuels. One of the strategies proposed for reduction of atmospheric CO_2 is to capture CO_2 gas generated by anthropogenic activities and inject it into underground geological repositories to be stored for thousands of years (Bachu, 2000; Gunter et al., 1997; Holloway, 1997). One potential risk associated with underground CO_2 storage is the possibility of leakage; CO_2 gas could escape from the repository, diffuse upward through the soil and return to the atmosphere. A naturally occurring underground CO_2 reservoir beneath Mammoth Mountain, California, began leaking after a swarm of earthquakes in 1989 created conduits for gas escape (Farrar et al., 1995; Gerlach et al., 1998; Hill, 1996; McGee and Gerlach, 1998; Rahn et al., 1996; Rogie et al., 2001). The

steady flux of CO_2 degassing from the relatively shallow magma reservoir (estimated to be within ~20 km of the surface) has resulted in elevated soil CO_2 concentrations that have killed the vegetation in several distinct areas (Sorey et al., 1996). This unique site provides a natural analog for examining potential effects of CO_2 leaks from engineered underground carbon storage reservoirs.

This field site also provides a unique opportunity to combine field observations and laboratory studies to examine how elevated CO_2 and associated vegetation mortality affect the rates of weathering of volcanic ash soils. By examining the factors affecting weathering of these soils, information on the validity of the presumed direct effect of CO_2 included in some models may be gained. Dissolution studies with whole soils also provide a useful complement to studies with pure minerals. Although weathering kinetics of pure minerals have been studied extensively in laboratory experiments, extrapolation of these results to field conditions has proven difficult. A need for dissolution studies with whole soils, rather than pure minerals, therefore, has been recognized (Schnoor, 1990).

1.2 Research Objectives and Scope

The primary objective of this project is to understand how the kinetics of soil mineral weathering are affected, both directly and indirectly, by elevated CO_2 concentrations. Information on the direct enhancement of dissolution by CO_2 (or lack thereof) is needed to evaluate the presumed direct relationship between CO_2 and weathering in soil weathering models. Indirect effects of elevated CO_2 on mineral

weathering are associated with decreasing pH and changes in vegetation (which could influence the profile of low-molecular-weight (LMW) organic acids in the soil solution). Based on evidence from experimental work using isolated minerals, these effects have the potential to change soil weathering rates significantly. Therefore, a combination of field-based observations and analysis, laboratory soil dissolution experiments, and model analysis was undertaken to examine and evaluate the direct and indirect effects of CO_2 on mineral weathering. The unique site at Mammoth Mountain, where volcanic ash soils have been exposed to extremely elevated soil CO_2 concentrations for the last 12 years, provides a natural laboratory to examine these effects. As a complement to the field-based work, laboratory studies were conducted to compare dissolution rates of soils from different sites and to examine independently the effects of the different factors influencing weathering rates (i.e., CO_2, pH, and changes in LMW organic acid concentrations).

Chapter 2 presents background on the geochemistry of mineral weathering, the direct and indirect effects of CO_2, methods of assessing soil mineral weathering rates and details of the field site. Chapter 3 discusses the results of a comparative characterization of the soils exposed to the anomalous CO_2 conditions at Mammoth Mountain with unexposed soils. Chemical and mineralogical differences between the soils are identified. Chapter 4 presents experiments designed to examine if the weathering histories of the exposed and unexposed soils would be reflected in the rates of their dissolution in the laboratory. Chapter 5 discusses experiments assessing the independent effects of pH, CO_2, and oxalate (a proxy for other organic acids) on the overall

dissolution rates of these soils. Chapter 6 critiques the inclusion of a direct effect of CO_2 on mineral weathering rates in a widely used soil chemistry model, PROFILE. Finally, in Chapter 7 the major results of this research are summarized and areas for future research are identified.

1.4 References

Bachu, S., 2000. Sequestration of CO_2 in geological media: criteria and approach for site selection in response to climate change. Energy Conversion and Management, 41: 953-970.

Berg, A., 1997. The Response of Soil Weathering to Climate Change: Laboratory and Modelling Studies, Royal Institute of Technology, Stockholm, Sweden.

Berg, A. and Banwart, S.A., 2000. Carbon dioxide mediated dissolution of Ca-feldspar: implications for silicate weathering. Chemical Geology, 163(1-4): 25-42.

Berner, R.A., 1992. Weathering, plants and the long-term carbon cycle. Geochimica et Cosmochimica Acta, 56: 3225-3231.

Berner, R.A., 1995. Chemical weathering and its effect on atmospheric CO_2 and climate. In: A.F. White and S.L. Brantley (Editors), Chemical Weathering Rates of Silicate Minerals. Reviews in Mineralogy. Mineralogical Society of America, Washington D.C.

Brady, P.V. and Carroll, S.A., 1994. Direct effects of CO_2 and temperature on silicate weathering: Possible implications for climate control. Geochimica et Cosmochimica Acta, 58(8): 1853-1856.

Bruno, J., Stumm, W., Wersin, P. and Brandberg, F., 1992. On the influence of carbonate in mineral dissolution: I. The thermodynamics and kinetics of hematite dissolution in bicarbonate solutions at T=25^{o}C. Geochim. Cosmochim. Acta, 56: 1139-1147.

Farrar, C.D. et al., 1995. Forest-killing diffuse CO_2 emission at Mammoth Mountain as a sign of magmatic unrest. Nature, 376: 675-678.

Gaillardet, J., Dupre, B., Louvat, P. and Allegre, C.J., 1999. Global silicate weathering and CO_2 consumption rates deduced from the chemistry of large rivers. Chemical Geology, 159: 3-30.

Gerlach, T.M., Doukas, M.P., McGee, K.A. and Kessler, R., 1998. Three-year decline of magmatic CO_2 emissions from soils of a Mammoth Mountain tree kill: Horseshoe Lake, CA, 1995-1997. Geophysical Research Letters, 25(11): 1947-1950.

Grandstaff, D.E., 1977. Some kinetics of bronzite orthopyroxene dissolution. Geochimica et Cosmochimica Acta, 41: 1097-1103.

Gunter, W.D., Wiwchar, B. and Perkins, E.H., 1997. Aquifer disposal of CO_2-rich greenhouse gases: extension of the time scale of experiment for CO_2-sequestering reactions by geochemical modelling. Mineralogy and Petrology, 59: 121-140.

Hill, D.P., 1996. Earthquakes and carbon dioxide beneath Mammoth Mountain, California. Seismological Research Letters, 67: 8-15.

Holloway, S., 1997. An overview of the underground disposal of carbon dioxide. Energy Conversion and Management, 38: S193-S198.

Lagache, M., 1965. Contribution a l'etude de l'alteration des feldspaths, dans l'eau, entre 100 et 200 C, sous diverses pressions de CO_2, et application a la synthese des mineraux argileux. Bull. Soc. Franc. Miner. Crist, 88: 223-253.

Lasaga, A.C., Soler, J.M., Ganor, J., Burch, T.E. and Nagy, K.E., 1994. Chemical-weathering rate laws and global geochemical cycles. Geochimica et Cosmochimica Acta, 58(10): 2361-2386.

Marshall, H.G., Walker, J.C.G. and Kuhn, W.R., 1988. Long-term climate change and the geochemical cycle of carbon. Journal of Geophysical Research, 93: 791-801.

McGee, K.A. and Gerlach, T.M., 1998. Annual cycle of magmatic CO_2 in a tree-kill soil at Mammoth Mountain, California: Implications for soil acidification. Geology, 26(5): 463-466.

Osthols, E. and Malmstrom, M., 1995. Dissolution kinetics of ThO_2 in acids and carbonate media. Radiochimica acta, 68(2): 113-119.

Rahn, T.A., Fessenden, J.E. and Wahlen, M., 1996. Flux chamber measurements of anomalous CO_2 emission from the flanks of Mammoth Mountain, California. Geophysical Research Letters, 23(14): 1861-1864.

Rogers, J.R., Bennett, P.C. and Choi, W.J., 1998. Feldspars as a source of nutrients for microorganisms. American Mineralogist, 83: 1532-1540.

Rogie, J.D., Kerrick, D.M., Sorey, M.L., Chiodini, G. and Galloway, D.L., 2001. Dynamics of carbon dioxide emission at Mammoth Mountain, California. Earth and Planetary Science Letters, 188: 535-541.

Schnoor, J.L., 1990. Kinetics of chemical weathering: A comparison of laboratory and field weathering rates. In: W. Stumm (Editor), Aquatic chemical kinetics: Reaction rates of processes in natural waters. John Wiley and Sons, New York, pp. 475-504.

Sorey, M.L. et al., 1996. Invisible CO_2 gas killing trees at Mammoth Mountain, California. U.S. Geological Survey.

Sverdrup, H. and Warfvinge, P., 1993. Calculating field weathering rates using a mechanistic geochemical model PROFILE. Applied Geochemistry, 8: 273-283.

Volk, T., 1987. Feedback between weathering and atmospheric CO_2 over the last 100 million years. American Journal of Science, 287: 763-779.

Chapter 2

BACKGROUND

2.1 Geochemical Interactions Involved in Soil Mineral Weathering

2.1.1 Introduction to Mineral Weathering

The dissolution of minerals in rocks and soils by water and its solutes is a process generally referred to as chemical weathering. This process begins when primary minerals formed at high temperatures and pressures within the earth's interior are exposed to circulating waters at or near the earth's surface. As soil minerals dissolve, protons are consumed and cations are released. The resulting dissolved species may be taken up by plants as nutrients, translocated through the soil to groundwater or rivers, or, under favorable conditions, re-precipitated as secondary minerals. This process is illustrated in the following reaction for the weathering of the primary mineral K-feldspar to the secondary mineral kaolinite accompanied by some complete dissolution.

$$K_2O \cdot Al_2O_3 \cdot 6SiO_{2(s)} + (2+6n)H^+ + (5-3n)H_2O =$$

$$2K^+ + (4+n)H_2SiO_3 + 2nAl^{3+} + (1-n)Al_2O_3 \cdot 2SiO_2 \cdot 2H_2O_{(s)} \qquad (1)$$

Chemical weathering is one of the primary processes of soil formation, thus the kinetics of chemical weathering has implications for soil development, acid neutralization and global biogeochemical cycling.

2.1.2 The Surface Chemistry of Mineral Weathering

The kinetics of chemical weathering must be understood by considering the chemistry taking place at the scale of the mineral surface. Four sequential steps are involved in chemical weathering: (1) transport of reactive species (e.g., H^+, OH^-, ligands, etc.) from the bulk solution to the mineral surface, (2) interaction of these reactive species with the surface metal centers (which destabilizes the bonds between the surface metal centers and crystal lattice), (3) detachment of the metal ion from the surface, and (4) transport of the reaction products (i.e., the metal ions) from the surface to the bulk solution (Stumm, 1987). Chemical weathering may occur under two different regimes: transport-controlled dissolution and surface-controlled dissolution. In transport-controlled dissolution, the rate-limiting supply of reactants or removal of products generates a concentration gradient between the surface and bulk solution (Stumm, 1992). In surface-controlled dissolution, the rate-determining step is the detachment of the surface complex at the solid-liquid interface (Schnoor, 1990). Disagreement on which of these two regimes best represents mineral dissolution in the environment prevailed for many years, until detailed examination of surface morphology (by scanning electron microscopy) and surface composition (by X-ray photoelectron spectroscopy) of weathered feldspar grains provided evidence of etch-pits (Berner and Holdren, 1979). Images of rough, highly etched mineral surfaces demonstrated that surface reactions were controlling, because mineral grains would be rounded if dissolution were controlled by diffusion. Currently, chemical weathering of most minerals in the environment is

considered to be surface controlled, although transport control may prevail under certain conditions and time scales (Schnoor, 1990).

Transition state theory states that the rate of a chemical reaction is controlled by the decomposition of an activated complex (Lowry and Richardson, 1987). This theory applies generally to all chemical reactions, and can be applied to the reactions between solids and solutes involved in chemical weathering. One challenge to applying this theory to mineral weathering is that the concentration of the activated complex at the mineral surface generally cannot be determined (Oelkers, 2001). The precursor to the activated complex, however, is assumed to be a more readily quantifiable surface species with the same chemical composition but lower energy.

$$mineral + aqueous\ species = precursor\ surface\ complex = activated\ complex = products \quad (2)$$

Therefore, according to transition state theory, the dissolution rate of a mineral, R_{diss}, is proportional to the concentration of the surface species (or complex) involved in the rate determining reaction step, which is usually taken to be the detachment of the metal center from the lattice (Oelkers, 2001).

$$R_{diss} \propto [surface\ complex] \quad (3)$$

This relationship only holds if the solution is undersaturated (i.e., the system is far from equilibrium) so that the net rate of dissolution, R_{diss}^{net}, is equal to R_{diss}.

2.1.3 Factors Affecting Mineral Weathering Rates

Rates of chemical weathering in soils are determined by the composition and characteristics of soil minerals, as well as the chemical composition of infiltrating solution and the hydrologic and temperature regime of the local environment (Sparks, 1989). The roots of plants may also play a physical role by exposing new surfaces to weathering (Berner, 1997). The reactivity of different minerals is highly variable (Chadwick and Chorover, 2001) and dependent on crystallinity (Eggleton, 1986) and surface area (Morel and Hering, 1993; Sposito, 1984), so soils with different mineral compositions may have distinctly different rates of mineral weathering. Solution composition can influence (net) dissolution rates (Devidal et al., 1997; Kraemer and Hering, 1997; Murakami et al., 1998; Oelkers and Gislason, 2001; Oelkers and Schott, 1998) by determining the solution saturation state and hence the thermodynamic driving force for (net) dissolution. Laboratory studies have confirmed that temperature accelerates dissolution (Brady and Carroll, 1994; Gwiazda and Broecker, 1994; White and Blum, 1995), and field studies show that rainfall enhances soil weathering rates (Brady et al., 1999; Hinkley, 1975).

2.1.3.1 Rate Dependence on pH

Laboratory studies on specific, isolated minerals have shown that dissolution rates are influenced by pH (Amrhein and Suarez, 1992; Blum and Lasaga, 1988; Brady and Walther, 1989; Casey and Westrich, 1991; Malmstrom and Banwart, 1997). Dissolution rates are generally pH-independent in the near-neutral pH range and increase both in the acid range with decreasing pH and in the alkaline range with increasing pH (Blum and Lasaga, 1988; Blum and Stillings, 1995). This pH dependence is attributed to the protonation or deprotonation of surface hydroxyl groups, which enhances dissolution by facilitating polarization, weakening and breaking of the metal-oxygen bonds of the crystal lattice. Many studies have quantified the hydrogen ion dependence of dissolution, rate $\alpha [H^+]^n$, by calculating and reporting the fractional order n (Etringer, 1989; Grandstaff, 1977; Malmstrom and Banwart, 1997; Pokrovsky and Schott, 2000; Wollast, 1967). Values of n for most feldspars are around 0.5, but reported values range from 0.19 for diopside (Chen and Brantley, 1998) to 0.98 for anorthite (Sverdrup, 1990).

2.1.3.2 The Role of Low-Molecular-Weight (LMW) Organic Acids

Among the various forms of organic carbon found in soils, low-molecular-weight (LMW) organic acids are of particular interest for mineral weathering, because they are ubiquitous in nature and can form stable complexes with polyvalent cations that accelerate mineral weathering (Drever and Stillings, 1997). The effects of organic acids on mineral dissolution have been studied extensively and it is well established that some LMW organic acids accelerate aluminosilicate mineral dissolution (Drever and Stillings,

1997; Drever and Vance, 1994; Fox and Comerford, 1990; Gwiazda and Broecker, 1994). Low-molecular-weight organic acids in soils are excreted from plant roots, leached from litter and other organic material, and produced by bacteria and fungi, which are often associated with the rhizosphere, the root zone. Variations in the nature and quantity of soil organic matter exist among different ecosystems but also within a single site, due to the heterogeneity of soils, spatial variation in vegetation, roots and insect and earthworm activity (Tate, 1987). Most experimental studies have focused on dissolution involving moderately strong ligands like oxalate and suggest that high concentrations of organic acids can increase silicate dissolution rates by a factor of 2 to 3 (Welch and Ullman, 1993).

2.1.3.3 Additive Effects

The rates of proton-promoted dissolution (R_H) and ligand-promoted dissolution (ΣR_L, where L includes both organic and inorganic ligands) are generally taken to contribute additively to the overall dissolution rate R_{diss} though some synergistic effects have been observed (Kraemer et al., 1998). Then

$$R_{diss} = R_H + \Sigma R_L \qquad (4)$$

This expression holds for systems sufficiently undersaturated that the back reaction (i.e., precipitation) can be neglected. As saturation is approached, the observed (net) dissolution rate decreases such that

$$R_{diss}^{net} = R_{diss} - R_{pptn} \quad (5)$$

with $R_{diss}^{net} = 0$ at equilibrium (Kraemer and Hering, 1997). Thus, ligands can increase observed dissolution rates by direct interaction with the surface metal centers (i.e., contributing to R_L) or indirectly by lowering the pH (i.e., contributing to R_H) or by stabilizing the dissolved metal in solution (i.e., decreasing R_{pptn}) (Drever and Stillings, 1997).

2.1.3.4 Mineral Weathering and CO_2

Mineral weathering is a primary sink for atmospheric CO_2 over geologic time, because chemical weathering of minerals is associated the conversion of atmospheric CO_2 to HCO_3^-, as represented in the following simple weathering reaction of the primary mineral enstatite:

$$CaSiO_{3(s)} + 2CO_2 + 3H_2O = H_4SiO_4 + 2HCO_3^- + Ca^{2+} \quad (6)$$

The bicarbonate released into solution is then transferred to rivers and eventually to the ocean where, in the presence of dissolved Ca^{2+} and Mg^{2+}, half of the carbon is removed from the oceans as Ca-Mg carbonate minerals (Berner, 1997).

$$2HCO_3^- + Ca^{2+} = CaCO_{3(s)} + CO_2 + H_2O \quad (7)$$

The rate of mineral dissolution reactions, therefore, determines the importance of mineral weathering as a sink for atmospheric CO_2.

Although the reaction (eq. 6) reflects the consumption of CO_2 in mineral weathering, the reaction stoichiometry cannot be taken to represent the mechanism by which CO_2 effects mineral weathering. The overall reaction does not indicate whether or not CO_2 interacts directly with the mineral surface to affect the dissolution rate; this question is a current area of debate.

CO_2 is included explicitly in the above reaction to represent the fact that interactions between water and CO_2 (and other weak acids) are responsible for the dissociation of water to form H^+, which is the constituent that actually promotes the dissolution reaction. By substituting the products of the reaction of CO_2 and water from reaction 8 below, reaction 6 can be re-written (reaction 9) without CO_2:

$$H_2O + CO_2 = H^+ + HCO_3^- \quad (8)$$

$$CaSiO_{3(s)} + 2H^+ + H_2O = H_4SiO_4 + Ca^{2+} \quad (9)$$

Elevated soil CO_2 concentrations and high concentrations of LMW organic acids occur in the rhizosphere as the result of root and microbial respiration from root

respiration and root and microbial metabolism, and in areas of decaying organic matter. This carbon transferred to the soil by roots is derived from atmospheric CO_2 taken up by plants during photosynthesis. Both CO_2 and organic acids may reduce soil pH and thus increase proton-enhanced dissolution. As discussed above, a direct interaction between organic acids and minerals has also been well documented. However, some controversy exists regarding whether or not CO_2 interacts directly with the mineral surface to promote dissolution.

Weathering rates measured at high temperature (100-200^{o}C) and high P_{CO_2} (2-20 bar) have been shown to be proportional to $P_{CO_2}^{0.3}$ (Lagache, 1965). This apparent fractional dependence on P_{CO_2} has been attributed either to adsorption of CO_2 (Sverdrup, 1990) or as simply a pH effect (apparently the initial pH of the experiments with CO_2 was lower) (Brady, 1991; Helgeson et al., 1984). Despite the uncertainty, this relationship has been assumed to hold for CO_2 values typical of soil environments in several geochemical models (Marshall et al., 1988; Sverdrup and Warfvinge, 1993; Volk, 1987). Several studies attempting to verify this relationship have shown that, at low pH, weathering is not directly affected by CO_2 concentration (Brady and Carroll, 1994; Grandstaff, 1977; Wogelius and Walther, 1991), whereas both decreases (Wogelius and Walther, 1991) and increases (Berg and Banwart, 2000; Osthols and Malmstrom, 1995) in dissolution rates have been observed with increased CO_2 at alkaline pH, in addition to observations of no effect (Knauss et al., 1993; Malmstrom et al., 1996).

2.2 Quantifying Soil Mineral Weathering Rates

2.2.1 Introduction to Different Approaches

Quantifying mineral weathering rates in soils is relevant to the understanding of watershed-scale processes as well as global-scale processes. On the watershed scale, rates of cation release from mineral dissolution affect nutrient availability in soils (Rogers et al., 1998), buffering capacity against acidification (Schnoor, 1990), and the chemistry of the soil, ground and surface waters within a watershed. On the global scale, mineral weathering regulates cation fluxes to the world's rivers and oceans (Gaillardet et al., 1999; Lasaga et al., 1994) and is the primary sink for atmospheric CO_2 over geologic time (Berner, 1995). Much work, therefore, has been done attempting to quantify the rates of mineral weathering occurring in soils; this work can be divided into three categories: 1) field-based approaches, 2) laboratory dissolution studies, and 3) computational modeling (Kolka et al., 1996).

Field-based studies designed to quantify mineral weathering rates usually involve either a mass balance approach using soil solute fluxes on the scale of an entire watershed (Gaillardet et al., 1999; Hinkley, 1975; White and Blum, 1995) or a mineral or elemental depletion approach relative to a conservative tracer (April et al., 1986; Langan et al., 1996). Laboratory dissolution experiments measure the release of elements from a specific isolated mineral or whole soil under controlled conditions. Several different reactor types have been used to determine weathering rates in the laboratory, including batch (Asolekar et al., 1991; Bennett et al., 1988; Brady and Carroll, 1994; Huertas et al., 1999; White and Claassen, 1980) and flow-through (Kalinowski et al., 1998; Pokrovsky

and Schott, 2000; van Grinsven et al., 1992) reactors. Among the flow-through systems, vessels containing solids well mixed in solution (Kraemer et al., 1998), a thin-film of solid material (Malmstrom and Banwart, 1997), and columns of solid material through which the solution must percolate have all been used (Dahlgren et al., 1989). Benefits of laboratory studies include the ease of manipulation of specific parameters including pH, ionic strength, temperature, and concentration and types of organic material. The obvious limitations of laboratory studies relate to the fact that the full complexity of a natural system can never be incorporated into a laboratory experiment.

2.2.2 Field versus Laboratory Derived Rates

Weathering rates determined in laboratory experiments with pure minerals are often several orders of magnitude higher than rates estimated from field studies (April et al., 1986; Drever and Clow, 1995; Kolka et al., 1996; Schnoor, 1990; van Grinsven et al., 1992; Velbel, 1990; Velbel, 1989). Weathering rates calculated at the watershed scale are normalized to unit area of catchment (and expressed in units of kmoles hectare^{-1} year^{-1}) while rates derived from laboratory studies are normalized to surface area of the mineral (and reported as mole m^{-2} h^{-1}). To compare weathering rates calculated from field and laboratory based approaches, therefore, the surface area of minerals exposed to weathering in the field must be estimated.

It has been proposed that overestimations of the surface area of soil in contact with percolating water result in underestimations of field weathering rates (Schnoor, 1990; Swoboda-Colberg and Drever, 1993). Heterogeneity within a sample also provides

uncertainty in soil surface area measurements. Soils are composed of a mixture of different mineral phases with different surface areas (i.e., clays and oxides have much higher surface areas than other minerals), so variability exists in how well the total measured surface represents the actual mineral surface undergoing weathering (Drever and Clow, 1995; Hodson and Langan, 1999). The two common methods of determining soil surface area, the B.E.T. method using N_2 adsorption and the geometric approximation method, often give different values (Blum and Stillings, 1995), providing another complication. These uncertainties associated with surface area represent one of several possible explanations for the general discrepancy between field and laboratory dissolution rates.

In addition to issues related to surface area, other proposed causes of the discrepancy between field and laboratory derived dissolution rates have been discussed in the literature. The aging of mineral surfaces and the formation of protective secondary layers may retard weathering rates in the field; already-weathered soil minerals in the field may be less reactive than unreacted pure minerals used in laboratory dissolution experiments (Velbel, 1995). The accumulation of solutes in the field may inhibit dissolution as solute concentrations approach saturation with respect to various possible solid phases (Burch et al., 1993; Chou and Wollast, 1985; Lasaga et al., 1994; Oelkers et al., 1994). It has also been recognized that lower field weathering rates may also reflect the influence of hydrologic conditions and a shift from surface-controlled dissolution (under laboratory conditions) to transport-controlled dissolution (Kolka et al., 1996; Schnoor, 1990).

2.2.3 Computational Modeling of Weathering Rates

Among efforts to understand the various factors contributing to the discrepancies between field and laboratory weathering rates, computational modeling of weathering processes has been developed in recent years to integrate the many interacting processes within inherently complex soil systems. Computational modeling offers a way to assimilate the data derived from laboratory experiments and, in so doing, attempts to incorporate the inherent complexity of the natural soil system included in field-based calculations. Although all soil chemistry models incorporate chemical weathering processes in some simplified way, the PROFILE model is unique in that it includes a detailed, geochemical weathering sub-model, in which weathering rates are calculated as a function of soil mineralogy, solute composition, and other input parameters (Sverdrup and Warfvinge, 1993). The kinetic information incorporated into the model is derived from an extensive review of laboratory dissolution experiments. For 15 sites in Scandinavia, Central Europe, and North America, calculated weathering rates agreed with the field-derived rates to within ± 20% (Sverdrup and Warfvinge, 1993).

2.2.4 Need for Dissolution Experiments with Whole Soils

An additional approach to bridging the gap between laboratory and field based weathering rates involves conducting laboratory dissolution experiments on whole soils rather than pure minerals. Actual soils are composed of mixtures of crystalline minerals, organic matter, and non-crystalline phases, which interact and react simultaneously (Schnoor, 1990). Extrapolation from specific minerals to whole soils is complicated by

the different responses of various mineral phases to the factors affecting weathering rates. Laboratory weathering experiments conducted on actual soils rather than pure minerals can provide kinetic information that incorporates a soil's complex composition. Although this complexity complicates the interpretation of experimental results, such experiments may help to resolve the discrepancy between predicted field and laboratory weathering rates and are valuable in understanding behavior of a particular soil of interest. Although a few reported studies have examined dissolution rates of whole soils (Asolekar, 1991; Asolekar et al., 1991; Etringer, 1989; van der Salm et al., 2000), these studies are relatively few compared to the plethora of dissolution studies on pure minerals. To my knowledge, such studies have not been performed with volcanic ash soils.

2.3 The Field Site

2.3.1 Mammoth Mountain, California

Mammoth Mountain is a large dormant volcano located on the southwestern rim of the Long Valley Caldera at the southern end of the Mono-Inyo volcanic chain in the eastern Sierra Nevada range in California (map shown in Fig. 3.1a). Elevated concentrations of soil CO_2 are derived from the venting of magmatic CO_2 from a reservoir estimated to be about 20 km below the surface. This CO_2 exposure has caused the death of coniferous trees in several distinct areas (Fig. 2.1) on Mammoth Mountain, California (Farrar et al., 1995; Hill, 1996; McGee and Gerlach, 1998; Rahn et al., 1996; Rogie et al., 2001). The initiation of CO_2 degassing has been attributed to a swarm of

small earthquakes in 1989 (Gerlach et al., 1998; Hill et al., 1990); tree mortality in this area was first observed in 1990 (Farrar et al., 1995). High concentrations of soil CO_2 can cause tree mortality either by preventing the tree roots from absorbing O_2 needed for respiration or by interfering with nutrient uptake (Sorey et al., 1996).

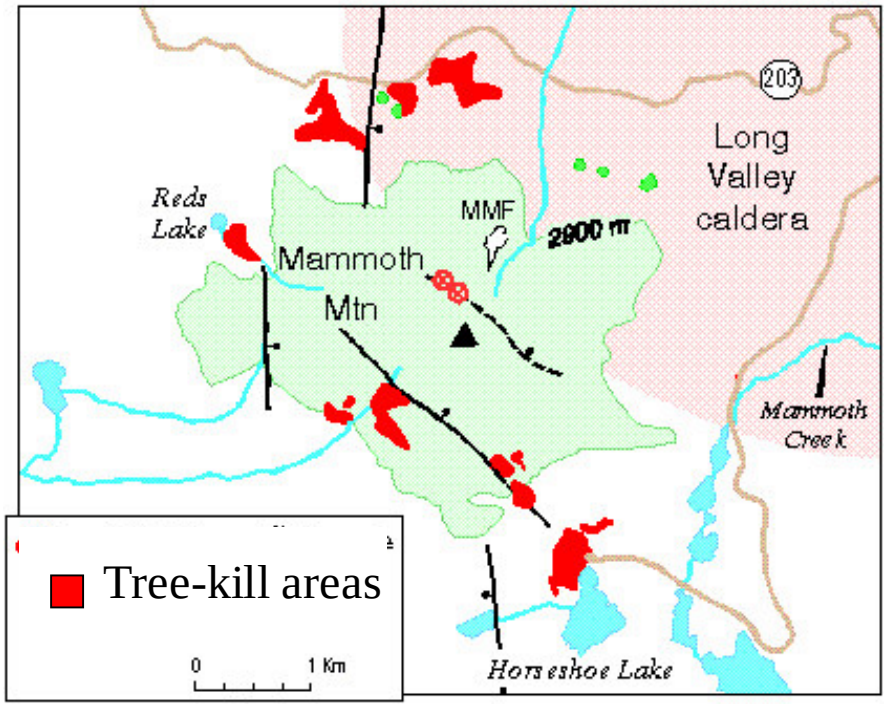

Figure 2.1 - Schematic map (courtesy of U.S.G.S.) showing the eight distinct areas of tree-kill caused by high soil CO_2 concentrations on the flanks of Mammoth Mountain, California. Soil samples used in this study were collected from the large tree-kill area north of Horseshoe Lake.

2.3.2 Horseshoe Lake Tree-Kill Area

Among the eight different locations on the flanks of the mountain where seepage of CO_2 through the soil has killed trees, the largest and most accessible area borders Horseshoe Lake on the southeast side of the mountain (Fig. 2.1 and 2.2). Extensive U.S. Geological Survey monitoring of the fluxes of soil gas is ongoing at this site. Surveys of

soil gas in the upper 70 cm of the soil have documented CO_2 concentrations ranging from 20-90% within the tree-kill areas (Fig. 3b). The concentrations of CO_2 in the adjacent healthy forest areas are at background levels of < 1% (Farrar et al., 1995; McGee and Gerlach, 1998; Rogie et al., 2001). Soil CO_2 concentrations vary seasonally with accumulation in the winter underneath the snow-pack and a sudden decrease during spring snow-melt (McGee and Gerlach, 1998).

Figure 2.2 - Aerial photograph of Mammoth Mountain and Horseshoe Lake (Courtesy of U.S.G.S.). The Horseshoe Lake high-CO_2 area is the treeless area just above Horseshoe Lake.

The $\delta^{13}C$ values of the CO_2 in soil gases outside the Horseshoe Lake tree-kill area are within the ranges expected in a typical forest soil (-19 to -25 ‰). At these unaffected sites, the CO_2 present has been produced by respiration and is steadily lost to the

atmosphere by diffusion (Farrar et al., 1995). The $\delta^{13}C$ values in the gas within the tree-kill areas show distinct magmatic characteristics (-3 to -5 ‰), and are similar to the values of magmatic gas collected at the Mammoth Mountain fumarole (Farrar et al., 1995).

The Horseshoe Lake high-CO_2, tree-kill area occupies ~145,000 m^2 on 15-60% slopes at elevations of 2700 - 2800 m (McGee and Gerlach, 1998). The vegetation in the area is dominated by lodgepole pine (Biondi and Fessenden, 1999). Winter snow-pack commonly exceeds 3 m but the soils remain unfrozen due to the insulating effect of the snow-pack (McGee and Gerlach, 1998), and water infiltrates readily into the soil (Seney and Gallegos, 1995).

2.3.3 Volcanic Ash Soils

Although the geological parent material of Mammoth Mountain consists largely of granitic rock, the upper meters of the soil are derived from volcanic ash from the Inyo eruption, 650-550 years ago (Miller, 1985; Sieh, 2000). Volcanic ash soils are distinguished by a high percentage of non-crystalline volcanic glass and unique clay-size mineral assemblages often dominated by non-crystalline components (Dahlgren et al., 1993). Metastable solid phases with short-range-order, including allophane, imogolite, and ferrihydrite are often formed as weathering products of volcanic glasses because of their rapid weathering rates (Dahlgren et al., 1993). The volcanic ash soils found at Mammoth Mountain, therefore, have a particularly low resistance to chemical weathering compared to other soils due to the predominance of volcanic glass and other non-crystalline phases (Dahlgren et al., 1993). Decadal exposure of volcanic tephra to natural

weathering conditions has been found to produce distinct differences in the solid phases present in the weathered (as compared with the parent) material (Dahlgren et al., 1997). Thus, the decade-long exposure of the young volcanic soil at Mammoth Mountain to elevated soil CO_2 concentrations may have caused observable differences in soil characteristics and soil mineral weathering rates.

2.3.4 Previous Research at the Site

Recent research on the Mammoth Mountain high-CO_2 areas has focused primarily on monitoring and characterizing the CO_2 fluxes and their relationship to seismic activity in the region (Farrar et al., 1999; Farrar et al., 1995; Gerlach et al., 1998; Hill, 1996; McGee and Gerlach, 1998; Rahn et al., 1996; Rogie et al., 2001; Sorey et al., 1998; Sorey et al., 1996). One study assessed the response of vegetation to the CO_2 degassing (Biondi and Fessenden, 1999) and another discussed possible effects of changing soil acidity on mobilization of aluminum (McGee and Gerlach, 1998). To date, however, the soil mineralogy and soil chemistry of this unique site have not been characterized nor have laboratory dissolution studies been conducted using these soils.

2.4 References

Amrhein, C. and Suarez, D.L., 1992. Some factors affecting the dissolution kinetics of anorthite at 25°C. Geochimica et Cosmochimica Acta, 56: 1815-1826.

April, R., Newton, R. and Coles, L.T., 1986. Chemical weathering in two Adirondack watersheds: Past and present-day rates. Geological Society of America Bulletin, 97: 1232-1238.

Asolekar, S.R., 1991. The Role of Chemical Weathering in the Neutralization of Acid Rain, University of Iowa, 200 pp.

Asolekar, S.R., Valentine, R.L. and Schnoor, J.L., 1991. Kinetics of Chemical Weathering in B Horizon Spodosol Fraction. Water Resources Research, 27(4): 527-532.

Bennett, P.C., Melcer, M.E., Siegel, D.I. and Hassett, J.P., 1988. The dissolution of quartz in dilute aqueous solutions of organic acids at 25°C. Geochimica et Cosmochimica Acta, 52: 1521-1530.

Berg, A. and Banwart, S.A., 2000. Carbon dioxide mediated dissolution of Ca-feldspar: implications for silicate weathering. Chemical Geology, 163(1-4): 25-42.

Berner, R.A., 1995. Chemical weathering and its effect on atmospheric CO_2 and climate. In: A.F. White and S.L. Brantley (Editors), Chemical Weathering Rates of Silicate Minerals. Reviews in Mineralogy. Mineralogical Society of America, Washington D.C.

Berner, R.A., 1997. The rise of plants and their effect on weathering and atmoshpheric CO_2. Science, 276(5312): 544-546.

Berner, R.A. and Holdren, G.R., Jr., 1979. Mechanism of feldspar weathering - II. Observations of feldspars from soils. Geochimica et Cosmochimica Acta, 43: 1173-1186.

Biondi, F. and Fessenden, J.E., 1999. Response of lodgepole pine growth to CO_2 degassing at Mammoth Mountain, California. Ecology, 80(7): 2420-2426.

Blum, A. and Lasaga, A.C., 1988. Role of surface speciation in the low-temperature dissolution of minerals. Nature, 331: 431-433.

Blum, A.E. and Stillings, L.L., 1995. Feldspar dissolution kinetics. In: A.F. White and S.L. Brantley (Editors), Chemical Weathering Rates of Silicate Minerals. Reviews in Mineralogy. Mineralogical Society of America, Washington D.C., pp. 291-351.

Brady, P.V., 1991. The Effect of Silicate Weathering on Global Temperature and Atmospheric CO_2. Journal of Geophysical Research, 96(B11): 18,101-18,106.

Brady, P.V. and Carroll, S.A., 1994. Direct effects of CO_2 and temperature on silicate weathering: Possible implications for climate control. Geochimica et Cosmochimica Acta, 58(8): 1853-1856.

Brady, P.V. et al., 1999. Direct measurement of the combined effects of lichen, rainfall, and temperature on silicate weathering. Geochimica et Cosmochimica Acta, 63(19/20): 3293-3300.

Brady, P.V. and Walther, J.V., 1989. Controls on silicate dissolution rates in neutral and basic pH solutions at 25°C. Geochimica et Cosmochimica Acta, 53: 2823-2830.

Burch, T.E., Nagy, K.L. and Lasaga, A.C., 1993. Free energy dependence of albite dissolution kinetics at 80°C and pH 8.8. Chemical Geology, 105: 137-162.

Casey, W.H. and Westrich, H.R., 1991. Dissolution rates of plagioclase at pH = 2 and 3. American Mineralogist, 76: 211-217.

Chadwick, O.A. and Chorover, J., 2001. The chemistry of pedogenic thresholds. Geoderma, 100: 321-353.

Chen, Y. and Brantley, S.L., 1998. Diopside and anthophyllite dissolution at 25 degrees and 90 degrees C and acid pH. Chemical Geology, 147(3-4): 233-248.

Chou, L. and Wollast, R., 1985. Steady-state kinetics and dissolution mechanisms of albite. American Journal of Science, 285: 963-993.

Dahlgren, R., Dragoo, J. and Ugolini, F., 1997. Weathering of Mt. St. Helens Tephra under a Cryic-Udic Climate Regime. Soil Sci. Soc. Am. J, 61: 1519-1525.

Dahlgren, R., Shoji, S. and Nanzyo, M., 1993. Mineralogical Characteristics of Volcanic Ash Soils. In: S. Shoji, R. Dahlgren and M. Nanzyo (Editors), Volcanic Ash Soils, Genesis, Properties, and Utilization. Developments in Soil Science. Elsevier, Amsterdam, London, NY, Tokyo.

Dahlgren, R.A., Driscoll, C.T. and McAvoy, D.C., 1989. Aluminum precipitation and dissolution rates in spodosol Bs horizons in the Northeastern USA. Soil Science Society of America Journal, 53: 1045-1052.

Devidal, J.L., Schott, J. and Dandurand, J.L., 1997. An experimental study of the dissolution and precipitation kinetics of kaolinite as a function of chemical affinity and solution composition at 150°C, 40 bars, and pH 2, 6.8 and 7.8. Geochimica et Cosmochimica Acta, 61: 5165-5186.

Drever, J.I. and Clow, D.W., 1995. Weathering Rates in Catchments. In: A.F. White and S.L. Brantley (Editors), Chemical Weathering Rates of Silicate Minerals. Reviews in Mineralogy. Mineralogical Society of America, Washington D.C., pp. 463-481.

Drever, J.I. and Stillings, L.L., 1997. The role of organic acids in mineral weathering. Colloids and Surfaces A: Physiochemical and Engineering Aspects, 120: 167-181.

Drever, J.I. and Vance, G.F., 1994. Role of soil organic acids in mineral weathering processes. In: E.D. Pittman and M.D. Lewan (Editors), Organic Acids in Geological Processes. Springer-Verlag, Berlin Heidelberg, pp. 138-161.

Eggleton, R.A., 1986. The relation between crystal structure and silicate weathering rates. In: S.M. Colman and D.P. Dethier (Editors), Rates of Chemical Weathering of Rocks and Minerals. Academic Press, Inc, Orlando, FL, pp. 21-40.

Etringer, M.A., 1989. The Hydrogen Ion Dependence of the Chemical Weathering Rate of a Tunbridge Series Soil from Lead Mountain, Maine at 15°C. Master of Science Thesis, University of Iowa.

Farrar, C.D., Neil, J.M. and Howle, J.F., 1999. Magmatic Carbon Dioxide Emissions at Mammoth Mountain, California, USGS, Sacramento, CA.

Farrar, C.D. et al., 1995. Forest-killing diffuse CO_2 emission at Mammoth Mountain as a sign of magmatic unrest. Nature, 376: 675-678.

Fox, T.R. and Comerford, N.B., 1990. Low-molecular weight organic acids in selected forest soils of the southeastern USA. Soil Science Society of America Journal, 54(4): 1139-1144.

Gaillardet, J., Dupre, B., Louvat, P. and Allegre, C.J., 1999. Global silicate weathering and CO_2 consumption rates deduced from the chemistry of large rivers. Chemical Geology, 159: 3-30.

Gerlach, T.M., Doukas, M.P., McGee, K.A. and Kessler, R., 1998. Three-year decline of magmatic CO_2 emissions from soils of a Mammoth Mountain tree kill: Horseshoe Lake, CA, 1995-1997. Geophysical Research Letters, 25(11): 1947-1950.

Grandstaff, D.E., 1977. Some kinetics of bronzite orthopyroxene dissolution. Geochimica et Cosmochimica Acta, 41: 1097-1103.

Gwiazda, R.H. and Broecker, W.S., 1994. The separate and combined effects of temperature, soil pCO_2, and organic acidity on silicate weathering in the soil environment: formulation of a model and results. Global Biogeochemical Cycles, 8(2): 141-155.

Helgeson, H.C., Murphy, W.M. and Aagaard, P., 1984. Thermodynamic and kinetic constraints on reaction rates among minerals and aqueous solutions. II. Rate constants, effective surface area, and the hydrolysis of feldspar. Geochimica et Cosmochimica Acta, 58: 2405-2432.

Hill, D.P., 1996. Earthquakes and carbon dioxide beneath Mammoth Mountain, California. Seismological Research Letters, 67: 8-15.

Hill, D.P. et al., 1990. The 1989 earthquake swarm beneath Mammoth Mountain, California: an initial look at the 4 May through 30 September activity. Bulletin of the Seismological Society of America, 80(2): 325-339.

Hinkley, T.K., 1975. Weathering mechanisms and mass balance in a high Sierra Nevada watershed, distribution of alkali and alkaline earth metals in components of parent rock and soil, snow, soil moisture and stream flow. Thesis, California Institute of Technology, Pasadena, CA.

Hodson, M.E. and Langan, S.J., 1999. The influence of soil age on calculated mineral weathering rates. Applied Geochemistry, 14: 387-394.

Huertas, F.J., Chou, L. and Wollast, R., 1999. Mechanism of kaolinite dissolution at room temperature and pressure Part II: Kinetic study. Geochimica et Cosmochimica Acta, 63(19/20): 3261-3275.

Kalinowski, B.E., Faith-Ell, C. and Schweda, P., 1998. Dissolution kinetics and alteration of epidote in acidic solutions at 25^{o}C. Chemical Geology, 151: 181-197.

Knauss, K.G., Nguyen, S.N. and Weed, H.C., 1993. Diopside dissolution kinetics as a function of pH, CO_2, temperature, and time. Geochimica et Cosmochimica Acta, 57: 285-294.

Kolka, R.K., Grigal, D.F. and Nater, E.A., 1996. Forest soil mineral weathering rates: use of multiple approaches. Geoderma, 73: 1-21.

Kraemer, S.M., Chiu, V.Q. and Hering, J.G., 1998. Influence of pH and competitive adsorption on the kinetics of ligand-promoted dissolution of aluminum oxide. Environ. Sci. Technol., 32: 2876-2882.

Kraemer, S.M. and Hering, J.G., 1997. Influence of solution saturation state on the kinetics of ligand-controlled dissolution of oxide phases. Geochim. Cosmochim. Acta, 61(14): 2855-2866.

Lagache, M., 1965. Contribution a l'etude de l'alteration des feldspaths, dans l'eau, entre 100 et 200 C, sous diverses pressions de CO_2, et application a la synthese des mineraux argileux. Bull. Soc. Franc. Miner. Crist, 88: 223-253.

Langan, S.J., Reynolds, B. and Bain, D.C., 1996. The calculation of base cation release from mineral weathering in soils derived from palaeozoic greywackes and shales in upland UK. Geoderma, 69: 275-285.

Lasaga, A.C., Soler, J.M., Ganor, J., Burch, T.E. and Nagy, K.E., 1994. Chemical-weathering rate laws and global geochemical cycles. Geochimica et Cosmochimica Acta, 58(10): 2361-2386.

Lowry, T.H. and Richardson, K.S., 1987. Mechanism and Theory in Organic Chemistry. Harper & Row, New York, 1090 pp.

Malmstrom, M. and Banwart, S., 1997. Biotite dissolution at 25^{o}C: The pH dependence of dissolution rate and stoichiometry. Geochimica et Cosmochimica Acta, 61(14): 2279-2799.

Malmstrom, M., Banwart, S., Lewenhagen, J., Duro, L. and Bruno, J., 1996. The dissolution of biotite and chlorite at 25^{o}C in the near-neautral pH region. Journal of Contaminated Hydrology, 21: 201-213.

Marshall, H.G., Walker, J.C.G. and Kuhn, W.R., 1988. Long-term climate change and the geochemical cycle of carbon. Journal of Geophysical Research, 93: 791-801.

McGee, K.A. and Gerlach, T.M., 1998. Annual cycle of magmatic CO_2 in a tree-kill soil at Mammoth Mountain, California: Implications for soil acidification. Geology, 26(5): 463-466.

Miller, C.D., 1985. Holocene eruptions at the Inyo volcanic chain, California: Implications for possible eruptions in Long Valley caldera. Geology, 13: 14-17.

Morel, F.M.M. and Hering, J.G., 1993. Principles and applications of aquatic chemistry. John Wiley & Sons, Inc., New York, 588 pp.

Murakami, T., Kogure, T., Kadohara, H. and Ohnuki, T., 1998. Formation of secondary minerals and its effect on anorthite dissolution. American Mineralogist, 83: 1209-1219.

Oelkers, E.H., 2001. General kinetic discription of multioxide silicate mineral and glass dissolution. Geochimica et Cosmochimica Acta, 65(21): 3703-3719.

Oelkers, E.H. and Gislason, S.R., 2001. The mechanism, rates and consequences of basaltic glass dissolution: I. An experimental study of the dissolution rates of basaltic glass as a function of aqueous Al, Si, and oxalic acid concentration at 25 ^{o}C and pH = 3 and 11. Geochimica et Cosmochimica Acta, 65(21): 3671-3681.

Oelkers, E.H. and Schott, J., 1998. Does organic acid adsorption affect alkali-feldspar dissolution rates? Chemical Geology, 151: 235-245.

Oelkers, E.H., Schott, J. and Devidal, J.L., 1994. The effect of aluminum, pH, and chemical affinity on the rates of aluminosilicate dissolution reactions. Geochimica et Cosmochimica Acta, 58: 2011-2024.

Osthols, E. and Malmstrom, M., 1995. Dissolution kinetics of ThO_2 in acids and carbonate media. Radiochimica acta, 68(2): 113-119.

Pokrovsky, O.S. and Schott, J., 2000. Kinetics and mechanism of forsterite dissolution at 25 degrees C and pH from 1 to 12. Geochimica et Cosmochimica Acta, 64(19): 3313-3325.

Rahn, T.A., Fessenden, J.E. and Wahlen, M., 1996. Flux chamber measurements of anomalous CO_2 emission from the flanks of Mammoth Mountain, California. Geophysical Research Letters, 23(14): 1861-1864.

Rogers, J.R., Bennett, P.C. and Choi, W.J., 1998. Feldspars as a source of nutrients for microorganisms. American Mineralogist, 83: 1532-1540.

Rogie, J.D., Kerrick, D.M., Sorey, M.L., Chiodini, G. and Galloway, D.L., 2001. Dynamics of carbon dioxide emission at Mammoth Mountain, California. Earth and Planetary Science Letters, 188: 535-541.

Schnoor, J.L., 1990. Kinetics of chemical weathering: A comparison of laboratory and field weathering rates. In: W. Stumm (Editor), Aquatic chemical kinetics: Reaction rates of processes in natural waters. John Wiley and Sons, New York, pp. 475-504.

Seney, J.P. and Gallegos, J.A., 1995. Soil survey of Inyo National Forest, west area, California. U.S. Department of Agriculture, Forest Service, Washington D.C., 365 pp.

Sieh, K., 2000. Personal Communication. Professor of Geology, California Institute of Technology, Pasadena, CA.

Sorey, M.L. et al., 1998. Carbon dioxide and helium emissions from a reservoir of magmatic gas beneath Mammoth Mountain, California. Journal of Geophysical Research, 103(B7): 15,303-15,323.

Sorey, M.L. et al., 1996. Invisible CO_2 gas killing trees at Mammoth Mountain, California. U.S. Geological Survey.

Sparks, D.L., 1989. Rates of Chemical Weathering, Kinetcis of soil chemical processes. Academic Press, Inc, San Diego, pp. 146-162.

Sposito, G., 1984. The Surface Chemistry of Soils. Oxford University Press, New York, 234 pp.

Stumm, W., 1987. Aquatic Surface Chemistry: Chemical processes at the particle-water interface. John Wiley & Sons, NY, 520 pp.

Sverdrup, H. and Warfvinge, P., 1993. Calculating field weathering rates using a mechanistic geochemical model PROFILE. Applied Geochemistry, 8: 273-283.

Sverdrup, H.U., 1990. The kinetics of base cation release due to chemical weathering. Lund University Press, 246 pp.

Swoboda-Colberg, N.G. and Drever, J.I., 1993. Mineral dissolution rates in plot-scale field and laboratory expeirments. Chemical Geology, 105: 51-69.

Tate, R.L.I., 1987. Soil Organic Matter, Biological and Ecological Effects. John Wiley & Sons, New York, 291 pp.

van der Salm, C., Westerveld, J.W. and Verstraten, J.M., 2000. Release of Al from inorganic and organic compounds in a sandy podzol, during laboratory experiments. Geoderma, 96: 173-198.

van Grinsven, H.J.M., van Riemsdijk, W.H., Otjes, R. and Breemen, N.v., 1992. Rates of aluminum dissolution in acid sandy soils observed in column experiments. Journal of Environmental Quality, 21: 439-447.

Velbel, M., 1990. Influence of temperature and mineral surface characteristics on feldspar weathering rates in natural and artificial systems: A first approximation. Water Resources Research, 26(12): 3049-3053.

Velbel, M.A., 1989. Effect of chemical affinity on feldspar hydrolysis rates in two natural weathering systems. Chemical Geology, 78: 245-253.

Velbel, M.A., 1995. Interaction of Ecosystem Processes and Weathering Processes. In: S.T. Trudgill (Editor), Solute Modelling in Catchment Systems. John Wiley & Sons Ltd., New York, pp. 193-209.

Volk, T., 1987. Feedback between weathering and atmospheric CO_2 over the last 100 million years. American Journal of Science, 287: 763-779.

Welch, S.A. and Ullman, W.J., 1993. The effect of organic acids on plagioclase dissolution rates and stoichiometry. Geochimica et Cosmochimica Acta, 57: 2725-2736.

White, A.F. and Blum, A.E., 1995. Effects of climate on chemical weathering in watersheds. Geochimica et Cosmochimica Acta, 59(9): 1729-1747.

White, A.F. and Claassen, H.C., 1980. Kinetic model for the short-term dissolution of a rhyolitic glass. Chemical Geology, 28: 91-109.

Wogelius, R.A. and Walther, J.V., 1991. Olivine dissolution at 25^{o}C: Effects of pH, CO_2, and organic acids. Geochimica et Cosmochimica Acta, 55(4): 943-954.

Wollast, R., 1967. Kinetics of alteration of K-feldspars in buffered solutions at low temperature. Geochimica et Cosmochimica Acta, 31: 635-648.

Chapter 3

COMPARATIVE CHARACTERIZATION OF VOLCANIC ASH SOILS EXPOSED TO DECADE-LONG ELEVATED CARBON DIOXIDE CONCENTRATIONS AT MAMMOTH MOUNTAIN, CALIFORNIA*

*Adapted from Stephens and Hering, 2002. *Chemical Geology*. Vol. 186. No. 3-4. p. 289-301

3.1 Introduction

Elevated concentrations of soil CO_2 derived from the venting of magmatic CO_2 have caused the death of coniferous trees in several distinct areas on Mammoth Mountain, California (Farrar et al., 1995; Hill, 1996; McGee and Gerlach, 1998; Rahn et al., 1996; Rogie et al., 2001). The initiation of CO_2 degassing has been attributed to a swarm of small earthquakes in 1989 (Gerlach et al., 1998; Hill et al., 1990); tree mortality in this area was first observed in 1990 (Farrar et al., 1995). High concentrations of soil CO_2 can cause tree mortality either by preventing the tree roots from absorbing O_2 needed for respiration or by interfering with nutrient uptake (Sorey et al., 1996). Surveys of soil gas in the upper 70 cm of the soil have documented CO_2 concentrations ranging from 20-90% within the tree-kill areas (Fig. 3.1b). The concentrations of CO_2 in the adjacent healthy forest areas are at background levels of < 1% (Farrar et al., 1995; McGee and Gerlach, 1998; Rogie et al., 2001). Soil CO_2 concentrations vary seasonally with accumulation in the winter underneath the snow-pack and a sudden decrease during spring snow-melt (McGee and Gerlach, 1998).

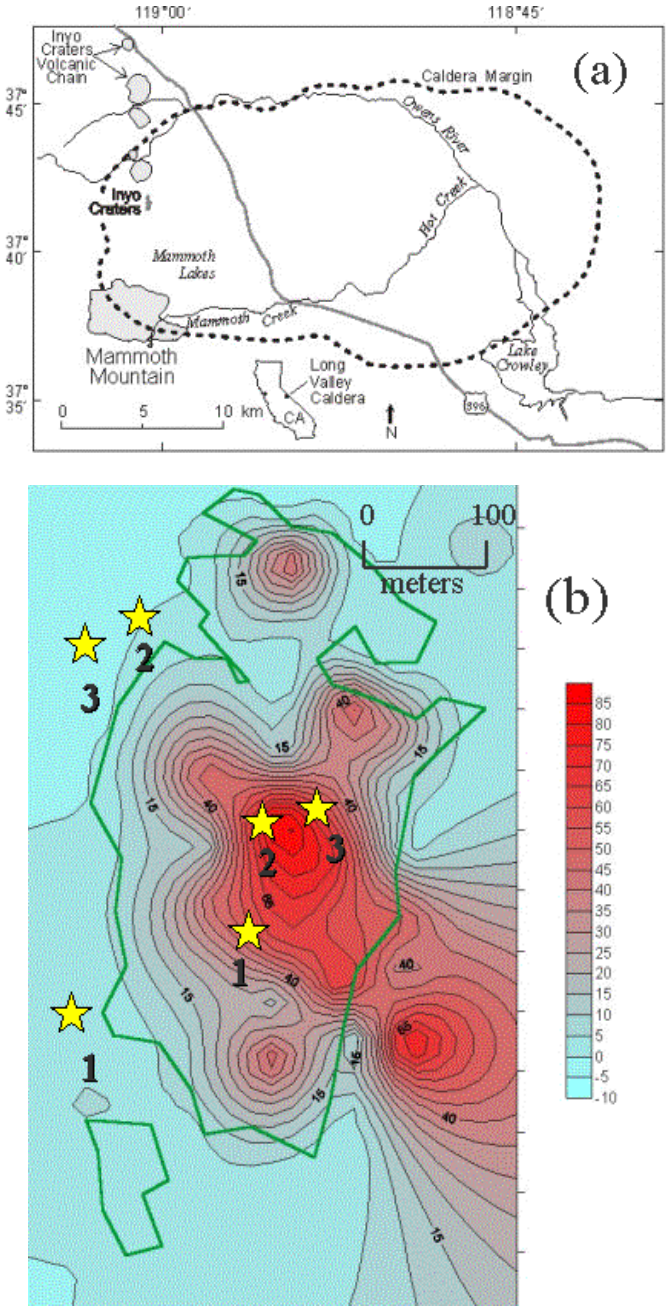

Figure 3.1 - (a) Map showing location of study area, Mammoth Mountain, California, and its relation to the Long Valley Caldera (courtesy of U.S.G.S.). (b) Map of Horseshoe Lake high-CO_2, tree-kill area and surroundings with contours representing percent CO_2 in soil gas (courtesy of Dave Parker, U.C. Riverside). Sampling sites within and outside the anomalous area are marked with a star. The exact locations of sampling locations are high-CO_2 Site 1 N 37°36’46.3 W 119°01’16.7, Control Site 1 N 37°36’46.5 W 119°01’23.6, high-CO_2 Site 2 N 37°36’47.6 W 119°01’13.2, Control Site 2 N 37°36’46.4 W 119°01’05.2, high-CO_2 Site 3 N 37°36’49.8 W 119°01’12.0, Control Site 3 N 37°36’46.1 W 119°01’04.6.

The tree-kill areas provide a natural laboratory to examine the response of soil mineral weathering to elevated CO_2 concentrations in conjunction with possible changes in organic acid composition resulting from vegetation mortality. Increased soil CO_2 concentrations cause a decrease in the pH of the soil solution and thus may (indirectly) increase weathering rates. Whether or not CO_2 itself has a direct effect on mineral weathering is not well understood. Some low molecular weight (LMW) organic acids produced in soils have been shown to accelerate mineral weathering (Drever and Stillings, 1997; Drever and Vance, 1994; Fox and Comerford, 1990; Gwiazda and Broecker, 1994).

The volcanic ash soils found at Mammoth Mountain have a particularly low resistance to chemical weathering compared to other soils due to the predominance of volcanic glass and other non-crystalline phases (Dahlgren et al., 1993). Decadal exposure of volcanic tephra to natural weathering conditions was found to produce distinct differences in the solid phases present in the weathered (as compared with the parent) material (Dahlgren et al., 1997). Thus, it may be anticipated that the decade-long exposure of the young volcanic soils at Mammoth Mountain to elevated soil CO2 concentration may result in differences in soil characteristics.

Recent research on the Mammoth Mountain high-CO_2 areas has focused primarily on monitoring and characterizing the CO_2 fluxes and their relationship to seismic activity in the region (Farrar et al., 1999; Farrar et al., 1995; Gerlach et al., 1998; Hill, 1996; McGee and Gerlach, 1998; Rahn et al., 1996; Rogie et al., 2001; Sorey et al., 1998; Sorey et al., 1996). One study assessed the response of vegetation to the CO_2 degassing

(Biondi and Fessenden, 1999) and another discussed possible effects of changing soil acidity on mobilization of aluminum (McGee and Gerlach, 1998). To date, however, the soil mineralogy and soil chemistry of this unique site have not been characterized. This paper presents a comparison of the soil chemistry and mineralogy and LMW organic acid composition in soils from a high-CO_2 and an adjacent control area.

3.2 Background

3.2.1 The Field Site

The soils analyzed for this study were sampled within and outside the Horseshoe Lake tree-kill, high-CO_2 area on Mammoth Mountain, located along the southwestern edge of the Long Valley Caldera (Fig. 3.1a). The Horseshoe Lake tree-kill area occupies ~145,000 m^2 on 15-60% slopes at elevations of 2700-2800 m (McGee and Gerlach, 1998). The vegetation in the area is dominated by lodgepole pine (Biondi and Fessenden, 1999). Winter snow-pack commonly exceeds 3 m but the soils remain unfrozen due to the insulating effect of the snow-pack (McGee and Gerlach, 1998), and water infiltrates readily into the soil (Seney and Gallegos, 1995). Mean annual soil temperature is ~5 ^oC and annual precipitation is ~90 cm per year (80-90 % falls as snow) (McGee and Gerlach, 1998).

Although the geological parent material consists largely of granitic rock, the upper meters of the soil are derived from volcanic ash from the Inyo eruption, 650-550 years ago (Miller, 1985; Sieh, 2000). Volcanic ash soils are distinguished by a high percentage of non-crystalline volcanic glass and unique clay-size mineral assemblages

often dominated by non-crystalline components (Dahlgren et al., 1993). Metastable solid phases with short-range-order, including allophane, imogolite, and ferrihydrite are often formed as weathering products of volcanic glasses because of their rapid weathering rates (Dahlgren et al., 1993). Because of the comparatively rapid time-scale for weathering of volcanic ash soils (Dahlgren et al., 1993), the Mammoth Mountain soils may respond rapidly to changes in weathering conditions. Seasonal variations in the weathering rates at Mammoth Mountain are expected in response to precipitation and hydrologic flow patterns with minimal weathering in the dry summer months, accelerating weathering in the late fall and winter as the soils become moist, and maximum weathering in the late spring during snow-melt (McGee and Gerlach, 1998).

3.2.2 Soil Mineral Weathering

Rates of chemical weathering in soils are determined in part by the composition and characteristics of soil minerals. Mineral reactivity is highly variable (Chadwick and Chorover, 2001) and dependent on crystallinity (Eggleton, 1986) and surface area (Morel and Hering, 1993; Sposito, 1984). The chemical composition of infiltrating solution and the hydrologic and temperature regime of the local environment also play a large role in determining the chemical weathering rates in a given soil (Sparks, 1989).

Mineral dissolution necessarily involves four general steps: (1) transport of reactive species (e.g., H^+, OH^-, ligands, etc.) from the bulk solution to the mineral surface, (2) interaction of these reactive species with the surface metal centers (which destabilizes the bonds between the surface metal centers and crystal lattice), (3)

detachment of the metal ion from the surface, and (4) transport of the reaction products (i.e., the metal ions) from the surface to the bulk solution. In transport-controlled dissolution, the rate-limiting supply of reactants or removal of products generates a concentration gradient between the surface and bulk solution (Stumm, 1992). In surface-controlled dissolution, the detachment step is usually considered to be rate limiting. The rates of proton-promoted dissolution (R_H) and ligand-promoted dissolution (ΣR_L, where L includes both organic and inorganic ligands) are generally taken to contribute additively to the overall dissolution rate R_{diss} though some synergistic effects have been observed (Kraemer et al., 1998). Then

$$R_{diss} = R_H + \Sigma R_L$$

This expression holds for systems sufficiently undersaturated that the back reaction (i.e., precipitation with rate R_{pptn}) can be neglected. As saturation is approached, the observed (net) dissolution rate, R_{diss}^{net}, decreases such that

$$R_{diss}^{net} = R_{diss} - R_{pptn}$$

with $R_{diss}^{net} = 0$ at equilibrium (Kraemer and Hering, 1997). Thus, ligands can increase observed dissolution rates by direct interaction with the surface metal centers (i.e., contributing to R_L) or indirectly by lowering the pH (i.e., contributing to R_H) or by stabilizing the dissolved metal in solution (i.e., decreasing R_{pptn}) (Drever and Stillings, 1997).

Increased concentrations of CO_2 could influence observed dissolution rates indirectly by decreasing pH. A direct role for CO_2 in mineral weathering has been

proposed but is still controversial. Weathering rates measured at high temperature (100-200°C) and high P_{CO_2} (2-20 bar) have been shown to be proportional to $P_{CO_2}^{0.3}$ (Lagache, 1965). This apparent fractional dependence on P_{CO_2} has been attributed either to adsorption of CO_2 (Sverdrup, 1990) or as simply a pH effect (apparently the initial pH of the experiments with CO_2 was lower) (Brady, 1991; Helgeson et al., 1984). Despite this uncertainty, this relationship has been assumed to hold for CO_2 values typical of soil environments in several geochemical models (Marshall et al., 1988; Sverdrup and Warfvinge, 1993; Volk, 1987). Several studies attempting to verify this relationship have shown that, at low pH, weathering is not directly affected by CO_2 concentration (Brady and Carroll, 1994; Grandstaff, 1977; Wogelius and Walther, 1991), whereas both decreases (Wogelius and Walther, 1991) and increases (Berg and Banwart, 2000; Osthols and Malmstrom, 1995) in dissolution rates have been observed with increased CO_2 at alkaline pH, in addition to observations of no effect (Knauss et al., 1993; Malmstrom et al., 1996).

Weathering rates determined in the laboratory for many minerals (Langmuir, 1997) and for some whole soils (Asolekar et al., 1991) are often much higher than field weathering rates estimated from watershed-scale element budgets (April et al., 1986; Velbel, 1989). One source of uncertainty in this comparison is the mineral surface area exposed to weathering in the field. However, lower field weathering rates may also reflect the influence of hydrologic conditions and a shift from surface-controlled dissolution (under laboratory conditions) to transport-controlled dissolution (Kolka et al., 1996; Schnoor, 1990).

3.3 Methods

3.3.1 Sampling

Samples were collected in September 1999 and June 2000 from a total of six sites (Fig. 3.1b), three within and three outside the Mammoth Mountain Horseshoe Lake high-CO_2 area (unless otherwise noted, the results presented here are from the samples collected in September 1999). The sites were carefully selected based on extensive U.S.G.S. monitoring data of the soil CO_2 concentrations (Rogie, 2001), (Rogie et al., 2001). The sites within the high-CO_2 area were selected in regions of vegetation mortality where measured soil CO_2 concentrations are > 20% throughout the year and the control sampling sites in regions of healthy vegetation with background levels (< 1%) of soil CO_2. Each of the three control sites was chosen to correspond to one of the three high-CO_2 sites (based on elevation, slope and aspect) in an attempt to minimize differences other than the vegetation and CO_2 concentration. The high-CO_2 site 1 and control site 1 are 200 m apart at an elevation of 2780 m and are on a slope of 50% facing east. The high-CO_2 site 2 and control site 2 are 300 m apart at an elevation of 2710 m and a slope of 20% facing southeast. The high-CO_2 site 3 and control site 3 are 300 m apart at an elevation of 2700 m and are on relatively flat terrain.

As is characteristic of volcanic ash soils (Shoji et al., 1993), these soils have a distinct organic litter layer (0-5 cm), a dark-colored organic A-horizon (5-45 cm) - where, in most of the soil pits, two distinct organic rich horizons (5-15 cm and 15-45 cm) could be distinguished - and a yellowish-brown B-horizon with minimal visible organic material (45-60 cm). Samples were taken from each of these horizons and homogenized

before analysis. With the exception of pH and soil moisture measurements, the results presented here are from analysis of B-horizon soils sampled from a depth ranging from 45-60 cm. Although more intense weathering would be expected in the surface horizons, this comparative study focused on the subsurface B-horizon in an attempt to minimize variability associated with the vegetation mortality in the surface horizons. Samples were stored in polypropylene bags and refrigerated until they were analyzed. Within 48 hours of sampling, upon return to the lab, pH and soil moisture were measured on the fresh soil samples; the remainder of the samples were dried and sieved through a 2 mm sieve and subsequently used in all other analyses.

3.3.2 Chemical Analyses

Soil pH was measured in aqueous suspensions (at a 1:2 (w/w) soil-to-water ratio) following a 20 minute equilibration. Soil moisture percentage was determined gravimetrically by measuring the difference in weight of the field-moist fresh sample and the same sample dried in an oven at 60^{o}C for 48 hours. Particle-size distribution was determined by the pipette method (Gee and Bauder, 1986). BET-N_2 surface areas of whole soils (< 2-mm) and the clay size fraction (<2-μm) were measured using a Gemini 2360 Surface Area Analyzer (Micromeritics Instrument Corp., Norcross, GA). Elemental analysis was performed by Chemex Laboratories on whole soil samples (< 2-mm) and on sand, silt and clay size fractionated samples using x-ray fluorescence (XRF) spectrometry. Percent weight of major elements as oxides was determined based on comparison with a certified standard reference material (SY-4, Canadian Certified

Reference Materials Project) and organic carbon was estimated based on weight loss on ignition at 1010 ^{o}C. Three selective dissolution analyses were performed on both the high-CO_2 and control soils. In the dithionite-citrate dissolution procedure, 0.5 g of soil sample was mixed with 25 ml of 0.68 M sodium citrate, 0.4 g of dithionite powder ($Na_2S_2O_4$) was added and the suspension was shaken overnight in an end-over-end shaker (Carter, 1993). For dissolution with acid-ammonium-oxalate, 0.25 g of soil sample was mixed vigorously with 0.2 M ammonium oxalate adjusted to pH 3 in the dark for 2 hours (McKeague and Day, 1966). For the pyrophosphate dissolution, 0.3 g of soil sample was mixed with 30 ml of 0.1 M sodium-pyrophosphate and shaken overnight in an end-over shaker (Carter, 1993). After each of these extraction procedures, the solutions were centrifuged and the supernatant was filtered with a cellulose acetate 0.2 μm filter and analyzed for Al, Si, Fe, Ca and K by inductively coupled plasma mass spectroscopy (ICP-MS).

Low-molecular-weight (LMW) organic acids and total organic carbon (TOC) were measured in aqueous extracts from soils collected in June 2000. Soil samples were extracted with water in a 1:2 (w/w) ratio shaken on an end-over shaker overnight. The suspension was then centrifuged at 4400 rpm for 10 minutes, the supernatant was filtered through a 0.45 μm filter and this aqueous extract was frozen until analyzed. LMW organic acids were analyzed by ion chromatography using a Dionex IonPac AS11 4 mm analytical column (and corresponding guard column) with detection by conductivity. Each run lasted 25 minutes using an eluent of NaOH with a concentration gradient of 0.50 mM to 38 mM. Concentrations of LMW organic acids were determined based on

comparison with standards. TOC in the soil extracts was determined by high temperature catalytic oxidation using a Shimadzu TOC-5000A Total Organic Carbon Analyzer. The percentage of TOC accounted for by the measured concentrations of LMW organic acids was calculated.

Replicate analyses with different sub-samples of soil were performed for all methods to assess the reproducibility of each method and the level of heterogeneity within each homogenized soil sample.

3.3.3 Mineralogical Analyses

Thin sections of the bulk (< 2 mm) size fraction soil were prepared and examined under a petrographic microscope. A minimum of 400 points of a grid on each slide were counted. Powder X-ray diffraction (XRD) analysis was performed on whole soil samples and clay-size fraction samples using a Scintag Pad V X-ray Powder Diffractometer using Cu K-α radiation generated with a 40 kV accelerating potential and 35 mA tube current. Samples were step scanned for 2 s at a rate of 0.01 ^{o}/min at a 0.01^{o} 2θ step. Diffractograms were obtained for samples treated following standard methods, including Mg and K saturation, glycolation, and heating to 550^{o}C (Whittig and Allardice, 1986). A Philips EM430 TEM at an accelerating voltage of 300kV was used to examine samples of the < 2 μm fraction for the presence of allophane, imogolite or ferrihydrite. Magnetite was separated from the bulk sample by using a magnet.

3.4 Results and Discussion

3.4.1 pH measurements

The measured pH was approximately 5.0 in the high-CO_2 soil and approximately 5.6 in the control soil (Fig. 3.2). The pH was lower in the surface horizons than at depth, probably due to the higher concentration of soluble organic acids closer to the surface (Zabowski and Sletten, 1991). Since the ambient soil CO_2 concentrations are not maintained during sample collection and analysis, it is reasonable that the pH measured in the high-CO_2 soil is higher than the pH of 3.9 - 4.15 predicted for soil solution calculated based on CO_2 concentration data (McGee and Gerlach, 1998). The measured pH is similar to that of water (pH 5.3) from a well in the high-CO_2 area and lower than that of water (pH 7.0) from a near-by well outside the high-CO_2 area (Farrar et al., 1999).

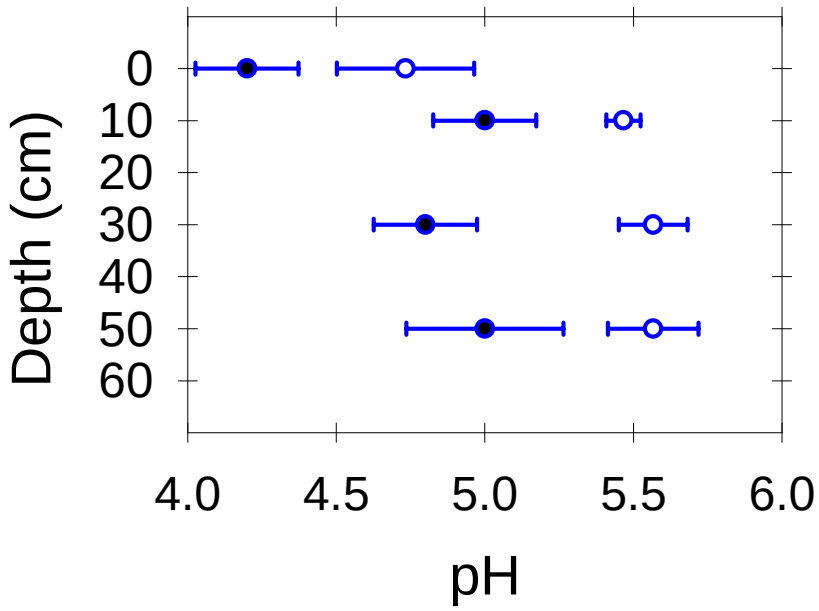

Figure 3.2 - pH measurements, average and standard deviation of samples within the high-CO_2 soil (solid circles) and in the control soil (open circles) collected in September, 1999.

Average soil pH in the Hubbard Brook Experimental Forest decreased to 4.3 from an original pH of 5.1 after trees were felled and left in place (Nodvin et al., 1988). This decrease in pH following a disturbance in vegetation has been attributed to accelerated mineralization of organic matter (Nodvin et al., 1988). It is possible, therefore, that the observed decrease in pH is due in part to the vegetation mortality in addition to the increased acidity from the high-CO_2.

3.4.2 Percent soil moisture

Although no distinct difference was observed in the moisture content of the high-CO_2 and control soils in the samples collected in early June during the snowmelt (Fig. 3.3a), the high-CO_2 soil was moister than the control soil in the samples collected in September, at the end of the summer (Fig. 3.3b). This difference in soil moisture content of the September samples probably reflects the absence of evapotranspiration by live trees throughout the dry summer months in the high-CO_2 soil.

3.4.3 Particle size distribution

The Mammoth Mountain B-horizon soils have a low clay content of less than 2% by weight, while the sand and silt-size particles make up 75-80% and 18-26% of the soil, respectively. Comparison with the results of a simultaneous analysis of a standard soil with a known particle size distribution indicates that the range of values for sand and silt reflect variations among the different sampling sites rather than error in the method. Rates of chemical weathering in volcanic ash soils are often estimated from the quantity

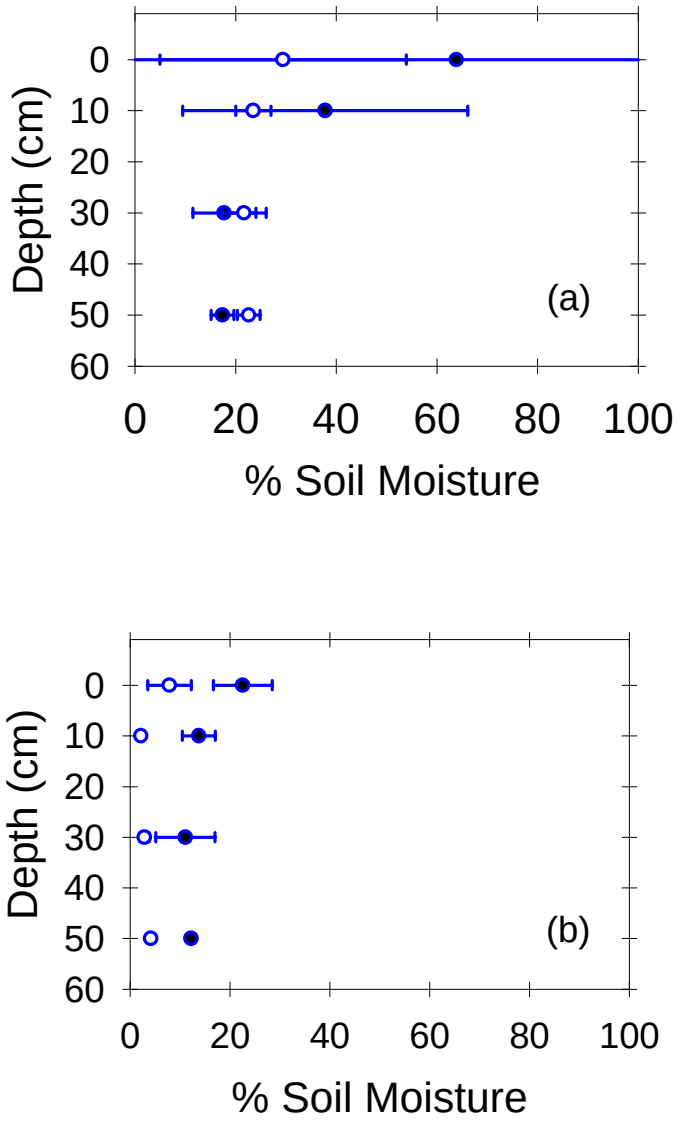

Figure 3.3 - Percent soil moisture, average and standard deviation of samples within the high-CO_2 soil (solid circles) and the control soil (open circles) collected in (a) June 2000, and (b) September, 1999. % soil moisture = 100*((fresh weight – dry weight) / dry weight)

of clay formed (Dahlgren et al., 1993). However, since the clay content of soils from both the high-CO_2 and control soils is comparable to the error of the method (± 1%) (Gee and Bauder, 1986), no comparison can be made between the sites.

3.4.4 Specific surface area

Specific surface areas measured in both whole soil samples (Fig. 3.4a) and clay-size fractions (Fig. 3.4b) are greater in the high-CO_2 soil than in the control soil.

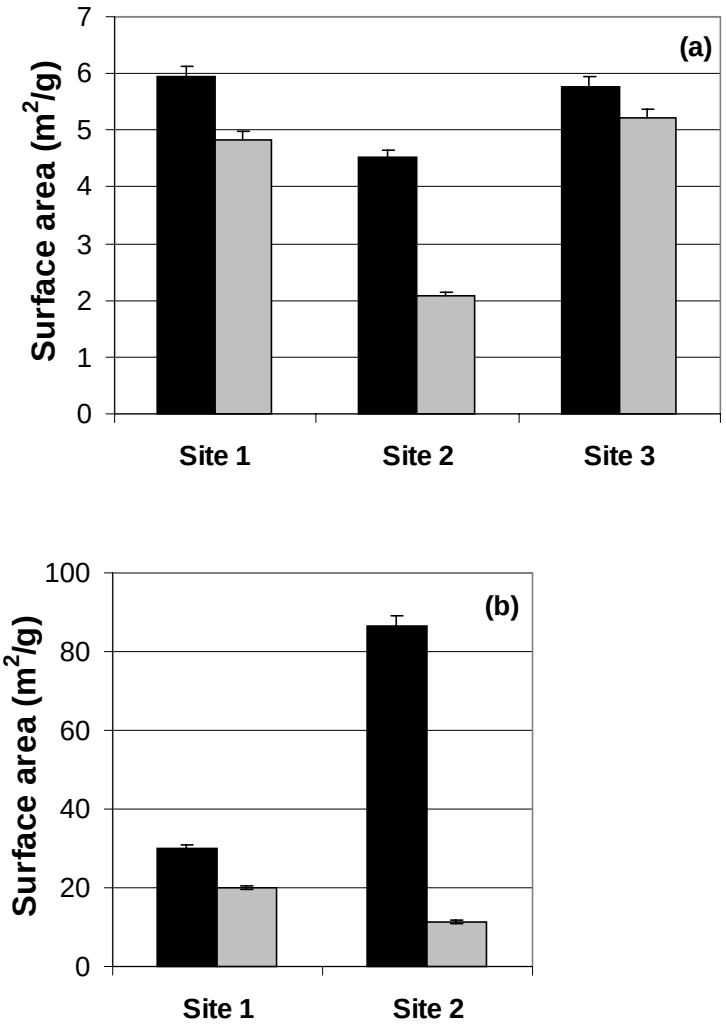

Figure 3.4 – Specific surface area measurements in B-horizon soils collected in September, 1999. Average and standard deviation of replicate measurements a) whole soil samples, b) clay size fraction. An insufficient quantity of the clay fraction from Site 3 precluded analysis. Black = high-CO_2 soil Grey = control soil

Replicate measurements on soil samples from each site were consistent (as shown by the error bars in Fig. 3.4). Thus the differences among the high-CO_2 and control sites can be attributed to heterogeneity of the soil. Soil surface areas as measured by the BET-N_2 technique generally increase with soil age because the weathering process alters the mineral surface and breaks down soil particles (White, 1995). Thus, the higher surface area of the soil from the high-CO_2 sites suggest that they have experienced more intense weathering than the soil from the control sites with lower surface area.

3.4.5 Mineralogical analysis

Bulk mineralogy of the soil was evaluated by XRD and visual examination using a petrographic microscope. The soils are predominantly composed of volcanic glass (50-60%). Plagioclase and K- feldspars, quartz, hornblende, magnetite (~2%), and cristobolite occur as accessory minerals. Halloysite, kaolinite, and vermiculite were identified by XRD in the clay size fraction. Ferrihydrite was identified by TEM analysis of the clay size fraction but neither allophane or imogolite was detected. Low intensities and poor signal-to-noise ratios were observed in the X-ray diffractograms of these samples consistent with the high percentage of non-crystalline material in these soils (details of mineralogical analysis are discussed in Appendix A). Thus, although distinct clay minerals were identified, any quantitative differences between the clay mineralogy of the high-CO_2 and control soils that may have resulted from 10 years of different weathering conditions were too subtle to be observed.

3.4.6 Elemental analysis

Analysis of the major elemental composition of the soils is shown in Table 3.1. Compared to the control samples, the high-CO_2 soil is slightly enriched in Si and depleted in Al. This pattern suggests that Al may have been preferentially weathered from the high-CO_2 soils either because the high-CO_2 soils were subject to more intense weathering or because less organic matter is available to bind Al in the high-CO_2 soil (see Section 4.8). The other major elements do not show any consistent differences between the high-CO_2 and control soils. Variability in the other major elements indicates a high

Table 3.1
Major elemental chemistry of the inorganic fraction of the bulk (< 2 mm) soil (in wt %)
All other elements are less than 1%

		SiO_2	Al_2O_3	K_2O	Na_2O	Fe_2O_3	CaO
High CO_2	1	72.7	14.3	4.4	3.5	2.8	1.2
	2	73.4	13.8	4.8	3.4	2.3	1.0
	3	73.7	13.3	5.0	3.6	1.7	0.9
Control	1	72.4	14.5	4.5	3.5	2.3	1.0
	2	70.6	15.1	4.2	3.7	2.7	1.4
	3	69.2	16.8	3.9	3.9	3.0	1.7
Precision[b]		± 0.3	± 0.4	± 0.05	± 0.2	± 0.3	± 0.03

[b] Based on replicate analyses

degree of spatial heterogeneity in the bulk mineralogy. As was found in another decade-long study of weathering of volcanic material (Dahlgren et al., 1997), total elemental analysis may not be a sufficiently sensitive technique to identify distinct differences in weathering in short-term studies.

3.4.7 Selective extractions

Three selective dissolution analyses were performed using dithionite-citrate, ammonium oxalate, and sodium pyrophosphate as extractants. The results shown in Figure 3.5 and 3.6 indicate differences in soil mineralogy between the high-CO_2 and control sites.

3.4.7.1 Dithionite-citrate extraction

In the dithionite-citrate extractions, the quantities of extractable Al and Si (DC-Al and DC-Si) are consistently lower in the high-CO_2 soil compared to the control soil (Fig. 3.5a,b). No consistent pattern was observed for iron extracted by dithionite-citrate (DC-Fe) (Fig. 3.5c). The dithionite-citrate extraction is generally assumed to dissolve crystalline oxide phases, non-crystalline phases and organically complexed Al and Fe (Mehra and Jackson, 1960). Approximately 1.5-8.5% of Al, 0.6-1.3% of Si, and 14-46% of Fe was leached from these soils in this extraction.

3.4.7.2 Acid oxalate extraction

The results of the acid ammonium oxalate dissolution show trends similar to the dithionite-citrate results for Al (AO-Al), Si (AO-Si) and Fe (AO-Fe). More AO-Al and AO-Si are extracted from the control soil than from the high-CO_2 soil from each site while AO-Fe varies considerably (Fig. 3.6a-c). The oxalate extraction dissolved <1.5% of Si, up to 7% of Al, and a highly variable 2-26% of Fe. Acid ammonium oxalate extraction of soils has been shown to dissolve non-crystalline materials selectively

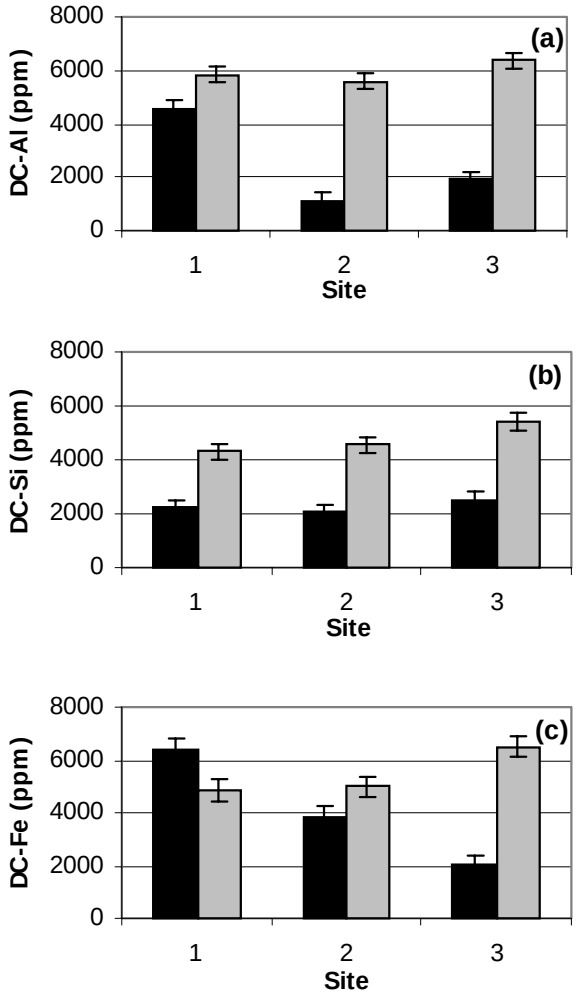

Figure 3.5 - Dithionite-citrate selective extraction results from B-horizon soil collected in September, 1999. Extractable (a) Al (DC-Al), (b) Si (DC-Si), (c) Fe (DC-Fe). Error bars represent range of duplicate samples. Black = high-CO_2 soil Grey = control soil

(Fey and Roux, 1977), although it may also partially dissolve magnetite (Baril and Bitton, 1969) and some layer silicates (Carter, 1993).

3.4.7.3 Pyrophosphate extraction

The results of the Na-pyrophosphate dissolution show considerable variability in the quantities of Fe (P_2O_5-Fe) and Al (P_2O_5-Al) extracted (Fig. 3.6d, e). Unlike the other

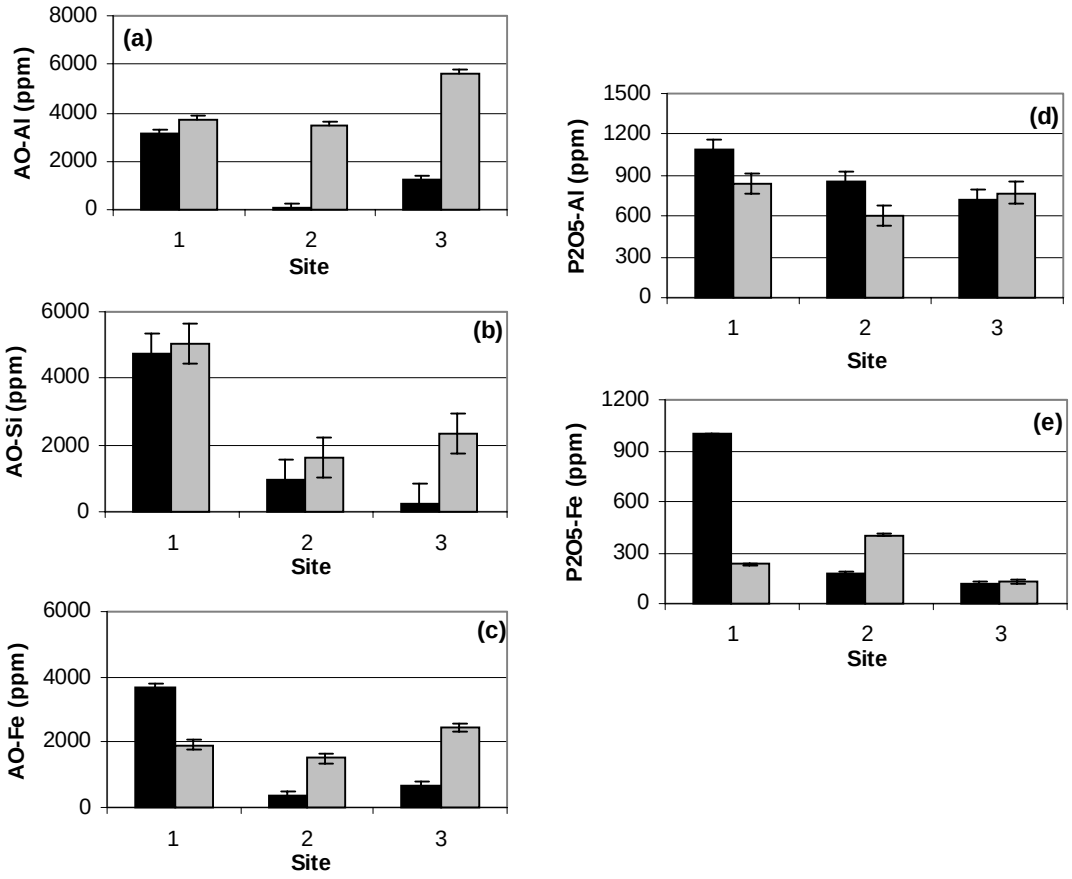

Figure 3.6 – Acid-ammonium-oxalate and Na-pyrophosphate selective extraction results from B-horizon soil collected in September, 1999. Acid-ammonium-oxalate extractable (a) Al (AO-Al), (b) Si (AO-Si), and (c) Fe (A0-Fe), and sodium-pyrophosphate extractable (d) Al (P_2O_5-Al) and (e) Fe (P_2O_5-Fe). Error bars represent standard deviation of at least 3 replicate samples. Black = High-CO_2 soil Grey = control soil

dissolution methods, no clear trend is apparent in the comparison of the high-CO_2 and control soils. Na-pyrophosphate, which extracts organically-bound Fe and Al, dissolved <1.5% of total Al and only up to 7% of total Fe suggesting that organically-complexed metals are not a major soil component.

3.4.7.4 Interpretation and critique of results of selective extractions

A distinct difference in the mineralogy of the high-CO_2 soil compared to the control soil is indicated by differences in the efficiencies of the dithionite-citrate and acid-oxalate extraction for these soils. Although assignment of extractable metal concentrations to specific mineral phases can be unreliable (McCarty et al., 1998), we suggest that the observed patterns can be related to the weathering history of the soils. The extraction of less Al and Si by both extractants is, however, subject to different possible interpretations. This observation could be taken to indicate that the high-CO_2 soil has been subject to greater weathering intensity and thus more of the mineral phases extractable by dithionite-citrate and acid oxalate had been weathered out of the high-CO_2 soil compared to the control soil. Alternatively, if the dithionite-citrate and acid-oxalate extractable fractions are taken to correspond to weathering products, this observation could reflect less intensive weathering (i.e., less formation of weathering products) in the high-CO_2 soil. However, the Mammoth Mountain soils have been weathering for hundreds of years and, thus the weathering products accumulated over the last 10 years during the period of CO_2 degassing would be insignificant relative to the total accumulation of weathering products. Therefore, we suggest that the difference in extractable material between the high-CO_2 and control soils reflects more intense weathering in the high-CO_2 soil.

3.4.8 Organic Analysis

3.4.8.1 Total organic carbon

Organic carbon in these B-horizon soils makes up 3-5% of the total soil material, and there is less organic material in the high-CO_2 soil than in the control soil (Fig. 3.7a). Vegetation mortality in the high-CO_2 soil has halted the normal deposition of litter as well as the input of organic acids from roots. These effects might be even more pronounced in the upper soil horizons; the subsurface B-horizon was chosen for this comparative study in an attempt to minimize differences in the organic fraction expected from the vegetation mortality.

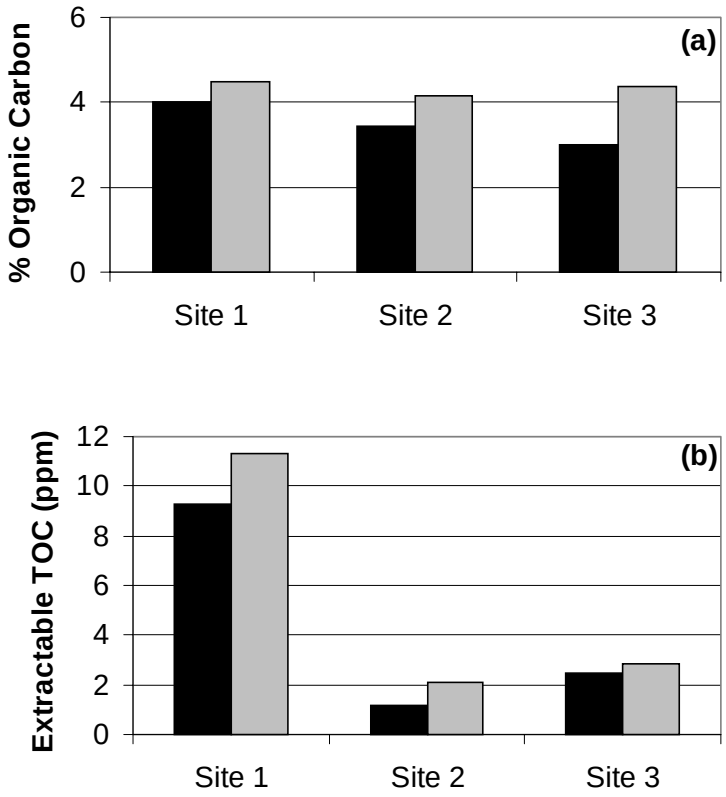

Figure 3.7 - (a) Total organic carbon % by weight. (b) Total organic carbon (TOC) in aqueous extracts of 1:2 (w/w) soil:water. Units of part per million (ppm) represent mg of organic carbon per kg of soil extract. Black = High-CO_2 soil Grey = control soil

3.4.8.2 Low-molecular-weight organic acids

Analysis of soil-water extracts by ion chromatography identified six primary organic acids present in the B-horizon soils: acetic, oxalic, citric, propionic, formic and malic (Table 3.2). Acetic acid is most abundant ranging from 40-100 μmol/kg, followed by formic, propionic, oxalic, citric, and malic acid with less than 3 μmol/kg. Concentrations of oxalic acid, which has been widely demonstrated to enhance mineral weathering (Drever and Stillings, 1997), range from 3-6 μmol/kg, consistent with

Table 3.2
Concentrations of LMW organic acids determined by ion chromatography (μmol/kg)

	High-CO_2 sites			Control Sites		
	1	2	3	1	2	3
Acetic	102.2	52.6	68.3	98.7	41.8	61.0
Formic	29.2	14.0	21.3	33.4	13.8	17.2
Propionic	21.1	22.8	27.8	21.3	9.6	16.2
Oxalic	6.1	3.6	4.5	5.3	3.1	3.7
Citric	2.4	0.8	0.5	4.9	ND[a]	1.6
Malic	2.8	1.7	1.7	1.6	0.8	1.4
% of TOC[b]	1.9	8.6	5.1	2.1	4.2	3.6

[a] Not detected

[b] Percent of extractable TOC accounted for by the sum of all measured LMW organic acids

measurements in other soils (Fox and Comerford, 1990). No clear or significant trends are observed in the comparison of the organic acid concentrations in the high-CO_2 and control soils.

The measured concentrations of LMW organic acids reflect a complex and dynamic balance between organic acid production and decomposition. LMW organic acids are produced primarily at plant roots and also by decomposition of organic matter

(Drever and Vance, 1994; Pohlman and McColl, 1988), so their concentrations may be dependent on micro-scale proximity to plant biomass. Seasonal variation in LMW organic acid concentrations is also likely, as organic acids can be removed by flushing during the spring snow-melt. Since our analysis of LMW organic acids was performed on soil samples collected in June just after the snow-melt, the organic acid concentrations and their relative abundance in the high-CO_2 and control soils may not be entirely representative. The similar abundance of LMW organic acids in the high-CO_2 and control soils suggests that these soil constituents do not contribute to the differences in weathering intensity experienced by these soils. However, a contribution of LMW organic acids to mineral weathering at these sites cannot necessarily be excluded because spatial and seasonal variations in LMW organic acid concentrations have not yet been examined.

3.4.8.3 Extractable total organic carbon and LMW organic acids

Total organic carbon (TOC) in the aqueous extracts is greater in the control soil than in the high-CO_2 soil (Fig. 3.7b), a result consistent with the vegetation mortality in the high-CO_2 soil and the higher percentage of organic matter measured in the control soil (Fig. 3.7a). The measured concentrations of LMW organic acid constitute only a small percentage of TOC, ranging from 2-9%, suggesting that the majority of extractable organic carbon in these soils is present as medium to high molecular-weight compounds, such as humic substances. Humic substances are thought to have only slight effects on

mineral dissolution and both inhibition and acceleration of mineral weathering (depending on pH) have been observed (Hering, 1995; Ochs, 1996; Ochs et al., 1993).

3.4.9 Temperature effect

An alternate explanation for differences in the weathering intensity of the high-CO_2 soil compared to the control soil could be temperature, since a temperature dependence of weathering of volcanic ash soils has been identified (Dahlgren et al., 1993). The CO_2 gas diffusing through the soil at Mammoth Mountain, however, is at ambient temperatures (Farrar et al., 1999), so no temperature difference between the sites is expected.

3.5 Conclusions

The results of this comparative characterization demonstrate some distinct differences between the high-CO_2 and control soils. The high-CO_2 soil is exposed to elevated soil CO_2 concentrations, lower pH, and higher soil moisture content (during late summer). It also exhibits a slight depletion of total Al and enrichment of total Si, and lower concentrations of extractable Al and Si than the control soils. The observed differences are consistent with the hypothesis that the high-CO_2 soil has experienced more intense weathering resulting from either the higher CO_2 concentrations or the lower pH or both. This hypothesis is supported by the observation that the concentrations of Si, Al, Mn and Fe measured in well-water within the Horseshoe Lake high-CO_2 area are

higher than those measured in nearby wells outside the anomalous area (Evans, 2001; Farrar et al., 1999).

Although we hypothesize that the high-CO_2 soil has experienced enhanced weathering, it is not possible to attribute this to direct effects of CO_2 on weathering rates (i.e., a contribution of R_L to R_{diss} where L = CO_2) because of the lower pH (which would tend to increase the rate of proton-promoted dissolution, R_H) and the potential changes in LMW organic acids due to vegetation mortality. Further work is needed to explain the observed differences between the high-CO_2 and control soils and to identify specific mechanisms by which altered weathering conditions (including elevated CO_2 concentrations, lower pH, and the vegetation mortality) determine weathering rates. Although concentrations of LMW organic acids measured in the high-CO_2 and control soils did not show any consistent trends, spatial and seasonal variations in organic acid concentrations need to be examined to determine whether organic acids might be contributing to enhanced weathering. In addition, laboratory soil dissolution experiments under controlled and varied CO_2 and organic acid concentrations may provide some insight into how elevated CO_2 concentrations at Mammoth Mountain affect the weathering of these volcanic-ash soils.

3.6 References

April, R., Newton, R. and Coles, L.T., 1986. Chemical weathering in two Adirondack watersheds: Past and present-day rates. Geological Society of America Bulletin, 97: 1232-1238.

Asolekar, S.R., Valentine, R.L. and Schnoor, J.L., 1991. Kinetics of Chemical Weathering in B Horizon Spodosol Fraction. Water Resources Research, 27(4): 527-532.

Baril, R. and Bitton, G., 1969. Teneurs élevées de fer libre et identification taxonnomique de certain sols due Québec contenant de la manetite. Canadian Journal of Soil Science, 52: 19-26.

Berg, A. and Banwart, S.A., 2000. Carbon dioxide mediated dissolution of Ca-feldspar: implications for silicate weathering. Chemical Geology, 163(1-4): 25-42.

Biondi, F. and Fessenden, J.E., 1999. Response of lodgepole pine growth to CO_2 degassing at Mammoth Mountain, California. Ecology, 80(7): 2420-2426.

Brady, P.V., 1991. The Effect of Silicate Weathering on Global Temperature and Atmospheric CO_2. Journal of Geophysical Research, 96(B11): 18,101-18,106.

Brady, P.V. and Carroll, S.A., 1994. Direct effects of CO_2 and temperature on silicate weathering: Possible implications for climate control. Geochimica et Cosmochimica Acta, 58(8): 1853-1856.

Carter, M.R., 1993. Soil Sampling and Methods of Analysis. Lewis Publishers, Boca Raton, Florida.

Chadwick, O.A. and Chorover, J., 2001. The chemistry of pedogenic thresholds. Geoderma, 100: 321-353.

Dahlgren, R., Dragoo, J. and Ugolini, F., 1997. Weathering of Mt. St. Helens Tephra under a Cryic-Udic Climate Regime. Soil Sci. Soc. Am. J, 61: 1519-1525.

Dahlgren, R., Shoji, S. and Nanzyo, M., 1993. Mineralogical Characteristics of Volcanic Ash Soils. In: S. Shoji, R. Dahlgren and M. Nanzyo (Editors), Volcanic Ash Soils, Genesis, Properties, and Utilization. Developments in Soil Science. Elsevier, Amsterdam, London, NY, Tokyo.

Drever, J.I. and Stillings, L.L., 1997. The role of organic acids in mineral weathering. Colloids and Surfaces A: Physiochemical and Engineering Aspects, 120: 167-181.

Drever, J.I. and Vance, G.F., 1994. Role of soil organic acids in mineral weathering processes. In: E.D. Pittman and M.D. Lewan (Editors), Organic Acids in Geological Processes. Springer-Verlag, Berlin Heidelberg, pp. 138-161.

Eggleton, R.A., 1986. The relation between crystal structure and silicate weathering rates. In: S.M. Colman and D.P. Dethier (Editors), Rates of Chemical Weathering of Rocks and Minerals. Academic Press, Inc, Orlando, FL, pp. 21-40.

Evans, W.C., 2001. Personal Communication. USGS.

Farrar, C.D., Neil, J.M. and Howle, J.F., 1999. Magmatic Carbon Dioxide Emissions at Mammoth Mountain, California, USGS, Sacramento, CA.

Farrar, C.D. et al., 1995. Forest-killing diffuse CO_2 emission at Mammoth Mountain as a sign of magmatic unrest. Nature, 376: 675-678.

Fey, M.V. and Roux, J.L., 1977. Properties and quantitative estimation of poorly crystalline components in sesquioxidic soil clays. Clays and Clay Mineralgy, 25: 285-294.

Fox, T.R. and Comerford, N.B., 1990. Low-molecular weight organic acids in selected forest soils of the southeastern USA. Soil Science Society of America Journal, 54(4): 1139-1144.

Gee, G.W. and Bauder, J.W., 1986. Particle-size Analysis. In: A. Klute (Editor), Methods of Soil Analysis Part I, Physical and Mineralogical Methods. Soil Science Society of America, Madison, WI, pp. 383-413.

Gerlach, T.M., Doukas, M.P., McGee, K.A. and Kessler, R., 1998. Three-year decline of magmatic CO_2 emissions from soils of a Mammoth Mountain tree kill: Horseshoe Lake, CA, 1995-1997. Geophysical Research Letters, 25(11): 1947-1950.

Grandstaff, D.E., 1977. Some kinetics of bronzite orthopyroxene dissolution. Geochimica et Cosmochimica Acta, 41: 1097-1103.

Gwiazda, R.H. and Broecker, W.S., 1994. The separate and combined effects of temperature, soil pCO_2, and organic acidity on silicate weathering in the soil environment: formulation of a model and results. Global Biogeochemical Cycles, 8(2): 141-155.

Helgeson, H.C., Murphy, W.M. and Aagaard, P., 1984. Thermodynamic and kinetic constraints on reaction rates among minerals and aqueous solutions. II. Rate constants, effective surface area, and the hydrolysis of feldspar. Geochimica et Cosmochimica Acta, 58: 2405-2432.

Hering, J.G., 1995. Interaction of organic-matter with mineral surfaces - effects on geochemical processes at the mineral-water interface, Aquatic Chemistry. Advances in Chemistry Series, pp. 95-119.

Hill, D.P., 1996. Earthquakes and carbon dioxide beneath Mammoth Mountain, California. Seismological Research Letters, 67: 8-15.

Hill, D.P. et al., 1990. The 1989 earthquake swarm beneath Mammoth Mountain, California: an initial look at the 4 May through 30 September activity. Bulletin of the Seismological Society of America, 80(2): 325-339.

Knauss, K.G., Nguyen, S.N. and Weed, H.C., 1993. Diopside dissolution kinetics as a function of pH, CO_2, temperature, and time. Geochimica et Cosmochimica Acta, 57: 285-294.

Kolka, R.K., Grigal, D.F. and Nater, E.A., 1996. Forest soil mineral weathering rates: use of multiple approaches. Geoderma, 73: 1-21.

Kraemer, S.M., Chiu, V.Q. and Hering, J.G., 1998. Influence of pH and competitive adsorption on the kinetics of ligand-promoted dissolution of aluminum oxide. Environ. Sci. Technol., 32: 2876-2882.

Kraemer, S.M. and Hering, J.G., 1997. Influence of solution saturation state on the kinetics of ligand-controlled dissolution of oxide phases. Geochim. Cosmochim. Acta, 61(14): 2855-2866.

Lagache, M., 1965. Contribution a l'etude de l'alteration des feldspaths, dans l'eau, entre 100 et 200 C, sous diverses pressions de CO_2, et application a la synthese des mineraux argileux. Bull. Soc. Franc. Miner. Crist, 88: 223-253.

Langmuir, D., 1997. Aqueous environmental geochemistry. Prentice Hall, Upper Saddle River, NJ.

Malmstrom, M., Banwart, S., Lewenhagen, J., Duro, L. and Bruno, J., 1996. The dissolution of biotite and chlorite at 25^{o}C in the near-neautral pH region. Journal of Contaminated Hydrology, 21: 201-213.

Marshall, H.G., Walker, J.C.G. and Kuhn, W.R., 1988. Long-term climate change and the geochemical cycle of carbon. Journal of Geophysical Research, 93: 791-801.

McCarty, D.K., Moore, J.N. and Marcus, W.A., 1998. Mineralogy and trace element association in an acid mine drainage iron oxide precipitate; comparison of selective extractions. Applied Geochemistry, 13: 165-176.

McGee, K.A. and Gerlach, T.M., 1998. Annual cycle of magmatic CO_2 in a tree-kill soil at Mammoth Mountain, California: Implications for soil acidification. Geology, 26(5): 463-466.

McKeague, J.A. and Day, J.H., 1966. Dithionite- and oxalate-extractable Fe and Al as aids in differentiating various classes of soils. Canadian Journal of Soil Science, 46: 13-26.

Mehra, O.P. and Jackson, M.L., 1960. Iron oxide removal from soils and clays by a dithionite-citrate system buffered with sodium bicarbonate. Clays and clay minerals, 7: 317-327.

Miller, C.D., 1985. Holocene eruptions at the Inyo volcanic chain, California: Implications for possible eruptions in Long Valley caldera. Geology, 13: 14-17.

Morel, F.M.M. and Hering, J.G., 1993. Principles and applications of aquatic chemistry. John Wiley & Sons, Inc., New York, 588 pp.

Nodvin, S.C., Driscoll, C.T. and Likens, G.E., 1988. Soil processes and sulfate loss at the Hubbard-Brook experimental forest. Biogeochemistry, 5(2): 185-199.

Ochs, M., 1996. Influence of humified and non-humified natural organic compounds on mineral dissolution. Chemical Geology, 132: 119-124.

Ochs, M., Brunner, I., Stumm, W. and Cosovic, B., 1993. Effects of root exudates and humic subatnces on weathering kinetics. Water, Air and Soil Pollution, 68: 213-229.

Osthols, E. and Malmstrom, M., 1995. Dissolution kinetics of ThO_2 in acids and carbonate media. Radiochimica acta, 68(2): 113-119.

Pohlman, A.A. and McColl, J.G., 1988. Soluble organics from forest litter and their role in metal dissolution. Soil Science Society of America Journal, 52: 265-271.

Rahn, T.A., Fessenden, J.E. and Wahlen, M., 1996. Flux chamber measurements of anomalous CO_2 emission from the flanks of Mammoth Mountain, California. Geophysical Research Letters, 23(14): 1861-1864.

Rogie, J.D., 2001. Personal Communication. Geological Engineer, USGS, Menlo Park, CA.

Rogie, J.D., Kerrick, D.M., Sorey, M.L., Chiodini, G. and Galloway, D.L., 2001. Dynamics of carbon dioxide emission at Mammoth Mountain, California. Earth and Planetary Science Letters, 188: 535-541.

Schnoor, J.L., 1990. Kinetics of chemical weathering: A comparison of laboratory and field weathering rates. In: W. Stumm (Editor), Aquatic chemical kinetics:

Reaction rates of processes in natural waters. John Wiley and Sons, New York, pp. 475-504.

Seney, J.P. and Gallegos, J.A., 1995. Soil survey of Inyo National Forest, west area, California. U.S. Department of Agriculture, Forest Service, Washington D.C., 365 pp.

Shoji, S., Dahlgren, R. and Nanzyo, M., 1993. Terminology, concepts and geographic distribution of volcanic ash soils. In: S. Shoji, M. Nanzyo and R.A. Dahlgren (Editors), Volcanic Ash Soils, Genesis, Properties and Utilization. Developments in soil science 21. Elsevier, Amsterdam, pp. 288.

Sieh, K., 2000. Personal Communication. Professor of Geology, California Institute of Technology, Pasadena, CA.

Sorey, M.L. et al., 1998. Carbon dioxide and helium emissions from a reservoir of magmatic gas beneath Mammoth Mountain, California. Journal of Geophysical Research, 103(B7): 15,303-15,323.

Sorey, M.L. et al., 1996. Invisible CO_2 gas killing trees at Mammoth Mountain, California. U.S. Geological Survey.

Sparks, D.L., 1989. Rates of Chemical Weathering, Kinetcis of soil chemical processes. Academic Press, Inc, San Diego, pp. 146-162.

Sposito, G., 1984. The Surface Chemistry of Soils. Oxford University Press, New York, 234 pp.

Stumm, W., 1992. Chemistry of the solid-water interface : processes at the mineral-water and particle-water interface in natural systems. Wiley, New York.

Sverdrup, H. and Warfvinge, P., 1993. Calculating field weathering rates using a mechanistic geochemical model PROFILE. Applied Geochemistry, 8: 273-283.

Sverdrup, H.U., 1990. The kinetics of base cation release due to chemical weathering. Lund University Press, 246 pp.

Velbel, M.A., 1989. Effect of chemical affinity on feldspar hydrolysis rates in two natural weathering systems. Chemical Geology, 78: 245-253.

Volk, T., 1987. Feedback between weathering and atmospheric CO_2 over the last 100 million years. American Journal of Science, 287: 763-779.

White, A.F., 1995. Chemical weathering rates of silicate minerals in soils. In: A.F. White and S.L. Brantley (Editors), Chemical Weathering Rates of Silicate Minerals. Mineralogical Society of America, Washington DC, pp. 407-463.

Whittig, L.D. and Allardice, W.R., 1986. X-ray diffraction techniques. In: A. Klute (Editor), Methods of soil analysis. Part 1. ASA and SSSA, Madison WI, pp. 331-362.

Wogelius, R.A. and Walther, J.V., 1991. Olivine dissolution at 25^{o}C: Effects of pH, CO_2, and organic acids. Geochimica et Cosmochimica Acta, 55(4): 943-954.

Zabowski, D. and Sletten, R.S., 1991. Carbon dioxide degassing effects on the pH of Spodosol soil solutions. Soil Science Society of America Journal, 55: 1456-1461.

Chapter 4

LABORATORY DETERMINATION OF DISSOLUTION RATES OF MAMMOTH MOUNTAIN SOILS

4.1 Introduction

Understanding the kinetics of chemical weathering is an essential part of improving our knowledge of global geochemical cycles. Primary minerals formed at high temperatures and pressures within the earth's interior weather as they are exposed to circulating waters at the earth's surface. Chemical weathering is, therefore, one of the primary soil forming processes. Soils develop as mineral dissolution alters parent material and releases dissolved solutes that are either leached downward or precipitated to form secondary (authigenic) minerals. The rate of this weathering process in soils is dependent on the mineral composition of the soil, the local hydrology and climate, and the chemistry of the soil solution.

Much of the current understanding of the kinetics of weathering has been derived from laboratory experiments conducted using specific minerals or synthesized solid phases. Actual soils, however, are composed of mixtures of crystalline minerals, organic matter, and non-crystalline phases, which interact and react simultaneously (Schnoor, 1990). Weathering rates determined in the laboratory for pure minerals are often several orders of magnitude higher than rates estimated from field studies (Kolka et al., 1996; van Grinsven et al., 1992; Velbel, 1990); these discrepancies have been attributed to difficulties in estimating mineral surface areas for field studies and differences in hydrologic regimes in laboratory and field experiments (Schnoor, 1990; van der Salm et

al., 1996; Velbel, 1990). Laboratory weathering experiments conducted on actual soils rather than pure minerals provide kinetic information that incorporates a soil's complex composition. Although this complexity complicates the interpretation of experimental results, such experiments may help to resolve the discrepancy between predicted field and laboratory weathering rates and are valuable in understanding behavior of a particular soil of interest.

Although several researchers have conducted laboratory dissolution experiments on whole soils (Asolekar et al., 1991; Etringer, 1989; Schnoor, 1990), such studies have not, to my knowledge, been performed with volcanic ash soils. Soils derived from volcanic ash have a particularly low resistance to chemical weathering due to the predominance of volcanic glass and other non-crystalline phases (Dahlgren et al., 1993). Over the last decade at Mammoth Mountain, California, volcanic ash soils have been exposed to anomalous environmental conditions; elevated soil CO_2 concentrations, from a magmatic source, have killed vegetation in several distinct areas. Comparative characterization of the soil exposed to these anomalous conditions and soil from a nearby unexposed area shows some distinct differences in the chemistry and the mineralogy (see Chapter 3) suggesting that the exposed soil may have experienced more intense weathering (Stephens and Hering, 2002).

This chapter reports on a set of laboratory pH-stat batch dissolution experiments on volcanic ash soils, modeled after similar experiments conducted on whole soils by Asolekar et al (1991), and designed to compare the mineral weathering regimes of the soils collected within and outside the high-CO_2 area at Horseshoe Lake on Mammoth

Mountain. These experiments tested the hypothesis that soil exposed to more intense weathering conditions in the field would exhibit slower rates of weathering than un-exposed soil in laboratory dissolution experiments. As a comparison with whole soils, dissolution experiments were also conducted with volcanic glass (obsidian), which represents both the parent material of the Mammoth Mountain soils and one of their dominant components.

4.2 Materials and Methods

4.2.1 The Volcanic Soils of Mammoth Mountain

The upper meters of soil on the flanks of Mammoth Mountain are derived from volcanic material ejected during explosive events during the Inyo eruption about 650-550 years ago (Miller, 1985; Sieh, pers. comm.). These violent eruptions deposited rhyolitic tephra consisting of glass, pumice, some crystals, and accidental lithic fragments downwind of the vents carpeting over 100 km^2 including Mammoth Mountain (Miller, 1985). Since the deposition of the volcanic parent material, these soils have been weathering and developing for about 600 years. Mineralogical analysis using a petrographic microscope and X-ray diffraction (XRD) (discussed in Chapter 3 with details in Appendix A) indicates that these soils are predominantly composed of volcanic glass (50-60%). Other major mineral phases, each estimated to be less than 10%, include plagioclase feldspar ((Na, Ca) $AlSi_3O_8$), K-feldspar ($AlSi_3O_8$), quartz (SiO_2), hornblende ($(Na, Ca)_2(Mg, Fe, Al)_5(Si,Al)_8O_{22}(OH)_2$), biotite ($K(Mg, Fe)_3Si_3(Al,Fe)O_{10}(OH,F)_2$) and

magnetite (Fe_3O_4); this is the same host of major mineral phases identified in the lava produced in the eruption (Sampson and Cameron, 1987). Halloysite ($Al_2Si_2O_5(OH)_4$), kaolinite ($Al_2Si_2O_5(OH)_4$), and vermiculite ($(Mg,Fe^{II},Al)_3(Si,Al)_4O_{10}(OH)_2 \cdot 4H_2O$) were identified in the clay size fraction by XRD. Under the petrographic microscope, iron oxide coatings were observed on some grains and hematite (Fe_2O_3) was identified. Transmission electron microscopy (TEM) identified ferrihydrite ($Fe_5HO_8 \cdot 4H_2O$) in the clay fraction.

The recent Inyo eruption was actually a series of eruptions of different types. The explosive eruptions that produced the pumaceous volcanic tephra, from which the upper meters of Mammoth Mountain soil are derived, were followed by eruptions that produced rhyolite flows (Miller, 1985) consisting of obsidian, a dense volcanic glass. The obsidian is more dense than the pumice material because the molten rock forming the rhyolite flows contained less dissolved water and volcanic gasses than that ejected in the explosive eruptions (U.S.G.S., 2002). Both the obsidian and the pumice material in the tephra are primarily non-crystalline because rapid cooling of the lava impedes crystal growth (Busch, 1997). Despite their physical differences, the tephra ejected over Mammoth Mountain and the obsidian from a nearby rhyolite flow are derived from the same lava and, therefore, have similar chemical compositions.

4.2.2 Experimental Procedure

Homogonized B-horizon soils were collected from a depth of 45-60 cm from 3 sites within and 3 sites outside the Mammoth Mountain Horseshoe Lake high-CO_2 area.

Each of the three control sites was chosen to correspond to one of the three high-CO_2 sites based on elevation, slope and aspect (details on sampling are discussed in Chapter 3). The soils were air dried and fractionated to the 63-125 μm size range (fine sand) by dry-sieving. The size-fractionated soil was pretreated by washing repeatedly in deionized water and sonicating in acetone to remove fines following the procedure of Etringer (1989). The washed and fractionated soil was dried overnight at 60^{o}C before being used in the experiments. BET-N_2 surface areas of the pre-treated soil before and after the dissolution experiment were measured using a Gemini 2360 Surface Area Analyzer (Micromeritics Instrument Corp., Norcross, GA). Uncertainty in the B.E.T. surface area measurements estimated based on replicate analyses of single samples is 10%, a value consistent with the uncertainty reported by other researchers (Gautier et al., 2001; Oelkers and Gislason, 2001). Elemental analysis was performed by Chemex laboratories by X-ray fluorescence (XRF) spectrometry reported as percent weight of major elements as oxides, and organic carbon was estimated based on weight loss on ignition at 1010^{o}C.

Batch experiments were conducted in a pH-stat system at 22^{o}C (room temperature) with 2 g of soil in 200 ml of water in a polypropylene beaker with a diameter and height of 4 and 8 cm respectively. A low pH of 2.78 was chosen for all of these experiments to allow for the determination of dissolution rates in a reasonable amount of time (~2 weeks) and to minimize formation of secondary phases expected at higher pH values. Soil particles were kept suspended by a motorized stirring rod (3 cm in diameter rotating at > 100 revolutions/min), and the amount of acid (H_2SO_4) added to the

system by a Mettler Toledo DL50 Graphix autotitrator to keep the pH at 2.78 was recorded over time.

Every 24 hours throughout each experiment the mixing was stopped for a brief time as the pH meter was calibrated and the solids were allowed to settle before a sample was taken. Uncertainties in the measured pH values and the associated acid addition throughout these pH-stat reactors arise from drift and error associated with an electrode that is constantly measuring pH over a period of weeks or months. Although the pH electrode was calibrated daily and replaced several times throughout the course of the project, occasional variation in the pre- and post-calibration measurements resulted in either an immediate considerable acid addition following the calibration if the post-calibration pH was higher than the pre-calibration pH or, if the post-calibration pH was lower, the calibration was followed by a period of time where no acid was added. A constant volume in the reactor was maintained by balancing the volume of solution sampled with the amount of acid added to the system in the preceding 24 hours, or by adding pH adjusted solution to the reactor to compensate for the volume sampled. Data have been corrected for changes in concentration as a result of sampling.

Samples taken from the system were filtered through a 0.02 μm Whatman Anopore™ aluminum oxide membrane filter and then analyzed by ICP-MS for Al, Si, Ca, Mg and Fe. Analytical constraints associated with measuring the two other major cations in these soils, Na and K, using ICPMS prevented successful monitoring of the release of these elements. The 0.02 μm filter was chosen to ensure that colloidal particles were not included in the ICPMS analysis; unfortunately, not until most of the

experiments had been completed was it realized that the filter was an aluminum oxide membrane and, therefore, not ideal for subsequent analysis of Al in solution. To assess whether the use of this filter influenced the Al measurements, a control dissolution experiment in which several samples was filtered through both the above mentioned aluminum oxide membrane filter and a 0.2 μm cellulose acetate filter demonstrated that the use of the aluminum oxide filter did not significantly influence the Al measurements (Appendix B, Fig. B.1); differences between the measurements were within the reproducibility error associated with the ICPMS measurement. Although the aluminum oxide filter was not the most appropriate choice, this control experiment provides reason to have confidence in the Al data. Uncertainties in the measurements of aqueous concentrations of Al, Si, Fe, Ca and Mg are estimated to be about 5%, based on the relative standard deviation of the mean of replicate measurements, the calibration uncertainty, and the error associated with dilution (each sample was diluted 10 fold before analysis).

Each experiment was conducted for a minimum of 300 hours. Weathering rates were calculated based on the steady-state amount of H^+ added to the system to keep a constant pH (μeq H^+ / m^2 hr), and release of Si and Al (μmole / m^2 hr); the rate is equal to the slope of the line that best fits the linear part of each data set. Following informal convention, the initial surface area was used to compute the dissolution rates (the final surface area was also measured and the implications of a change in surface area on dissolution rate is discussed in Section 4.3.7). Replicate experiments with different sub-

samples of the same samples were conducted to determine the reproducibility of the method and the heterogeneity within a single soil sample.

In addition to running these experiments with the soils from the different sites, the same experimental set up was used to determine the weathering rate of volcanic glass, in the form of obsidian, produced from the same eruption. The obsidian sample used in these experiments, collected from the nearby Deadman Creek obsidian flow by Daniel Sampson (Sampson and Cameron, 1987), was crushed and size fractionated into the same 63-125 μm size fraction as the soil. The obsidian sample was washed and the experiment was repeated as described above.

4.3 Results and Discussion

4.3.1 Characterization of Soils Prior to Dissolution Experiments

The cleaned and size-fractionated soil material used in these experiments shows some variation in elemental composition (Table 4.1), organic carbon (Fig. 4.1a) and surface area (Fig. 4.1b) among the high-CO_2 and control samples. High-CO_2 site 1 has a

Table 4.1
Elemental composition (in wt %) of the inorganic fraction of the 63-125μm samples
All other elements are less than 1%

		SiO_2	Al_2O_3	K_2O	Na_2O	Fe_2O_3	CaO
High CO_2	1	67.9	15.1	3.6	3.7	5.7	1.9
	2	74.2	13.6	4.4	3.9	2.0	1.2
	3	73.3	14.5	4.3	4.0	1.9	1.2
Control	1	72.3	14.1	4.2	3.9	2.8	1.6
	2	74.5	13.6	4.4	4.0	1.6	1.2
	3	73.7	14.0	4.2	4.0	1.9	1.4
Obsidian		71.1	13.7	4.9	4.7	2.5	1.1
Precision[b]		± 0.3	± 0.4	± 0.05	± 0.2	± 0.3	± 0.03

[b] Based on replicate analyses

higher Al and Fe content and a correspondingly lower Si content when compared to the other samples (Table 4.1). Each of the control samples has a higher percentage of organic carbon (3.5 - 5.5% by weight) compared to the high-CO_2 samples (< 2%) and a lower surface area (Fig. 4.1 a & b). High-CO_2 site 1 has the highest measured specific surface area (7.3 m^2/g) while the other samples range from 1.0 – 3.8 m^2/g. The higher

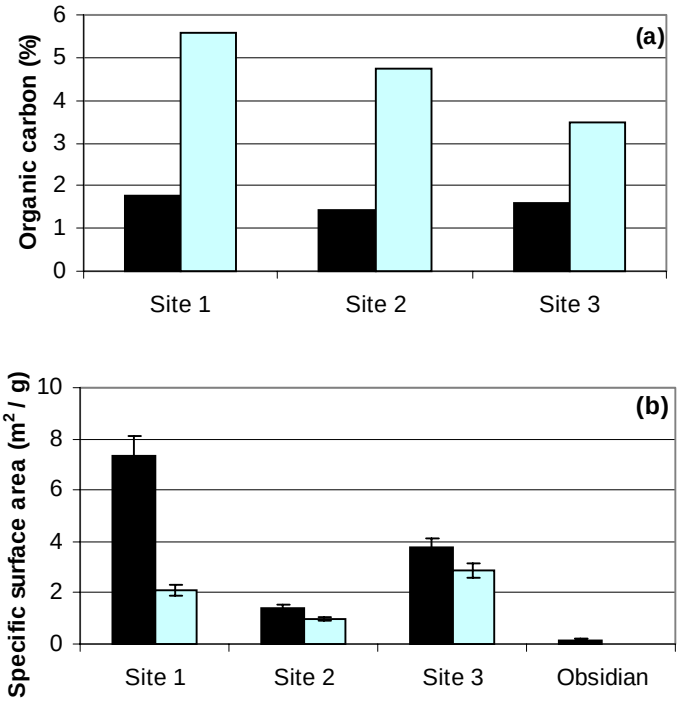

Figure 4.1 – Characteristics of the 63-125 μm size fraction used in the dissolution experiments, (a) Percent organic carbon. (b) Pre-dissolution specific surface area. Black = high-CO_2 soil, Grey = control soil.

specific surface area in high-CO_2 site 1 together with its higher Al and Fe content may reflect the presence of high-surface area Al and Fe oxides. The size-fractionated obsidian sample has a lower surface area (0.18 m^2/g) than any of the soil samples (Fig 4.1b). The elemental composition of the obsidian sample is very similar to the composition of the inorganic fraction of the soil samples (Table 4.1), consistent with the

predominance of this volcanic material in the soils. The jet-black appearance of obsidian is due to the presence of abundant crystallites (microscopic crystal growths); crystalline minerals in the form of phenocrysts occur throughout the samples (Fig. 4.2).

Figure 4.2 - Photograph of obsidian sample (about 5 cm across) collected from Deadman Creek obsidian flow by Daniel Sampson. Inclusions of small, white, crystals of crystobalite (SiO_2) are visible. This material was crushed, sieved to the 63-125 μm size fraction, and washed before being dissolved in the pH-stat batch reactor following the same protocol as the dissolution of the soil samples.

4.3.2 Determination of Weathering Rates

Weathering rates for these soils have been derived from three different sets of time-dependent data: 1) the cumulative addition of H^+ necessary to maintain a constant pH , 2) the cumulative release of Al, and 3) the cumulative release of Si. In each of these data

sets, a shift from parabolic to linear kinetics is observed after approximately 100 hours of dissolution as shown in Fig. 4.3 and 4.4. The initial nonlinear rapid dissolution is commonly observed in dissolution experiments and often attributed to the rapid dissolution of fine (submicron) particles adhering to surfaces. Although the cleaning procedure is an attempt to remove these fines, it has been demonstrated that submicron particles continue to adhere to soil mineral surfaces even after ultra sonic cleaning (Berner and Holdren, 1979). This nonlinear dissolution could also reflect the dissolution of highly soluble oxide coatings surrounding some mineral grains.

As the soil minerals dissolve, protons are consumed and cations are released into solution. This process is illustrated in the following reaction for the weathering of K-feldspar to kaolinite accompanied by some complete dissolution.

$$K_2O \cdot Al_2O_3 \cdot 6SiO_{2(s)} + (2+6n)H^+ + (5-3n)H_2O =$$

$$2K^+ + (4+n)H_2SiO_3 + 2nAl^{3+} + (1-n)Al_2O_3 \cdot 2SiO_2 \cdot 2H_2O_{(s)} \qquad (1)$$

Both alkali feldspars and volcanic glass are principal components of rhyolite, however the release of Si associated with glass dissolution does not consume protons because aqueous silica exists as a neutral species (H_2SiO_3 or $Si(OH)_4$) in acid and near-neutral pH conditions (Brady and Walther, 1990).

The cumulative addition of H^+ in μequivalents per m^2 of soil for control site 1 is plotted against time in Figure 4.3a. Figure 4.3b shows that the cumulative release of Al in μequivalents/m^2 accounts for most of the sum of the cumulative release of the

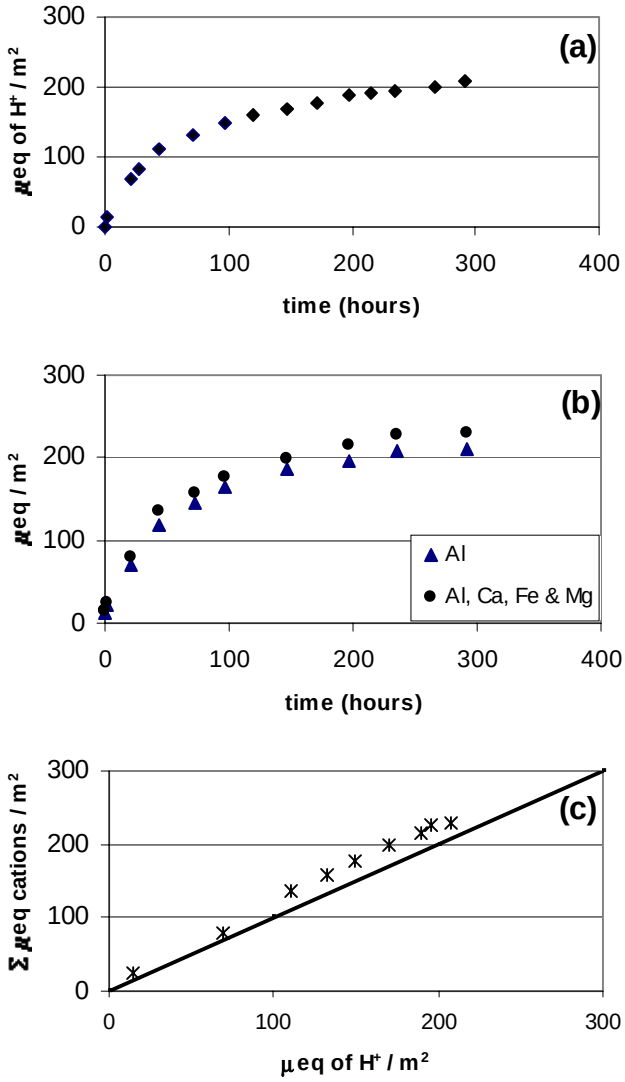

Figure 4.3 – Data from the dissolution of soil from control site 1, (a) µequivalents of H^+ consumed in the reactor vs. time, (b) µequivalents of measured cations released vs. time, (c) This plot of the sum of the µequivalents of Al, Ca, Fe, and Mg vs. the total µequivalents of H^+ consumed shows that the two data sets are comparable in magnitude for this sample. High variability in Al release (the dominant cation) among different samples and replicate experiments is not observed in H^+ consumption, so these two data sets are not comparable in magnitude for every sample.

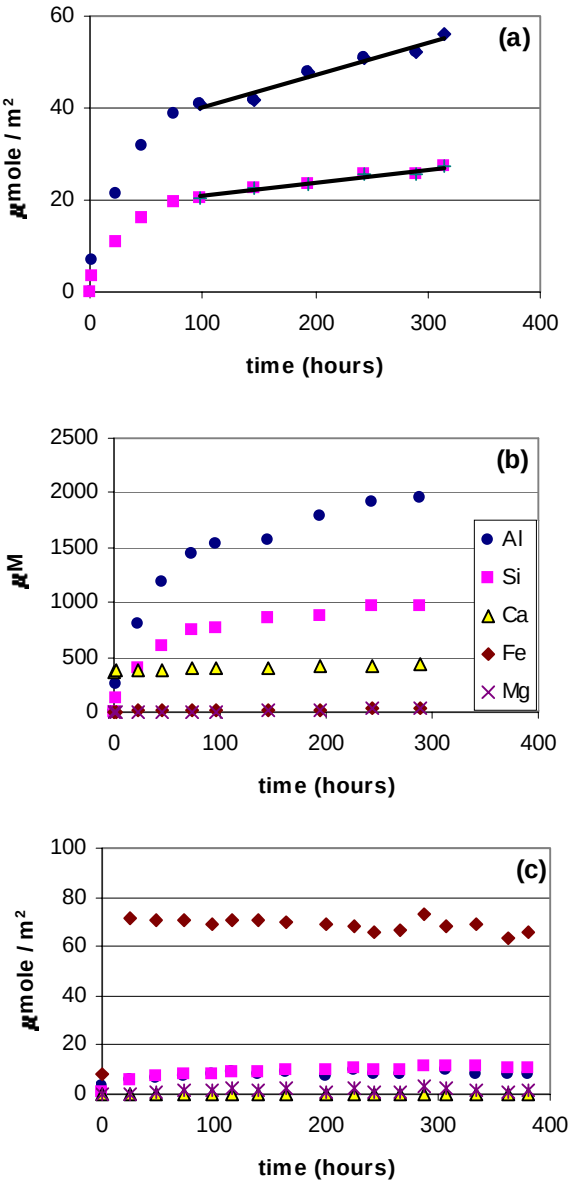

Figure 4.4 – (a) High-CO_2 site 3, release of Al and Si normalized to initial surface area vs. time. Slopes of linear portion of data, 0.07 µmole Al/m^2hr and 0.03 µmole Si/m^2hr, are calculated dissolution rates. (b) High-CO_2 site 3, cation release data in units of concentration (µM) vs. time. (c) Obsidian, release of cations normalized to initial surface area vs. time. Na and K were not measured due to analytical constraints using ICPMS.

measured cations (Al, Ca, Fe and Mg). The H^+ data and the sum of the μequivalents of measured cations are comparable in magnitude in the dissolution of soil from control site 1 (Fig. 4.3c). However, high variability in Al release (the dominant cation) among different samples and replicate experiments is not observed in H^+ consumption, so these two data sets are not comparable in magnitude for every sample. Although the magnitude of H^+ consumption and cation release is similar in soil from control site 1, rates derived from these two data sets do not correspond (discussed in Section 4.3.3).

Weathering rates were calculated from the release of Si and Al normalized to initial surface area of soil material in the reaction vessel (Fig. 4.4a). The rate derived from the Al data for high-CO_2 site 3 shown in Fig. 4.4a (0.07 μmole/m^2 hr), is higher than the rate derived from the Si data (0.03 μmole/m^2 hr), although both data sets show a similar time-dependent pattern of rapid initial release followed by linear dissolution. The differences in release rates of Al and Si may reflect the heterogeneous nature of these soils, which are a mixture of mineral particles with different solubilities and elemental compositions (discussed in more detail in Section 4.3.3).

Figure 4.4c shows the release of elements normalized to initial surface area for dissolution of the obsidian sample. The most striking differences between the elemental release of the obsidian sample and the whole soils are the large quantity of Fe initially released from the obsidian sample and the comparatively low concentrations of other cations released.

4.3.3 Comparison of Weathering Rates

Weathering rates derived from the H^+ addition data are substantially lower in the soil exposed to elevated CO_2 concentrations than in the control soil only for site 1 (Fig. 4.5a). Differences in replicate experiments may result from heterogeneity within a single sample and/or error associated with this method of determining weathering rate. The overall error of the H^+ and Si rates is estimated to be ± 20%, based on the standard deviation of the rates derived from the experiments done in triplicate. Differences in the rates observed in sites 2 and 3 are within the error and are, therefore, negligible. The initial hypothesis, that the soil exposed to elevated CO_2 may have consistently lower dissolution rates because it has been previously more intensely weathered in the field, is not confirmed by these data.

The weathering rates calculated from the dissolved silica data show a similar pattern as those determined from H^+ consumption for site 1 and the weathering rates of the high-CO_2 and control samples from sites 2 and 3 are, likewise, indistinguishable (Fig. 4.5b). Again, control site 1 has a reproducibly higher dissolution rate than any of the other samples.

Weathering rates calculated from the dissolved Al data show significant variability and the rates are not reproducible (Fig. 4.5c). The inconsistency of the Al-derived rates is likely caused by variation in quantities of some active Al phase within sub-samples of a given sample. Due to the high degree of variability in Al release rates among the sites and among replicate experiments, the Al release data do not appear to be useful in this comparison of calculated rates. Subsequent discussion of dissolution rates,

therefore, will focus primarily on those derived from the H^+ consumption and Si release data.

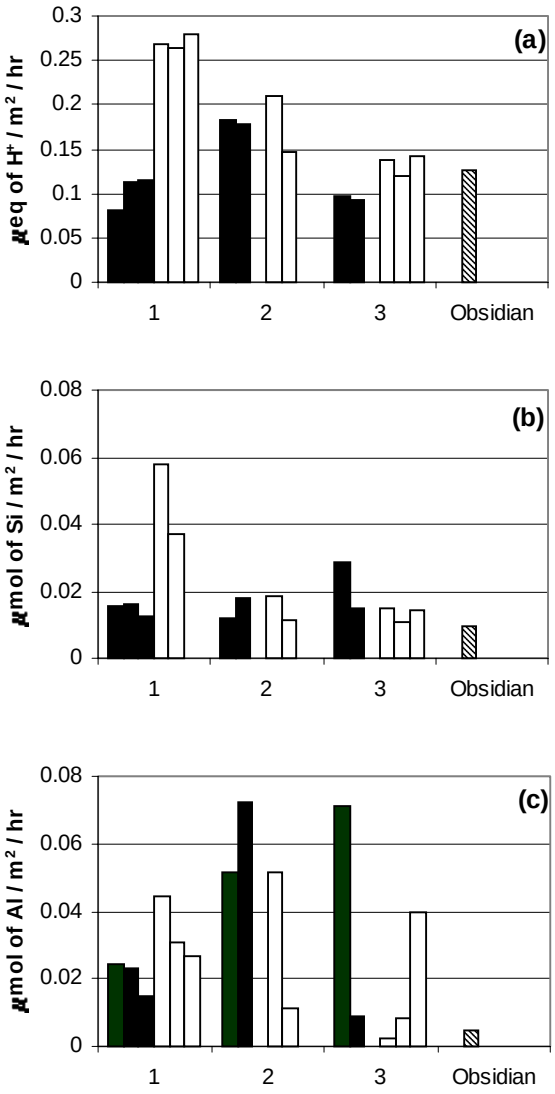

Figure 4.5 – Comparison of dissolution rates of soil samples from high-CO_2 and control sites 1, 2 and 3 and the obsidian sample in the pH-stat batch reactor at pH 2.78. Rates derived from steady-state data on (a) H^+ consumption (b) Si release and (c) Al release. Black = high-CO_2 soil White = control soil Diagonal stripes = obsidian sample

The rates of obsidian dissolution derived from the H^+ consumption, and Si and Al release data are 0.127 μeq/m^2 hr, and 0.01 and 0.005 μmole/m^2 hr respectively. The obsidian dissolution rates derived from the H^+ and Si data are similar to or lower than the rates calculated for the whole soil samples. The obsidian rate derived from the Al data is lower than all but one of the highly variable Al soil dissolution rates.

4.3.4 "Non-stoichiometric" Elemental Release

The ratios of elements released during dissolution do not correspond to the elemental ratios of the starting soil material (Table 4.2). Although the Al/Si molar ratio in the initial soil material is ~0.22, more Al was released than Si (Fig. 4.4a & b) resulting in Al/Si ratios during the linear portion of dissolution around 2.0. Although "stoichiometric" dissolution is expected during the steady-state dissolution of pure minerals, it has not been reported in other studies using whole soils (Asolekar, 1991; Asolekar et al., 1991). This is attributable to the different solubilities of the complex

Table 4.2
Molar ratios of major elements in the pre-dissolution soil and obsidian samples and characteristic ratios of elemental release during steady-state dissolution

		Al/Si	K/Si	Na/Si	Fe/Si	Ca/Si
High CO_2	1	0.25	0.09	0.09	0.13	0.04
	2	0.21	0.11	0.08	0.04	0.02
	3	0.22	0.11	0.09	0.04	0.03
Control	1	0.22	0.10	0.08	0.06	0.03
	2	0.21	0.10	0.09	0.03	0.03
	3	0.22	0.10	0.09	0.04	0.03
	obsidian	0.22	0.12	0.11	0.05	0.02
Released into solution						
	soil	2.0	NA[a]	NA	0.1	0.4
	obsidian	0.8	NA	NA	5.8	0.02

[a] Analytical constraints precluded the measurement of Na and K on the ICPMS

assemblages of minerals that are present in actual soils. The dissolution of the obsidian sample (Fig. 4.4c), which is a simpler material than the soil though not a pure mineral, exhibits an Al/Si ratios of 0.8, much closer to the bulk elemental ratio of 0.22. This difference may reflect highly soluble aluminum oxide phases that have developed in the soil, phases that are not present in the freshly crushed obsidian sample.

In addition to measuring the release of Al and Si, the accumulated concentrations of Fe, Ca and Mg were also monitored. The release of Fe in the soil dissolution experiments resulted in an Fe/Si ratio in solution similar to that of the initial solid material. In the obsidian dissolution experiment, however, Fe released in the rapid, initial phase was greater than the cumulative release of Al or Si (Fig. 4.4c), resulting in an extremely high Fe/Si ratio of 5.8 in solution. This rapid release of Fe, discussed in Section 4.3.2, occurred although the Fe/Si ratio of the obsidian sample is 0.05 which is comparable to the ratios in the soil samples. This initial release of Fe and the lack of measurable subsequent release of Fe suggests that some highly soluble Fe-oxides exposed at the obsidian surfaces after crushing may be dissolving rapidly at the beginning of this experiment.

The Ca/Si ratio of the initial solid material and that released into solution is the same for the obsidian sample (0.02), but in the dissolution of the soils Ca is preferentially released, resulting in a Ca/Si ratio of 0.4. This preferential release of Ca in the soils suggests the formation of some comparatively soluble Ca phases during soil development. The Ca/Si ratios for both the soil and the obsidian dissolution are constant throughout the experiment suggesting that the rate of dissolution of the soluble Ca phases

in the soil is close to that of the Si containing phases. The release of Mg in both the soil and the obsidian experiments was low.

4.3.5 Individual Contributors to Overall Dissolution Rates

The bulk soil dissolution rates discussed above can be interpreted as the sum of the dissolution rates of the (major) mineral phases present in the soils.

$$R_{bulk} = R_{volcanic\ glass} + R_{plagioclase} + R_{K\text{-}feldspar} + R_{quartz} + R_{hornblende} + R_{biotite} \quad (2)$$

Volcanic glass is the dominant constituent of these soils and is generally thought to weather more quickly than crystalline minerals (Dahlgren et al., 1993; Gislason and Eugster, 1987). It is reasonable to assume, therefore, that its rate of dissolution will be a dominant contributor to the overall rate. The dissolution rate measured for the obsidian sample was 0.01 μmole Si/m^2 hr which is on the same order but slightly lower than the average of 0.02 ± 0.013[1] μmole Si/m^2 hr calculated for the 14 soil dissolution experiments. The similarity of these rates confirms that volcanic glass may be the dominant mineral phase contributing to the overall soil dissolution rates.

$$R_{bulk} \sim R_{volcanic\ glass} \quad (3)$$

[1] The error represents one standard deviation of the mean.

The difference in dissolution rates for the bulk soil and the volcanic glass may be due to dissolution of other highly soluble mineral phases in the soils. Selected dissolution rates for the other major Si containing minerals present in these soils reported in the literature in the pH range 2-3 is compiled in Table 4.3. This comparison of rates determined by different researchers using different reactor types must be analyzed with caution, as poor reproducibility of rates determined in different laboratories has been well documented (Blum and Stillings, 1995). Nevertheless, this rough comparison suggests that the rate of dissolution of obsidian is comparable to rates reported for plagioclase and hornblende and faster than those rates for K-feldspar and quartz. In contrast, the dissolution rate reported for biotite is considerably faster than that for obsidian. Thus biotite, along with poorly crystalline phases that are not well defined, are possible candidates for soil minerals whose dissolution would yield higher dissolution rates for bulk soil than for the volcanic glass component.

4.3.6 Evidence Against Formation of Secondary Phases

The determination of the dissolution rate, R_{bulk}, in these experiments presumes that the system is far from equilibrium, that the dissolved Al and Si concentrations are undersaturated with respect to secondary minerals. As soils dissolve, solute concentrations accumulate in batch reactors and can come close to or exceed the solubility of secondary phases potentially influencing the apparent weathering rate. The measured concentrations (not normalized to surface area) of Al, Si, Ca, Fe and Mg in the reactor at each sampling time are shown for high-CO_2 site 3 in Figure 4.4b. Although at

Table 4.3
Weathering rates of minerals identified in Mammoth Mountain soils reported in the literature

Mineral	Formula	Temp °C	pH	Reactor	Weathering Rate μmol Si / m^2 hr	Reference
obsidian	SiO_2 + impurities	22	2.78	batch	$1.0 \times 10^{-2*}$	this study
				batch	$1.87 \times 10^{-2**}$	this study
plagioclase	$(Na,Ca)AlSi_3O_8$	25	3	batch	1.1×10^{-2}	Casey et al, 1991
		25	3	flow-through	9.8×10^{-3}	Stillings & Brantley, 1995
k-feldspar	$KAlSi_3O_8$	25	3	flow-through	5.9×10^{-3}	Stillings & Brantley, 1995
quartz	SiO_2	25	2.15	batch	1.1×10^{-3}	Brady & Walther, 1989
		25	3	batch	2.3×10^{-4}	Bennett, 1991
hornblende	$(Na,Ca)_2(Mg,Fe,Al)_5$-$(Si,Al)_8O_{22}(OH)_2$	25	3	flow-through	3.0×10^{-2}	Frogner & Schweda, 1998
biotite	$K(Mg,Fe)_3Si_3(Al,Fe)$-$O_{10}(OH,F)_2$	25	3	flow-through	2.0×10^{-1}	Malmstrom & Banwart,1997

* Calculated using initial surface area

** Calculated using final surface area (see section 4.3.7 for discussion)

low pH, high solubility minimizes these concerns, two steps were taken to test the effect of accumulated solutes on weathering rates. First, a sample that had been previously weathered for > 300 hours was re-suspended in fresh solution, essentially removing any accumulated cations and allowing the dissolution to continue. After re-suspension the rate of Si release was unchanged (Fig. 4.6), indicating that the solutes accumulated during the initial dissolution period did not affect the Si dissolution rate. The Al data did not display a steady, linear increase (shown in Appendix B, Fig. B.2), so the calculation of an Al release rate after re-suspension was not possible.

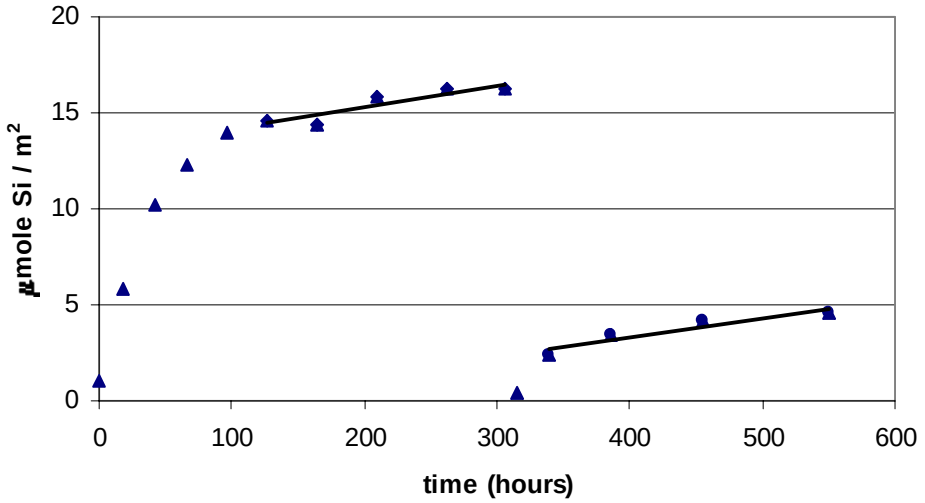

Figure 4.6 – Rates of Si release before and after re-suspension of soil from control site 3 in fresh solution at pH 2.78 normalized to pre-dissolution surface area are the same (0.01 µmole Si / m^2 hr). This demonstrates that accumulation of solutes in the batch reactors is not influencing the observed Si release rates.

In addition to this re-suspension experiment, solubility calculations for likely secondary minerals based on the maximum accumulated Al and Si concentrations at the end of each experiment were performed. Gibbsite, kaolinite and amorphous SiO_2 are

generally considered to be likely secondary products in Si and Al rich soils. To determine if precipitation of these phases was favorable, the ion activity product (Q) calculated from the maximum measured concentrations of accumulated Si and Al in the filtered solution were compared with the reported values of the solubility equilibrium constants, K_{sp}, for these phases at 25°C. Assuming that the measured cations (Al, Ca, Mg, and Fe) and the sulfate added as acid are the primary contributors to ionic strength, an ionic strength in the range of 0.01-0.02 was estimated and the Davies equation was used in the calculations to convert concentrations into activities. Saturation quotients (Q/K_{sp}) were evaluated for kaolinite:

$$Al_2Si_2O_5(OH)_{4(s)} + 6H^+ = 2Al^{3+} + 2H_4SiO_4 + H_2O \quad (4)$$

with $K_{sp} = 2.72 \times 10^7$ (Stumm and Morgan, 1996), for gibbsite:

$$Al(OH)_{3(s)} + 3H^+ = Al^{3+} + 3H_2O \quad (5)$$

with $K_{sp} = 1.28 \times 10^8$ (Stumm and Morgan, 1996), and for amorphous SiO_2:

$$SiO_2 + 2H_2O = Si(OH)_4^0 \quad (6)$$

with $K_{sp} = 1.95 \times 10^{-3}$ (Stumm and Morgan, 1996). Typical concentration ranges in the pH-stat reactors were 1500-2000 μM Al and 700-1000 μM Si. At the low pH (2.78) of these experiments, none of these batch systems approached saturation with respect to kaolinite, gibbsite or amorphous SiO_2. Values of the log of the saturation quotient are around -3 for kaolinite, around -2 for gibbsite, and around –1 for amorphous SiO_2. As will be discussed in Chapter 5, when similar experiments were conducted at higher pH values of 3.5 and 4.0, the solutions did reach saturation with respect to kaolinite and gibbsite (the solubility of amorphous SiO_2 is pH-independent in the acidic pH range).

4.3.7 A Decrease in Specific Surface Area Observed

Specific surface areas measured with the post-dissolution soil material and the obsidian sample were consistently and significantly lower than the pre-dissolution values; a reduction in specific surface area on the order of 40-80% was observed (Table 4.4). Most dissolution studies do not report post-dissolution measurements of specific surface area and follow the informal convention of normalizing dissolution rates to the initial specific surface area. Changes in specific surface area have been reported primarily where increased values were observed in the dissolution of pure minerals (Casey et al., 1989; Chen and Brantley, 1998; Gautier et al., 2001; Stillings et al., 1996; Stillings and Brantley, 1995). Decreases in specific surface area during dissolution experiments have also been reported and attributed either to the rapid dissolution of fine particles (Helgeson et al., 1984), or to the dissolution of Al and Si oxyhydroxide coatings in soils (Hodson et

Table 4.4
Effect of decreases in specific surface area (A) on normalized dissolution rates

Solid material	A (m^2/g)		% Decrease	dissolution rates (μeq H^+/m^2 hr) w/ initial A	w/ final A	R_{fin}/R_{init}
	initial	final	in A	R_{init}	R_{fin}	
High-CO_2 1	7.36	3.73	49.3	0.08	0.16	2.0
High-CO_2 1	7.36	4.38	40.4	0.11	0.19	1.7
High-CO_2 1	7.36	3.08	58.2	0.12	0.28	2.4
Control 1	2.13	0.42	80.0	0.27	1.34	5.0
Control 1	2.13	0.88	58.7	0.26	0.64	2.4
Control 1	2.13	0.55	74.0	0.28	1.08	3.8
High-CO_2 2	1.43	0.35	75.2	0.18	0.74	4.0
High-CO_2 2	1.43	0.39	72.9	0.18	0.65	3.7
Control 2	0.98	0.54	44.9	0.21	0.38	1.8
Control 2	0.98	0.47	52.4	0.15	0.31	2.1
High-CO_2 3	3.75	1.31	65.0	0.10	0.28	2.9
High-CO_2 3	3.75	1.28	65.9	0.09	0.27	2.9
Control 3	2.88	1.39	51.7	0.14	0.29	2.1
Control 3	2.88	1.00	65.2	0.12	0.34	2.9
Obsidian	0.18	0.09	49.8	0.13	0.28	2.2

al., 1998). In the latter case, specific surface area decreased by 61-94%, a range similar to that of the decreases observed in these soil dissolution experiments.

The loss of mass during the > 300 hours of dissolution determined by comparing the measured weights of the pre- and post-dissolution material was on the order of 1-4%. This is consistent with estimates of the amount of material dissolved during the experiments based on summing the concentrations of solutes released (0.5-2 %). This order of mass loss can be reconciled with the decrease in specific surface area if variations in specific surface area among different mineral phases and different particle sizes are considered. The highly soluble ultra fine particles may have been a major contributor to the initially measured specific surface area, but a minor contributor to the overall weight of the sample.

The significant decrease in specific surface area of these soils invited a more detailed analysis of when during the < 300 hours of dissolution this change was occurring. Dissolution experiments were conducted over varying periods of time with both a soil sample (control site 1) and the obsidian sample to assess the temporal component of the observed decrease in specific surface area (Fig. 4.7 a & b). In both the soil and the obsidian sample, the specific surface area reduction appears to be primarily occurring in the initial 100 hours or so, the same time period as the initial nonlinear portion of the H^+ consumption and Si release data. This suggests that the decrease in specific surface area is associated with the dissolution of fine particles and other highly soluble phases that occurs in the initial 100 hours.

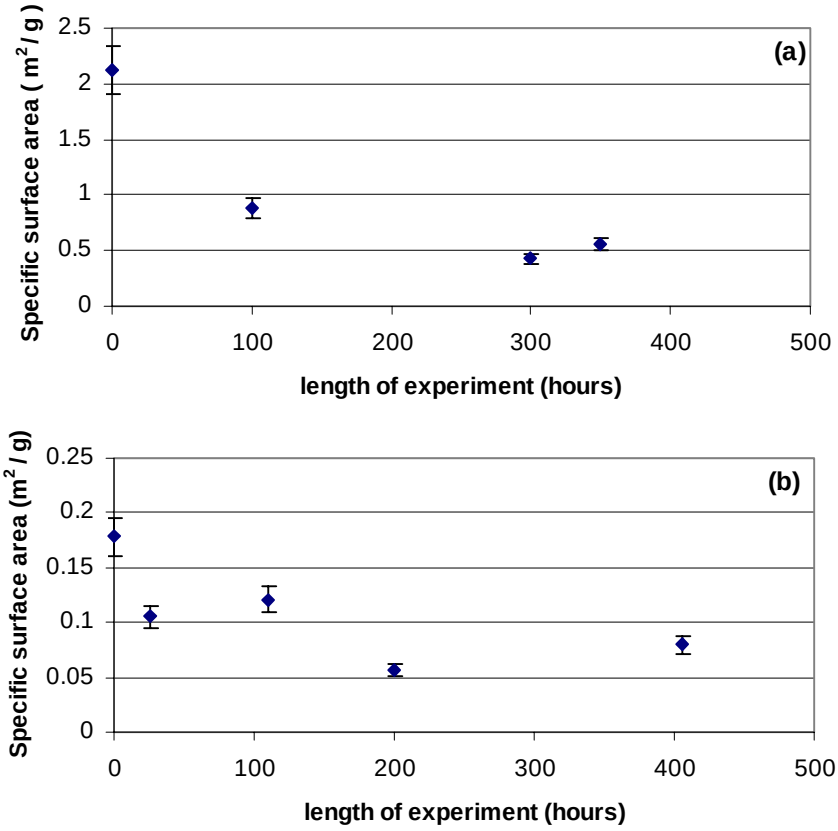

Figure 4.7 - Comparison of final specific soil surface area measurements after dissolution experiments of varying duration. t = 0 represents the initial soil surface area. Series of experiments with (a) soil from control site 1, (b) the obsidian sample. These experiments demonstrate that the decrease in surface area is associated primarily with the initial, rapid phase of dissolution.

The dissolution rates reported in the previous sections are derived from the linear portion of the dissolution data which occurs after the initial dissolution phase and, apparently, after the decrease in specific surface area. A more accurate calculation of the dissolution rates, therefore, would use the post-dissolution values rather than the initial values for specific surface area. When the dissolution rates are recalculated using the post-dissolution values, the rates increase by a factor of 1.7-5 (Table 4.4). This re-

calculation does not, however, change the pattern of relative rates shown in Fig 4.5; control site 1 still exhibits the highest dissolution rate.

To my knowledge, only two studies have reported dissolution rates that incorporate observed changes in specific surface area. In a study of albite dissolution, the final specific urface area was used to calculate dissolution rates (Burch et al., 1993). In a study of feldspar dissolution, a linear increase in specific surface area from the initial to final value with time was assumed and the specific surface area estimated for the time of sampling was used to calculate the dissolution rate (Stillings and Brantley, 1995). The observed changes in specific surface area observed in these experiments and their demonstrated effect on the calculated weathering rates provide reason to question the informal convention of normalizing all dissolution rates to initial surface area. The erroneous normalization of rates to initial values of specific surface area is a possible explanation for the well-documented poor reproducibility of rates determined in different laboratories by different researchers. In the attempt to compare the dissolution rate of obsidian determined in this study to rates of other minerals present in the soil in Table 4.3, the rate calculated using the final specific surface area is almost twice that of the rate determined by the initial value. To improve researchers' confidence in reported rates, the specific surface area of the solid material should always be measured before and after dissolution experiments, allowing for consideration of how to best calculate and report dissolution rates in each case.

4.4 Conclusions

This comparison of the laboratory determined dissolution rates of Mammoth Mountain soils does not show a distinct difference between the soils within and outside the high-CO_2 area. These experiments did not confirm the hypothesis that soil exposed to more intense weathering conditions in the field may display evidence of its weathering history by exhibiting slower weathering kinetics in controlled laboratory conditions. This method of determining soil dissolution rates, although it did not distinguish between the high-CO_2 and control soils, may be useful in understanding the kinetics of dissolution of an individual soil (as will be discussed in Chapter 5).

4.5 References

Asolekar, S.R., 1991. The Role of Chemical Weathering in the Neutralization of Acid Rain, University of Iowa, 200 pp.

Asolekar, S.R., Valentine, R.L. and Schnoor, J.L., 1991. Kinetics of Chemical Weathering in B Horizon Spodosol Fraction. Water Resources Research, 27(4): 527-532.

Bennett, P.C., 1991. Quartz dissolution in organic-rich systems. Geochimica et Cosmochimica Acta, 55: 1781-1797.

Berner, R.A. and Holdren, G.R., Jr., 1979. Mechanism of feldspar weathering - II. Observations of feldspars from soils. Geochimica et Cosmochimica Acta, 43: 1173-1186.

Blum, A.E. and Stillings, L.L., 1995. Feldspar dissolution kinetics. In: A.F. White and S.L. Brantley (Editors), Chemical Weathering Rates of Silicate Minerals. Reviews in Mineralogy. Mineralogical Society of America, Washington D.C., pp. 291-351.

Brady, P.V. and Walther, J.V., 1989. Controls on silicate dissolution rates in neutral and basic pH solutions at 25^{o}C. Geochimica et Cosmochimica Acta, 53: 2823-2830.

Brady, P.V. and Walther, J.V., 1990. Kinetics of quartz dissolution at low temperatures. Chemical Geology, 82: 253-264.

Burch, T.E., Nagy, K.L. and Lasaga, A.C., 1993. Free energy dependence of albite dissolution kinetics at 80^{o}C and pH 8.8. Chemical Geology, 105: 137-162.

Busch, R.M., 1997. Laboratory Manual in Physical Geology. Prentice Hall, Upper Saddle River, NJ, 280 pp.

Casey, W.H. and Westrich, H.R., 1991. Dissolution rates of plagioclase at pH = 2 and 3. American Mineralogist, 76: 211-217.

Casey, W.H., Westrich, H.R., Arnold, G.W. and Banfield, J.F., 1989. The surface chemistry of dissolving labradorite feldspar. Geochimica et Cosmochimica Acta, 53: 821-832.

Chen, Y. and Brantley, S.L., 1998. Diopside and anthophyllite dissolution at 25 degrees and 90 degrees C and acid pH. Chemical Geology, 147(3-4): 233-248.

Dahlgren, R., Shoji, S. and Nanzyo, M., 1993. Mineralogical Characteristics of Volcanic Ash Soils. In: S. Shoji, R. Dahlgren and M. Nanzyo (Editors), Volcanic Ash Soils, Genesis, Properties, and Utilization. Developments in Soil Science. Elsevier, Amsterdam, London, NY, Tokyo.

Etringer, M.A., 1989. The Hydrogen Ion Dependence of the Chemical Weathering Rate of a Tunbridge Series Soil from Lead Mountain, Maine at 15^{o}C. Master of Science Thesis, University of Iowa.

Frogner, P. and Schweda, P., 1998. Hornblende dissolution kinetics at 25 degrees C. Chemical Geology, 151(1-4): 169-179.

Gautier, J.M., Oelkers, E.H. and Schott, J., 2001. Are quartz dissolution rates proportional to BET surface areas? Geochimica et Cosmochimica Acta, 65(7): 1059-1070.

Gislason, S.R. and Eugster, H.P., 1987. Meteoric water-basalt interactions, I. A laboratory study. Geochimica et Cosmochimica Acta, 51: 2827-2840.

Helgeson, H.C., Murphy, W.M. and Aagaard, P., 1984. Thermodynamic and kinetic constraints on reaction rates among minerals and aqueous solutions. II. Rate constants, effective surface area, and the hydrolysis of feldspar. Geochimica et Cosmochimica Acta, 58: 2405-2432.

Hodson, M.E., Langan, S.J., Kennedy, F.M. and Bain, D.C., 1998. Variation in soil surface area in a chronosequence of soils from Glen Feshie, Scotland and its implications for minerals weathering rate calculations. Geoderma, 85: 1-18.

Kolka, R.K., Grigal, D.F. and Nater, E.A., 1996. Forest soil mineral weathering rates: use of multiple approaches. Geoderma, 73: 1-21.

Malmstrom, M. and Banwart, S., 1997. Biotite dissolution at 25^{o}C: The pH dependence of dissolution rate and stoichiometry. Geochimica et Cosmochimica Acta, 61(14): 2279-2799.

Miller, C.D., 1985. Holocene eruptions at the Inyo volcanic chain, California: Implications for possible eruptions in Long Valley caldera. Geology, 13: 14-17.

Oelkers, E.H. and Gislason, S.R., 2001. The mechanism, rates and consequences of basaltic glass dissolution: I. An experimental study of the dissolution rates of basaltic glass as a function of aqueous Al, Si, and oxalic acid concentration at 25 ^{o}C and pH = 3 and 11. Geochimica et Cosmochimica Acta, 65(21): 3671-3681.

Sampson, D.E. and Cameron, K.L., 1987. The Geochemistry of the Inyo Volcanic chain: multiple magma systems in the Long Valley Region, Eastern California. Journal of Geophysical Research, 92(B10): 10,403-10,421.

Schnoor, J.L., 1990. Kinetics of chemical weathering: A comparison of laboratory and field weathering rates. In: W. Stumm (Editor), Aquatic chemical kinetics: Reaction rates of processes in natural waters. John Wiley and Sons, New York, pp. 475-504.

Sieh, K., 2000. Personal Communication. Professor of Geology, California Institute of Technology, Pasadena, CA.

Stephens, J.C. and Hering, J.G., 2002. Comparative Characterization of Volcanic Ash Soils Exposed to Decade-Long Elevated Carbon Dioxide Concentrations at Mammoth Mountain, California. Chemical Geology, 186(3-4): 289-301.

Stillings, L.L., Drever, J.I., Brantley, S.L., Sun, Y. and Oxburgh, R., 1996. Rates of feldspar dissolution at pH 3-7 with 0-8 oxalic acid. Chemical Geology, 1322: 79-89.

Stillings, L.S. and Brantley, S.L., 1995. Feldspar dissolution at 25^{o}C and pH 3: Reaction stoichiometry and the effect of cations. Geochimica et Cosmochimica Acta, 59(8): 1483-1496.

Stumm, W. and Morgan, J.J., 1996. Aquatic Chemistry, Chemical Equilibria and Rates of Natural Waters. John Wiley & Sons, Inc., New York, 1022 pp.

U.S.G.S., 2002. Eruptions from the Inyo Chain about 600 years ago: sequence of events and effects in the Long Valley Caldera. USGS Volcano Hazards Program.

van der Salm, C., Verstraten, J.M. and Tiktak, A., 1996. The influence of percolation rate on the weathering rates of silicates in an E horizon of an Umbric Albaqualf. Geoderma, 73: 83-106.

van Grinsven, H.J.M., van Riemsdijk, W.H., Otjes, R. and Breemen, N.v., 1992. Rates of aluminum dissolution in acid sandy soils observed in column experiments. Journal of Environmental Quality, 21: 439-447.

Velbel, M., 1990. Influence of temperature and mineral surface characteristics on feldspar weathering rates in natural and artificial systems: A first approximation. Water Resources Research, 26(12): 3049-3053.

Chapter 5

FACTORS AFFECTING THE DISSOLUTION KINETICS OF VOLCANIC ASH SOILS: DEPENDENCIES ON pH, CO_2, AND OXALATE

5.1 Introduction

Quantifying the rates of mineral weathering and identifying factors that may affect them are important for understanding both watershed-scale and global-scale processes. Rates of cation release from mineral dissolution affect nutrient availability in soils, the capacity of soils to buffer acid deposition, and the composition of the soil-, ground- and surface waters within a watershed. On the global scale, rates of mineral weathering determine cation fluxes to rivers and oceans (Gaillardet et al., 1999; Lasaga et al., 1994), and weathering is the primary sink for atmospheric CO_2 over geological time (Berner, 1995).

Laboratory studies on isolated minerals have shown that dissolution rates are influenced by pH (Amrhein and Suarez, 1992; Blum and Lasaga, 1988; Brady and Walther, 1989; Casey and Westrich, 1991; Malmstrom and Banwart, 1997). Dissolution rates are generally pH-independent in the near-neutral pH range and increase both in the acid range with decreasing pH and in the alkaline range with increasing pH (Blum and Lasaga, 1988; Blum and Stillings, 1995). For mineral dissolution kinetics that are surface controlled (i.e., for which chemical reactions at the mineral-water interface determine the dissolution rates) (Stumm and Morgan, 1996), this pH dependence is attributed to the protonation or deprotonation of surface hydroxyl groups, which enhances dissolution by

facilitating polarization, weakening and breaking of the metal-oxygen bonds of the crystal lattice.

Solution composition can also influence (net) dissolution rates (Devidal et al., 1997; Kraemer and Hering, 1997; Murakami et al., 1998; Oelkers and Gislason, 2001; Oelkers and Schott, 1998) by determining the solution saturation state and hence the thermodynamic driving force for (net) dissolution. The acceleration of mineral dissolution by some low molecular weight organic acids (Drever and Stillings, 1997; Drever and Vance, 1994; Fox and Comerford, 1990; Gwiazda and Broecker, 1994) has been attributed primarily to the formation of complexes between organic acids and metal centers at the mineral surface which facilitates detachment of the metal center. Studies using ligands like oxalate suggest that high concentrations of organic acids (>1 mM) can increase dissolution rates of aluminosilicate minerals by a factor of 2 to 3 (Welch and Ullman, 1993).

Enhancement of dissolution rate by CO_2 has also been reported (Lagache, 1965; Sverdrup, 1990). Clearly, increased soil CO_2 could influence dissolution rates indirectly by decreasing pH. A direct role for CO_2 in mineral weathering has been proposed but is still controversial. Weathering rates measured at high temperature (100-200 ^{o}C) and high P_{CO_2} (2-20 bar) have been shown to be proportional to $P_{CO_2}^{0.3}$ (Lagache, 1965). The observed fractional dependence on P_{CO_2} has been attributed either to adsorption of CO_2 (Sverdrup, 1990) or simply to a pH effect (since the initial pH of the experiments with CO_2 was lower) (Brady, 1991; Helgeson et al., 1984). Despite this uncertainty, this relationship has been assumed to hold for CO_2 values typical of soil environments in

several geochemical models (Marshall et al., 1988; Sverdrup and Warfvinge, 1993; Volk, 1987). Several studies attempting to verify this relationship have shown that, at low pH, weathering is not directly affected by CO_2 concentration (Brady and Carroll, 1994; Grandstaff, 1977; Wogelius and Walther, 1991), whereas both decreases (Wogelius and Walther, 1991) and increases (Berg and Banwart, 2000; Bruno et al., 1992; Osthols and Malmstrom, 1995) in dissolution rates have been observed with increased CO_2 at alkaline pH, in addition to observations of no effect (Knauss et al., 1993; Malmstrom et al., 1996).

A schematic representation of the effects pH, CO_2 and organic acids on dissolution rates reported in the literature from experiments on isolated minerals is shown in Figure 5.1, which includes an approximate pH range for each effect. The organic acid dependence has been shown to predominate at moderately acidic to near-neutral pH ranges where proton-promoted dissolution is minimal (Welch and Ullman, 1993). The CO_2 dependence associated with the carbonate ion (Berg and Banwart, 2000) is relevant only in the basic pH range, while the proposed dependence on CO_2 reported by Lagache (1965) is pH independent.

Laboratory dissolution studies on isolated pure minerals or synthesized solid phases are the primary basis of the current understanding of weathering kinetics. Extrapolation from specific minerals to whole soils is complicated by the different responses of various mineral phases to the factors affecting weathering rates. Studies on how factors such as pH, CO_2 and organic acids affect the dissolution rates of whole soils could help to bridge this gap.

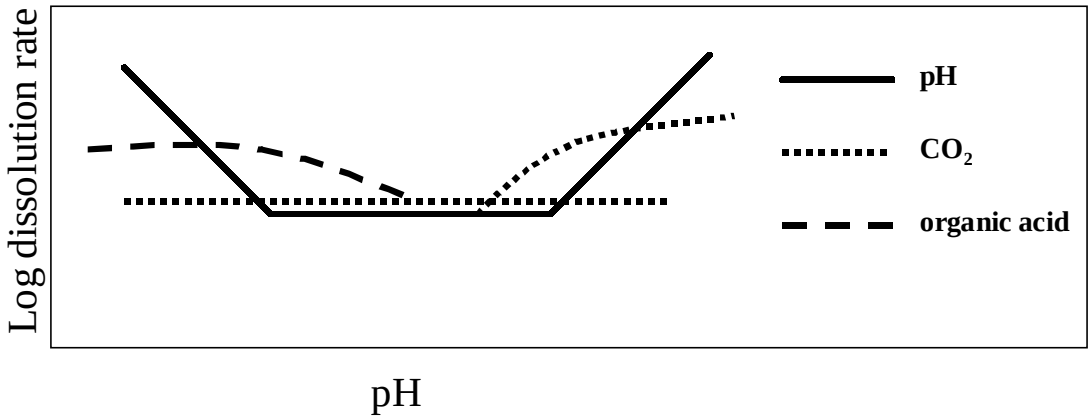

Figure 5.1 – Schematic representation of the pH ranges of possible pH, CO_2 and organic acid dependencies on dissolution rate. The straight line for CO_2 represents the proposed dependence of Lagache (1965) which is independent of pH (the placement of this line with respect to the others is arbitrary). The curved line for CO_2 represents the carbonate dependence proposed by Berg and Banwart (2000).

The relative importance of pH, CO_2 and LMW organic acids in determining rates of mineral dissolution is of particular interest in understanding the weathering of volcanic ash soils of Mammoth Mountain. In the last decade, several distinct areas on the flanks of Mammoth have been exposed to decreased pH, increased soil CO_2 and altered organic acid compositions compared to the typical soils on the mountain (as discussed in Chapter 3). This chapter reports on laboratory dissolution experiments designed to assess the effects of each of these three factors, pH, CO_2 and LMW organic acids, on the dissolution rate of the volcanic ash soils from Mammoth Mountain.

5.2 Materials and Methods

A single soil sample, collected from control site 3, a healthy forested site outside the Horseshoe Lake high-CO_2 area, was used in all experiments discussed in this chapter

(details of sampling location are discussed in Chapter 3). The soil was dried, sieved, washed and characterized as described in Chapter 4.

Two different experimental approaches were used to determine soil dissolution rates in the laboratory. The dependence of dissolution rates on pH and CO_2 was examined using the pH-stat reactor described in Chapter 4. The rate dependence on oxalate, chosen as a proxy for the general effect of LMW organic acids, was assessed using a continuously stirred flow-through reactor. In all experiments, weathering rates were calculated based on the steady-state release of Si and Al. Release of Si is generally considered to be the best tracer for aluminosilicate dissolution (Schnoor, 1990). However, in dissolution experiments of soils with their complex mixture of different Si and Al phases, the release of Al provides additional kinetic information on the dissolution of the Al phases. In the pH-stat batch experiments, weathering rates were also calculated based on H^+ consumption (μequivalents of H^+ / m^2 hr). All experiments were conducted at the ambient temperature of the laboratory (22 ± 1^oC).

5.2.1 pH-stat Batch Experiments

Batch experiments were conducted in a pH-stat system with 2 g of soil in 200 ml of water in a polypropylene beaker at pH 2.78, 3.5 and 4.0 and ambient (uncontrolled) CO_2. Experiments at pH 2.78 and 4.0 were repeated with pure CO_2 gas bubbling through the reactor so that the solutions were in equilibrium with a P_{CO_2} of 1 atm. Before being introduced into the reaction vessels the CO_2 gas was bubbled through two consecutive

vessels of water to saturate the gas. Further experimental details are provided in Chapter 4.

5.2.2 Flow-through Experiments

The flow-through experiments were conducted in continuously stirred polymethylmethcrylate reactors with a volume of approximately 50 ml (diameter and hight of vessels were ~3.75 cm and 4 cm respectively). Exact volumes for each reactor were determined gravimetrically. One gram of soil within each reactor was kept suspended by a magnetic stir plate and a teflon coated stirbar (SpinRing®) stirring at a rate greater than 100 revolutions/min elevated on four Teflon legs to minimize contact with the surface of the reactor. The effluent passed through a 0.025 μm mixed cellulose acetate and nitrate membrane Millipore filter mounted on a 47 mm polypropylene filter holder, which capped the reactors. A peristaltic pump was used to adjust the flow rate, which varied from 0.02 – 0.4 ml/min. The pumps were set at the relatively fast rate of 0.4 ml/min at the beginning of each experiment to minimize the length of time of the rapid initial dissolution stage; as the release of Al and Si stabilized the flow rate was reduced to 0.02 ml/min, where it was held constant during the later part of the experiment when steady-state dissolution rates were measured. To retard microbial growth, 1 milliliter of chloroform was added to each liter of inlet solution. The influent solutions, with an ionic strength of 0.01 M ($NaClO_4$), contained either 0 or 1 mM oxalate and were adjusted to either pH 4 or pH 5.

In the experiments without oxalate, the measured effluent pH was slightly (but not more than 0.2 pH units) higher than the influent pH. In the experiments with oxalate, the effluent pH increased considerably in the initial dissolution phase (an initial maximum pH of 4.7 and pH 6.1 for the pH 4 and pH 5 influent, respectively), but by the time steady state was reached the effluent pH had stabilized at 0.2 pH units above the influent pH.

Effluent was collected and measured for Si and Al using ICPMS. The net dissolution rate, R_{net} [μmol/m^2 hr], in the reactor is determined as:

$$R_{net} = \frac{1}{S \cdot A} * \frac{d[M]_{diss}}{dt} = \frac{1}{A} * [M]_{out} * \frac{q}{v}, \qquad (1)$$

where S is the solids concentration (g/l), A is the specific surface area of the solid (m^2/g), $[M]_{out}$ is dissolved concentrations of Si or Al in the effluent (mol/l), q is the flow rate (ml/hr) and V is the reactor volume (ml). Steady state dissolution rates were calculated from the Si and Al concentrations in the effluent once constant concentrations were measured in at least three consecutive samples (over 50 hours).

5.2.3 Oxalate Adsorption Methods

Batch adsorption experiments were conducted with oxalate concentrations of 1 mM prepared from reagent grade oxalic acid. Each solution was adjusted to pH 4 using concentrated reagent grade HCl and NaOH. Following the procedure of Stillings et al. (1998), each pH-adjusted aliquot was split; some was retained to measure the initial oxalate concentration while the rest was used in the adsorption experiments. The

experiments were conducted mixing 200 or 100 mg of the cleaned 63-125 μm soil size fraction and 10ml of pH-adjusted oxalate solution in centrifuge tubes rotating in an end-over shaker for 4 hours. The pH was checked and adjusted if necessary three times during the experiment: right after the soil was introduced to the solution, after 2 hours and after 4 hours. At each check the pH had drifted upward slightly to a maximum of pH 4.7. After 4 hours of mixing, the samples were filtered through a 0.02 μm aluminum oxide membrane filter[1] and then half of the sample was acidified for ICPMS analysis while the other half was analyzed for total oxalate by ion chromatography (IC). The IC method used was isocratic with an eluent composition of 5 mM NaOH. The concentration of oxalate adsorbed to the surface was calculated as:

$$Ox_{ads} = \frac{(Ox_i - Ox_f) \cdot V}{S \cdot A}, \qquad (2)$$

where Ox_{ads} is the total oxalate adsorbed to the soil surface (μmol/m^2), Ox_i and Ox_f are the pre- and post-reaction concentrations of total oxalate in solution (mM), S is the mass of the solid (g), and A is the specific surface area of the soil (m^2/g). During the 4 hours of shaking allowed for oxalate to adsorb, some Al dissolved into solution. Speciation calculations using MINEQL$^+$4.0 (Schecher and McAvoy, 1992) with the measured Al

[1] A discussion on this sub-optimal choice of filter can be found in Chapter 4. Control experiments conducted in the pH-stat batch experiments showed that the Al concentrations measured in solutions filtered through this aluminum oxide filter were the same as the concentration in solution filtered through a cellulose acetate filter (Appendix B, Fig. B.1). Although control experiments were not conducted under the specific conditions of the oxalate adsorption studies, the assumption that these filters did not influence the subsequent measurement of Al is made based on the similarity of conditions of the control experiments discussed in Chapter 4.

concentrations and the total oxalate concentrations, showed that the concentrations of free oxalate ($C_2O_4^{2-}$) and bioxalate ($HC_2O_4^-$) available for adsorption were far lower than the total concentrations in solution because oxalate forms strong aqueous complexes with Al.

5.3 Results and Discussion

5.3.1 Decrease in specific surface area

As discussed in Chapter 4, in all batch experiments the specific surface area measured after the dissolution experiment was 40-80% less than that measured initially (Table 4.4). Comparison of the final values from several experiments of varying duration shows that the observed decrease in specific surface area occurs primarily in the initial 100 or so hours (Fig. 4.7). This corresponds to the nonlinear phase of dissolution, which suggests that this decrease is associated with the rapid initial dissolution of fine particles or mineral coatings. The magnitude of the decrease in specific surface area was the same in the experiments conducted at pH 2.78, 3.5 and 4.0, even though the extent of initial dissolution varies at the different pH values (Table 5.1).

Table 5.1
Decrease in specific surface area (A) during the experiments and extent of initial dissolution

pH	A (m^2/g)		% Decrease	Extent of Initial Dissolution[a]
	initial	final	in A	μeq of H^+/m^2
2.78	2.88	1.39	51.7	217.0
2.78	2.88	1.00	65.2	303.5
3.5	2.88	1.08	62.5	153.8
4	2.88	1.11	61.6	69.9

[a] This value represents the amount of H^+ consumed at the point of transition from the initial nonlinear phase of dissolution to the linear steady-state phase

Since the dissolution rates are derived from the period of steady-state dissolution that follows the period of initial rapid dissolution, all dissolution rates reported in this chapter have been normalized to the post-dissolution measurements of specific surface area.

The final specific surface area of the soil from the flow-through experiments could not be reliably determined because finely ground particles of Teflon were produced by the abrasion of the stir-bar. The final value for specific surface area of the material taken from the flow-through reactors was the same or slightly higher than the initial value, reflecting the contribution of both Teflon particles and the soil. In the absence of reliable post-dissolution measurements of the soil from the flow-through reactors, post-dissolution values of specific surface area from the batch reactors (obtained at pH 4.0) were used to calculate dissolution rates for the flow-through experiments.

5.3.2 pH dependence

Dissolution rates of the Mammoth Mountain soil derived from the H^+ and Si data increase with decreasing pH in the pH range from 2.78 to 4.0, although rates derived from the Al release data do not show a pH dependence (Fig 5.2). The pH dependence in the H^+ and Si derived rates, and the lack of a pH dependence in the Al derived rates, is demonstrated more clearly in Figure 5.3, where the log of the rates is plotted against pH. As discussed in Chapter 4, weathering rates calculated from Al release data in replicate experiments are not reproducible. This inconsistency is likely caused by variation in quantities of some active Al phases within sub-samples of a given sample. This variability in Al release may explain the lack of a pH dependence of the Al rates.

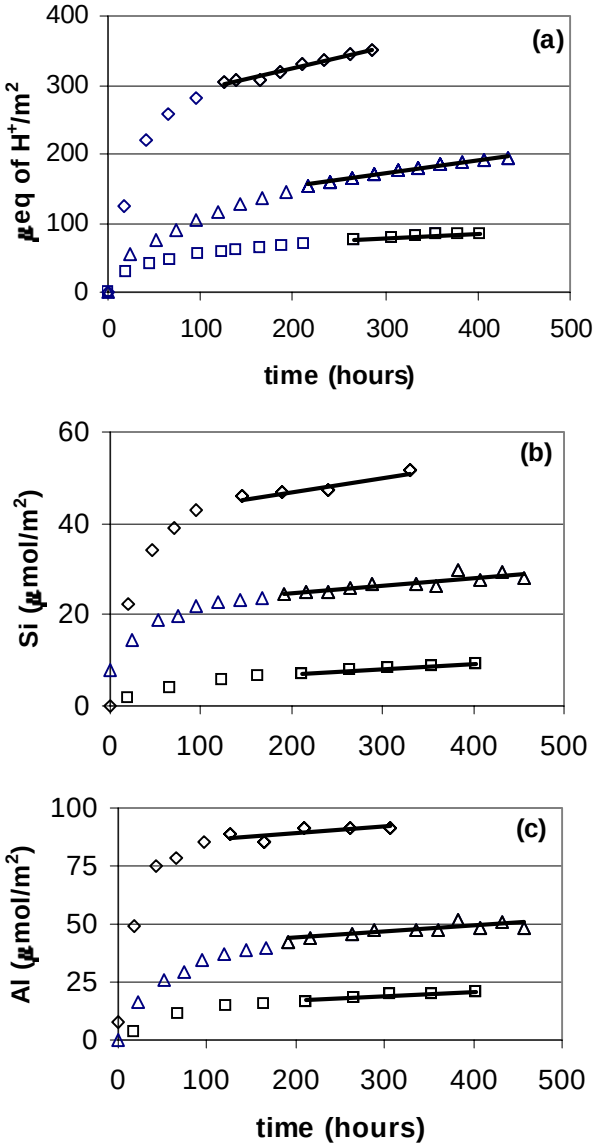

Figure 5.2 - pH dependence on soil dissolution rates derived from the pH-stat batch reactor experiments. (a) µequivalent of H^+ consumed per m^2 over time, (b) µmole of Si released per m^2 over time, and (c) µmole of Al released per m^2 over time. ◊ = pH 2.78, Δ = pH 3.5, and □ = pH 4.0. Dissolution rate is calculated as the slope of the linear portion of the data.

In all data sets, at each pH value, an initial nonlinear phase of dissolution is observed; the extent of the rapid initial dissolution decreases with increasing pH. The steady state dissolution rates calculated from the subsequent linear increase of both H^+ consumption and Si release with time exhibit fractional order hydrogen ion dependence of 0.50 (Fig. 5.3a) and 0.35 (Fig. 5.3b) respectively. The discrepancy between these values suggests that overall cation release (corresponding to H^+ consumption as discussed in section 4.3.2) of these soils has a greater dependence on pH than Si release. For a pure mineral, such difference between the cation and Si release rates indicates incongruent dissolution. However, for a soil composed of various minerals, including some phases such as aluminum and iron oxides that do not contain Si, the different dependencies on pH may simply reflect the variability of pH dependence among different minerals.

Many previous laboratory studies conducted with pure minerals (or, in limited studies, with whole soils) have demonstrated that the hydrogen ion dependence of dissolution is fractional order, where rate α $[H^+]^n$ (Etringer, 1989; Grandstaff, 1977; Malmstrom and Banwart, 1997; Pokrovsky and Schott, 2000; Wollast, 1967). A partial list of n values reported in the literature for whole soils or minerals relevant to Mammoth Mountain soils is presented in Table 5.2. Compared with some of the previously reported values of n, which range from 0.19 for diopside (Chen and Brantley, 1998) to 0.98 for anorthite (Sverdrup, 1990), the value of 0.27 derived from the Si data is low. The value of 0.47 from the H^+ data is similar to the value generally reported for feldspars, and both values are lower than the other value reported for whole soils. Thus, the dissolution rates of Mammoth Mountain soil are less strongly influenced by pH than those of Lead

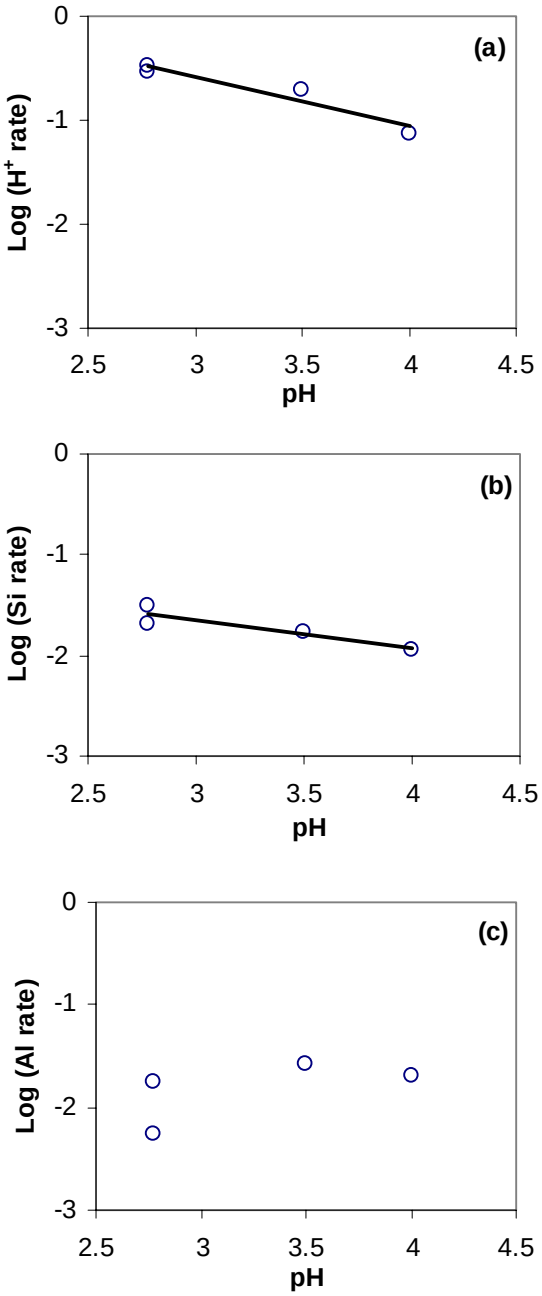

Figure 5.3 – The log of soil dissolution rates from batch pH-stat reactors derived from data on (a) H^+ consumption, (b) Si release, and (c) Al release, plotted against pH. Duplicate experiments were conducted at pH 2.78. The rate dependence on pH is evident in the H^+ and Si data and absent in the Al rates (which exhibit poor reproducibility). The slopes 0.47 and 0.27, for the H^+ and Si data respectively, give the fractional order hydrogen ion dependence of the dissolution rate.

Table 5.2
Selection of dissolution rate fractional order hydrogen ion dependences of soils and minerals reported in the literature

	Soil or Mineral	ZPC[a]	pH range	Temp (^{o}C)	Basis for rates	n	Reference
Soils	Mammoth Mountain Soil, CA	-	2.78 - 4.0	22	H^{+} consumption	0.47	this study
	Mammoth Mountain Soil, CA	-	2.78 - 4.0	22	Si release	0.27	this study
	Lead Mountain Soil, ME	-	2.7 - 4.0	15	H^{+} consumption	0.85	Asolekar et al, 1991
Minerals	K-feldspar	2-2.4	< 6	22-25	various[b]	~0.5	Blum & Stillings, 1995
	plagiocalse feldspars	2-2.4	< 5	25	various[b]	~0.5	Blum & Stillings, 1995
	quartz	2	<3	NA[c]	Si release	0.3	Sverdrup, 1990[d]
	quartz	2	< 7	25	Si release	0	Brady & Walther, 1989
	aluminum oxide	9.1	2.5 - 6	NA	Al release	0.3	Furrer & Stumm, 1983
	iron hydroxide	8.5	NA	NA	Fe release	0.48	Stumm et al., 1985
	hornblende	-	3 - 4	25	Si release	0.47	Frogner & Schweda, 1998

[a] Zero point of charge = pH at which net surface charge is zero (values compiled by Stumm, 1992)

[b] Rates derived from different parameters generally agree

[c] NA = information not available

[d] Not original source. In a review of quartz dissolution literature Sverdrup mentions this value but omits source

Mountain soil or some isolated minerals.

5.3.3 Lack of dependence on CO_2

The dissolution rates determined at pH 4.0 were nearly identical under both ambient and elevated (1 atm) P_{CO_2} (Table 5.3). At pH 2.78, the dissolution rates were slightly higher at 1 atm P_{CO_2} but still within experimental error of those at ambient conditions. These results with actual soil are consistent with previous reports showing no direct effect on dissolution rates of pure minerals under acidic conditions (Brady and Carroll, 1994; Grandstaff, 1977; Knauss et al., 1993), contradicting the proposed dependence on CO_2 reported by Lagache (1965). It can be inferred from these experiments, therefore, that the high soil CO_2 concentrations at Mammoth Mountain are not directly affecting the soil weathering.

5.3.4.1 Dependence on oxalate

The influence of low-molecular-weight (LMW) organic acids on soil dissolution rates was examined using oxalate as a proxy for the various LMW organic acids found in these soils (discussed in Chapter 3). Oxalic acid is commonly found in soils associated with forest litter, roots and fungi (Drever and Vance, 1994), and its effects have been widely studied in mineral dissolution experiments. The presence of 1 mM oxalate increased the rate of both Si and Al release in these soils during the period of rapid initial dissolution (Fig. 5.4) and once steady-state rates were achieved (Fig. 5.5). Without

Table 5.3

Lack of effect of CO_2 on Si disolution rates (μmole Si / m^2 hr) at constant acidic pH

Soil or Mineral	pH	T (^oC)	R_{CO2} [a]	R_{amb} [b]	R_{CO2} / R_{amb}	Reference
Mammoth Mountain soil, CA	2.78	22	0.04	0.03	1.3	this study[c]
Mammoth Mountain soil, CA	4	22	0.01	0.009	1.1	this study[c]
anorthite, augite	4	21	NA[d]	NA	~1	Brady & Carroll, 1994
bronzite	2.3 - 2.5	22	10^{-7}	10^{-7}	~1	Grandstaff, 1977

[a] Dissolution rate in presence of 1 atm CO_2

[b] Dissolution rate at ambient CO_2

[c] Error associated with this method of determining rates estimated to be 20% based on the standard deviation of triplicate experiments

[d] NA = information not available

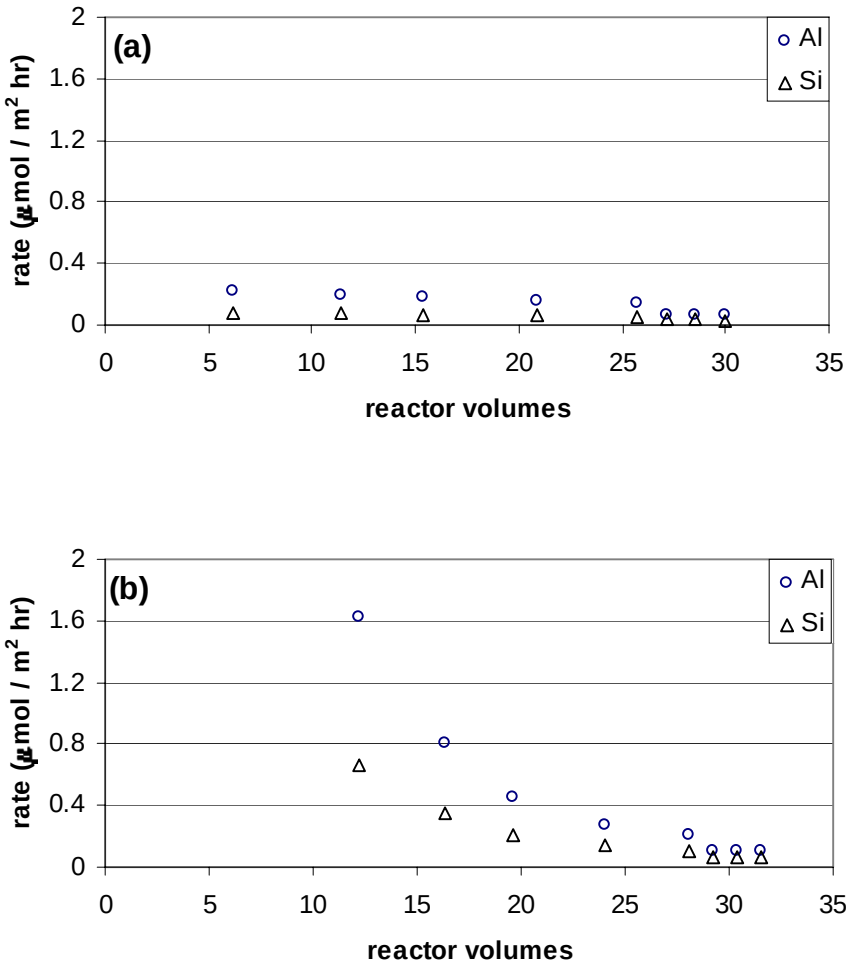

Figure 5.4 – Soil dissolution rates calculated from the flow-through reactors at pH 4 derived from the Al (o) and Si (Δ) data, (a) no oxalate, (b) 1 mM oxalate. The rates are plotted against reactor volumes rather than time, because the flow rate varied throughout the experiment as discussed in Section 5.2.2.

oxalate (Fig. 5.4a) the initial rates are only slightly faster than the steady-state rates, whereas in the presence of oxalate (Fig. 5.4b) the initial rates are an order of magnitude higher than the steady-state rates.

At both pH 4 and 5, higher steady-state dissolution rates were measured in the reactors with oxalate, however the degree of oxalate-enhanced dissolution is different for

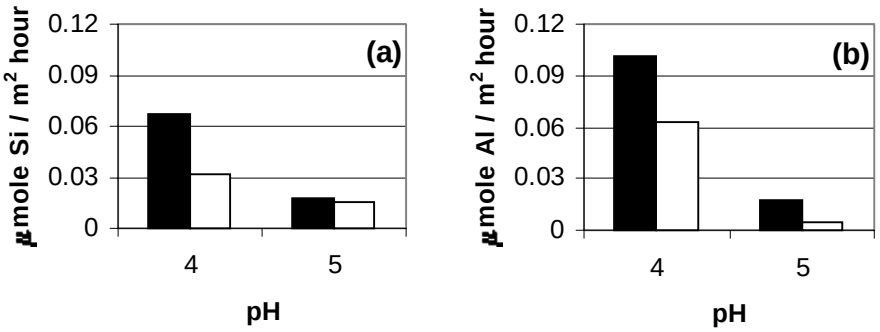

Figure 5.5 - Comparison of soil dissolution rates with 1 mM oxalate (solid) and without oxalate (open) at pH 4 and 5 in the flow-through reactors. Rates derived from the steady-state release of (a) Si and (b) Al.

Si and Al (Fig. 5.5). At pH 4, oxalate increased both the Si and Al release rates by about a factor of 2. At pH 5, the Si rate was slightly increased by oxalate while the Al rate was increased by about fourfold. The greater enhancement of Al release by oxalate at pH 5 than pH 4 is consistent with previous observations that ligand-enhanced dissolution is greatest in the pH range of 5-7.5 as proton-promoted dissolution becomes less important (Bennett and Casey, 1994; Welch and Ullman, 1993). The smaller effect of oxalate on Si release rates at pH 5 than at pH 4 was not, therefore, expected, but may be related to the differences in the mechanism by which oxalate promotes the release of Si and Al.

Oxalate forms stronger complexes in solution with Al (Mast and Drever, 1987), than with Si (Pokrovski and Schott, 1998; Poulson et al., 1997); comparable affinities are expected for Al and Si centers on mineral surfaces. Thus, oxalate enhances the dissolution of aluminosilicate minerals primarily by promoting detachment of Al centers. If the release of the Al destabilizes Si-O bonds sufficiently that Si is released stoichiometrically, congruent dissolution will be observed. Otherwise, dissolution will be

incongruent. In the presence of oxalate, both congruent (Blake and Walter, 1999; Mast and Drever, 1987) and incongruent (Huang and Kiang, 1972; Stillings et al., 1996; Welch and Ullman, 1993) dissolution of aluminosilicates has been reported in the literature; in cases of incongruent dissolution, Al was released preferentially to Si.

In whole soils, Al and Si released into solution may also derive from different phases. In addition to the numerous studies observing oxalate-enhanced dissolution of feldspars (Amrhein and Suarez, 1988; Blake and Walter, 1999; Manley and Evans, 1986; Mast and Drever, 1987; Stillings et al., 1996; Welch and Ullman, 1993), oxalate has also been shown to promote the dissolution of aluminum oxides (Axe and Persson, 2001; Fish and Kumar, 1994; Stumm and Furrer, 1987; Stumm et al., 1985) and quartz (Bennett, 1991; Poulson et al., 1997). The discrepancy between the rates of Al and Si release in whole soils may reflect the mixture of soil minerals undergoing dissolution.

5.3.4.2 Surface Concentration of Oxalate

The primary mechanism proposed for oxalate-enhanced dissolution is adsorption (Stillings et al., 1998); oxalate complexes with the structural cations at the mineral surface weakening bonds and facilitating bond breakage. The degree of oxalate-enhanced dissolution, therefore, is proportional to the amount of oxalate species sorbed at the surface (Schnoor, 1990). The oxalate-enhanced dissolution of these soils was observed at a single oxalate concentration, 1 mM. To aid in the interpretation of the observed oxalate-enhanced dissolution, a simple oxalate adsorption study was conducted to determine whether the concentration of oxalate on the soil surface during the

Table 5.4
Determination of surface oxalate concentration of soil at pH 4 and 1 mM oxalate

Soil (mg)	Al_{diss} (μM)[a]	Ox_{free} (μM)[b]	Ox_{tot} (μM)	Ox_{diss} (μM)	Ox_{ads} (μmol/m^2)[cd]
100	248	372	992	983	0.315
200	306	254.2	992	974	0.317
200	364	154.7	992	976	0.277

[a] Measured in solution by ICPMS after 4-hour adsorption equilibration time

[b] Bioxalate + oxalate = actual oxalate available to adsorb to surface, calculated by MINEQL using measured Al and total oxalate concentrations

[c] $Ox_{ads} = ((Ox_{tot}-Ox_{dis})*Volume) / (mass * A)$

[d] A = 2.88 m^2/g and volume is .01 L

dissolution experiments had reached a maximum. Table 5.4 shows that under the conditions of the dissolution experiments, pH 4 with 1 mM oxalate, the soil surface appears to be saturated with respect to oxalate at about 0.3 μmole of oxalate per m^2 of soil. Although the total oxalate concentration is the same in all three adsorption experiments, the free oxalate (the sum of the concentrations of $C_2O_4^{2-}$ and $HC_2O_4^-$ calculated in MINEQL) available to adsorb to the surface (i.e., not bound to the Al in solution) varies in each experiment based on how much Al dissolved during the 4 hour equilibration time. Ox_{ads} does not vary with Ox_{free}, suggesting that a surface maximum concentration has been reached under these conditions. If adsorption is assumed to be the primary mechanism for oxalate-enhanced dissolution, this apparent maximum surface concentration suggests that an increasing oxalate concentration above 1 mM in the dissolution experiments would not result in further enhancement of dissolution.

Another proposed mechanism for oxalate-enhanced dissolution involves the stabilization of dissolved metals increasing the thermodynamic driving force for the

dissolution reaction (Oelkers et al., 1994; Stillings et al., 1998). If this mechanism is operative, increases in oxalate beyond the concentration necessary to saturate the surface would result in further enhancement of dissolution.

The calculated surface concentration (0.3 μmole/m^2) is low compared to the reported surface concentration (5 μmole/m^2) of oxalate on a plagioclase feldspar under the same conditions, pH 4 and 1 mM oxalate (Stillings et al., 1998). Although dissolution experiments under the same conditions were not reported in that study of oxalate adsorption on feldspar, the same researcher reported that 1 mM oxalate increased feldspar dissolution rates by a factor of 2-5 at pH 3 and by a factor of 2-15 at pH 5-6 (Stillings et al., 1996). Although the surface oxalate concentration is lower, the enhancement of soil dissolution rates by oxalate in this study is roughly comparable to these reported values.

Bulk soil concentrations of oxalate measured in extracts from the Mammoth Mountain soils are 4-6 μmol/g soil (Stephens and Hering, 2002) or 0.8-1.2 μmole/m^2 (assuming a specific surface area of 5.0 m^2/g for whole soil discussed in Chapter 3). These measurements represent oxalate concentrations on the surface of the dry soil, not the total concentration in the soil and soil solution. The maximum surface concentration in the adsorption experiment (0.3 μmole/m^2) is the same order of magnitude as the oxalate concentrations measured from soil extracts (0.8-1.2 μmole/m^2).

5.3.5 Comparison of Rates in Batch and Flow-through Reactors

The dissolution rates derived from the flow-through reactors in this study are ~3 times faster than the rates determined from the pH-stat batch reactors for experiments conducted at the same pH (pH 4) without oxalate (Table 5.5). Dissolution rates reported for soils from Lead Mountain, Maine, also show a discrepancy among rates derived from different experimental set-ups; rates derived from soil column and fluidized bed reactors are an order of magnitude faster than rates derived from batch experiments, even though the pH in the fluidized bed experiments was higher.

Accumulation of solutes and the subsequent precipitation of secondary minerals is a well recognized, likely explanation for the observation of slower rates in batch experiments than in flow-through reactors. In batch reactors, as soils dissolve, solutes accumulate and their concentrations can come close to or exceed the solubility of secondary phases. To test the effect of accumulated solutes on weathering rates in the batch experiments, two steps were taken (discussed in more detail in Chapter 4): (1) dissolution rates before and after a sample was re-suspended in fresh solution were compared, and (2) solubility calculations for three likely secondary minerals, kaolinite, gibbsite and amorphous SiO_2, were performed. In the experimental approach, the same steady-state dissolution rates derived from all three data-sets, H^+, Si and Al, were observed after the solution change (Fig. 5.6), indicating that the solutes accumulated in the initial dissolution period did not affect the observed rates.

Table 5.5
Comparison of soil dissolution rates of this study and rates reported in the literature

Soil	Reactor type	pH	Oxalate (mM)	Rate (μmol Si / m^2 hr)[a]	Reference
Mammoth Mountain,CA	flow-through	4	0	0.032	this study
	flow-through	4	1	0.067	this study
	batch	4	0	0.009	this study
Lead Mountain, ME	soil column	3	0	0.0216	Schnoor , 1990
	fluidized bed	4	0	0.011	Swoboda-Colberg & Drever, 1993
	batch	3	0	0.003	Asolekar, 1991

[a] Although rates from literature are reported in mole Si/m^2/s, for ease of comparison all rates have been converted toμmol Si / m^2 hr.

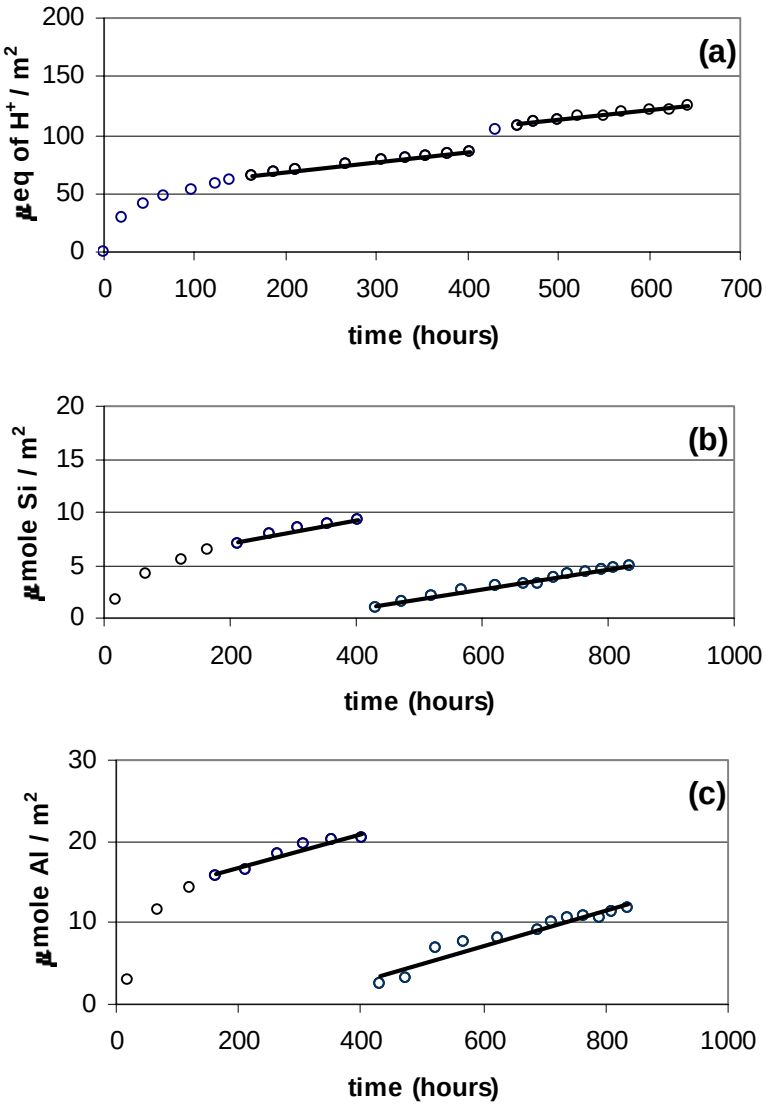

Figure 5.6 – No apparent change in dissolution rates was observed before and after fresh solution was added to soil suspension in the batch reactor at pH 4 (without oxalate). (a) H^+ consumption data, initial rate is 0.085 and subsequent rate is 0.084 µeq/m^2 hr, (b) Si release data, initial rate is 0.011 and subsequent rate is 0.010 µmol/m^2 hr, and (c) Al release data, initial rate is 0.021 and subsequent rate is 0.021 µmol/m^2 hr.

To determine whether precipitation of kaolinite, gibbsite or amorphous SiO_2 was favorable, the ion activity product (Q) calculated from the maximum measured concentrations of accumulated Si and Al in the filtered solution were compared with the reported values of the solubility equilibrium constants, K_{sp}, for these phases at 25°C. Assuming that the measured cations (Al, Ca, Mg, and Fe) and the sulfate added as acid are the primary contributors to ionic strength, an ionic strength of 0.004 and 0.002 were calculated for experiments at pH 3.5 and 4.0 respectively. The Davies equation was used in the calculations to convert concentrations into activities. Saturation quotients (Q/K_{sp}) were evaluated for kaolinite:

$$Al_2Si_2O_5(OH)_{4(s)} + 6H^+ = 2Al^{3+} + 2H_4SiO_4 + H_2O, \quad (3)$$

with $K_{sp} = 2.72 \times 10^7$ (Stumm and Morgan, 1996), for gibbsite:

$$Al(OH)_{3(s)} + 3H^+ = Al^{3+} + 3H_2O \ , \quad (4)$$

with $K_{sp} = 1.28 \times 10^8$ (Stumm and Morgan, 1996), and for amorphous SiO_2:

$$SiO_2 + 2H_2O = Si(OH)_4^0 \ , \quad (5)$$

with K_{sp} = 1.95 x 10-3 (Stumm and Morgan, 1996). Concentrations in the batch reactors were 200-500 μM Al and 35-300 μM Si. The solubility calculations based on these measured accumulated concentrations of Si and Al indicate that, at pH 3.5 and pH 4.0, solutions were at or within one-half log unit of saturation with respect to kaolinite and gibbsite, and around one log unit away from saturation with respect to amorphous SiO_2. At the low pH of 2.78, as discussed in Chapter 4, the solute concentrations were far from saturation with respect to kaolinite and gibbsite (by 3-5 log units). The solubility of amorphous SiO_2 is pH-independent in the acidic pH range. The experimental observation that an ion activity product in a soil solution is larger than or close to the corresponding solubility product constant is not prima facie evidence of precipitation (Sposito, 1984). However, having solute concentrations close to or exceeding saturation does reduce the confidence in observed dissolution rates. Despite these solubility calculations, the experimental test demonstrates that accumulated solutes are not affecting dissolution rates in the batch reactor.

Another possible explanation for the observation that dissolution rates in the flow-through experiments were faster than in batch reactors may be abrasion of particles in the flow-through reactors. The batch reactors were mixed with a paddle-stirrer and the flow-through reactors with a magnetically driven Teflon coated stir-bar. Although an elevated stir-bar was used to minimize contact with the surface of the reactor, the presence of finely ground particles of Teflon mixed in with the soil material at the end of the experiments demonstrated that some grinding and abrasion of particles occurred, which

could have enhanced dissolution rates by exposing fresh surface throughout the experiment.

5.3.6 Implications for Weathering of Mammoth Mountain Soils

The rates reported here for Mammoth Mountain volcanic ash soils are in the same range as the rates reported for the Lead Mountain podzols (Table 5.5). Higher rates in the volcanic ash soils were expected, since volcanic ash soils weather more quickly than other more crystalline soils. However, this comparison of rates does not preclude the possibility that the volcanic ash soils do, in fact, weather more rapidly than the Lead Mountain soils in the field. Extrapolation of laboratory dissolution rates to the field is complicated by other factors that will influence weathering rates under field conditions. In addition, the high variability in reported rates among different researchers and different laboratories must be considered as comparisons of laboratory determined dissolution rates are made. Blum and Stillings (1995) make this point very clearly as they review the voluminous literature on laboratory determined feldspar dissolution rates; they report, for example, that the highest and lowest measured rates of anorthite dissolution at pH 5 differ by 6 orders of magnitude (Blum and Stillings, 1995).

The identification of dependencies of soil dissolution rates on pH and organic acids and the absence of a dependence on CO_2 at low pH provides insight into how the soil dissolution rates may be changing in the anomalous area of Mammoth Mountain. These experiments suggest that the CO_2 degassing through the soil would not directly affect soil dissolution rates, however the reduction in pH and changes in organic acids

associated with the decomposing dead trees may be enhancing dissolution rates. The pH effect has been described quantitatively, and can be related to the measured decreases in pH in the high-CO_2 anomalous area. The effect of oxalate has only been observed at a single high concentration, and, since it is not currently understood how LMW organic acid compositions may have changed within the high-CO_2 anomalous area, the implications of the observed oxalate-enhanced dissolution are not as clear.

Low-molecular-weight (LMW) organic acids in soils are excreted from plant roots, leached from litter and other organic material, and produced by bacteria and fungi, which are often associated with the rhizosphere, the root zone. Due to the death of the vegetation within the high-CO_2 areas and the consequent decrease in exudate production by living roots, lower concentrations of organic acids might be expected. However, the increased amount of decomposing organic material and the associated microbial activity in the high-CO_2 soils may provide additional sources of organic acids. It is not obvious, therefore, whether the soils within the anomalous area at Mammoth Mountain are exposed to higher or lower concentrations of LMW organic acids. The results of a comparative analysis of LMW organic acid composition, discussed in Chapter 3, did not show distinct differences in LMW organic acids compositions in the high-CO_2 and control site. However, since this analysis of LMW organic acids was performed on soil samples collected in June just after the snow-melt, the organic acid concentrations and their relative abundance in the high-CO_2 and control soils may not be entirely representative. Spatial and seasonal variation in LMW organic acid concentrations have not yet been examined.

Although little is known about the microbial and fungal populations in the soils exposed to high-CO_2 at Mammoth Mountain, preliminary comparative investigations found that bacterial cell counts in the unexposed areas were 1,000-10,000 times higher than the counts within the anomalous area (Tsapin, 2000), and similarly the abundance of live ectomycorrhizal fungi root tips was greater in the unexposed than the exposed high-CO_2 area (Treseder, 2000). More detailed investigation of the microbial populations and spatial and temporal distributions of the concentrations of LMW organic acids in the Mammoth Mountain soils are needed to understand how LMW organic acids are affecting the mineral weathering regimes of these soils.

5.4 Conclusions

The dissolution rates of the volcanic-ash soils from Mammoth Mountain, California are dependent on pH and organic acid concentration, but are not affected directly by CO_2 (at low pH). These results are consistent with previous laboratory studies on specific minerals that have demonstrated pH and oxalate dependencies and a lack of effect of CO_2. To our knowledge, however, this study is the first to examine how dissolution rates of whole soils respond to these environmental factors. Given the observed sensitivity of these soils to both pH and organic acids, the following rate law can be used to describe the dissolution rates of these soils:

$$R_T = R_H + R_L \,, \qquad (6)$$

where R_T is the total overall dissolution rate; R_H is the proton-promoted rate, and R_L is the ligand-promoted rate. Additional research examining ligand-promoted dissolution of Mammoth Mountain soils in detail, and assessing the combined effects of pH and organic acids would improve understanding of the soil dissolution at the Mammoth site as well as the more general effects of factors on dissolution rates.

5.5 References

Amrhein, C. and Suarez, D.L., 1988. The use of a surface complexation model to describe the kinetics of ligand-promoted dissolution of anorthite. Geochim. Cosmochim. Acta, 52: 2785-2793.

Amrhein, C. and Suarez, D.L., 1992. Some factors affecting the dissolution kinetics of anorthite at 25°C. Geochimica et Cosmochimica Acta, 56: 1815-1826.

Asolekar, S.R., 1991. The Role of Chemical Weathering in the Neutralization of Acid Rain, University of Iowa, 200 pp.

Asolekar, S.R., Valentine, R.L. and Schnoor, J.L., 1991. Kinetics of Chemical Weathering in B Horizon Spodosol Fraction. Water Resources Research, 27(4): 527-532.

Axe, K. and Persson, P., 2001. Time-dependent surface speciation of oxalate at the water-boehmite (γ-AlOOH) interface: Implications for dissolution. Geochimica et Cosmochimica Acta, 65(24): 4481-4492.

Bennett, P.C., 1991. Quartz dissolution in organic-rich systems. Geochimica et Cosmochimica Acta, 55: 1781-1797.

Bennett, P.C. and Casey, W., 1994. Chemistry and mechanisms of low-temperature dissolution of silicates by organic acids. In: E.D. Pittman and M.D. Lewan (Editors), Organic Acids in Geological Processes. Springer-Verlag, Berlin Heidelberg, pp. 162-200.

Berg, A. and Banwart, S.A., 2000. Carbon dioxide mediated dissolution of Ca-feldspar: implications for silicate weathering. Chemical Geology, 163(1-4): 25-42.

Berner, R.A., 1995. Chemical weathering and its effect on atmospheric CO_2 and climate. In: A.F. White and S.L. Brantley (Editors), Chemical Weathering Rates of Silicate Minerals. Reviews in Mineralogy. Mineralogical Society of America, Washington D.C.

Blake, R.E. and Walter, L.M., 1999. Kinetics of feldspar and quartz dissolution at 70-80°C and near-neutral pH: Effects of organic acids and NaCl. Geochimica et Cosmochimica Acta, 63(13/14): 2043-2059.

Blum, A. and Lasaga, A.C., 1988. Role of surface speciation in the low-temperature dissolution of minerals. Nature, 331: 431-433.

Blum, A.E. and Stillings, L.L., 1995. Feldspar dissolution kinetics. In: A.F. White and S.L. Brantley (Editors), Chemical Weathering Rates of Silicate Minerals. Reviews in Mineralogy. Mineralogical Society of America, Washington D.C., pp. 291-351.

Brady, P.V., 1991. The Effect of Silicate Weathering on Global Temperature and Atmospheric CO_2. Journal of Geophysical Research, 96(B11): 18,101-18,106.

Brady, P.V. and Carroll, S.A., 1994. Direct effects of CO_2 and temperature on silicate weathering: Possible implications for climate control. Geochimica et Cosmochimica Acta, 58(8): 1853-1856.

Brady, P.V. and Walther, J.V., 1989. Controls on silicate dissolution rates in neutral and basic pH solutions at 25°C. Geochimica et Cosmochimica Acta, 53: 2823-2830.

Bruno, J., Stumm, W., Wersin, P. and Brandberg, F., 1992. On the influence of carbonate in mineral dissolution: I. The thermodynamics and kinetics of hematite

dissolution in bicarbonate solutions at T=25°C. Geochim. Cosmochim. Acta, 56: 1139-1147.

Casey, W.H. and Westrich, H.R., 1991. Dissolution rates of plagioclase at pH = 2 and 3. American Mineralogist, 76: 211-217.

Chen, Y. and Brantley, S.L., 1998. Diopside and anthophyllite dissolution at 25 degrees and 90 degrees C and acid pH. Chemical Geology, 147(3-4): 233-248.

Devidal, J.L., Schott, J. and Dandurand, J.L., 1997. An experimental study of the dissolution and precipitation kinetics of kaolinite as a function of chemical affinity and solution composition at 150°C, 40 bars, and pH 2, 6.8 and 7.8. Geochimica et Cosmochimica Acta, 61: 5165-5186.

Drever, J.I. and Stillings, L.L., 1997. The role of organic acids in mineral weathering. Colloids and Surfaces A: Physiochemical and Engineering Aspects, 120: 167-181.

Drever, J.I. and Vance, G.F., 1994. Role of soil organic acids in mineral weathering processes. In: E.D. Pittman and M.D. Lewan (Editors), Organic Acids in Geological Processes. Springer-Verlag, Berlin Heidelberg, pp. 138-161.

Etringer, M.A., 1989. The Hydrogen Ion Dependence of the Chemical Weathering Rate of a Tunbridge Series Soil from Lead Mountain, Maine at 15°C. Master of Science Thesis, University of Iowa.

Fish, W. and Kumar, A., 1994. Alteration of adsoprtion site heterogensity by ligand-promoted oxide dissolution, American Chemical Society Annual Spring Meeting. American Chemical Society, Anaheim, CA, pp. 231-ENVR.

Fox, T.R. and Comerford, N.B., 1990. Low-molecular weight organic acids in selected forest soils of the southeastern USA. Soil Science Society of America Journal, 54(4): 1139-1144.

Frogner, P. and Schweda, P., 1998. Hornblende dissolution kinetics at 25 degrees C. Chemical Geology, 151(1-4): 169-179.

Furrer, G. and Stumm, W., 1983. The role of surface coordination in the dissolution of δ–Al_2O_3 in dilute acids. Chimia, 37: 338-341.

Gaillardet, J., Dupre, B., Louvat, P. and Allegre, C.J., 1999. Global silicate weathering and CO_2 consumption rates deduced from the chemistry of large rivers. Chemical Geology, 159: 3-30.

Grandstaff, D.E., 1977. Some kinetics of bronzite orthopyroxene dissolution. Geochimica et Cosmochimica Acta, 41: 1097-1103.

Gwiazda, R.H. and Broecker, W.S., 1994. The separate and combined effects of temperature, soil pCO_2, and organic acidity on silicate weathering in the soil environment: formulation of a model and results. Global Biogeochemical Cycles, 8(2): 141-155.

Helgeson, H.C., Murphy, W.M. and Aagaard, P., 1984. Thermodynamic and kinetic constraints on reaction rates among minerals and aqueous solutions. II. Rate constants, effective surface area, and the hydrolysis of feldspar. Geochimica et Cosmochimica Acta, 58: 2405-2432.

Huang, W.H. and Kiang, W.C., 1972. Laboratory dissolution of plagioclase feldspars in water and organic acids at room temperature. American Mineralogist, 57: 1849-1859.

Knauss, K.G., Nguyen, S.N. and Weed, H.C., 1993. Diopside dissolution kinetics as a function of pH, CO_2, temperature, and time. Geochimica et Cosmochimica Acta, 57: 285-294.

Kraemer, S.M. and Hering, J.G., 1997. Influence of solution saturation state on the kinetics of ligand-controlled dissolution of oxide phases. Geochim. Cosmochim. Acta, 61(14): 2855-2866.

Lagache, M., 1965. Contribution a l'etude de l'alteration des feldspaths, dans l'eau, entre 100 et 200 C, sous diverses pressions de CO_2, et application a la synthese des mineraux argileux. Bull. Soc. Franc. Miner. Crist, 88: 223-253.

Lasaga, A.C., Soler, J.M., Ganor, J., Burch, T.E. and Nagy, K.E., 1994. Chemical-weathering rate laws and global geochemical cycles. Geochimica et Cosmochimica Acta, 58(10): 2361-2386.

Malmstrom, M. and Banwart, S., 1997. Biotite dissolution at 25^{o}C: The pH dependence of dissolution rate and stoichiometry. Geochimica et Cosmochimica Acta, 61(14): 2279-2799.

Malmstrom, M., Banwart, S., Lewenhagen, J., Duro, L. and Bruno, J., 1996. The dissolution of biotite and chlorite at 25^{o}C in the near-neautral pH region. Journal of Contaminated Hydrology, 21: 201-213.

Manley, E.P. and Evans, L.J., 1986. Dissolution of feldspars by low-molecular-weight aliphatic and aromatic acids. Soil Science, 141(2): 106-112.

Marshall, H.G., Walker, J.C.G. and Kuhn, W.R., 1988. Long-term climate change and the geochemical cycle of carbon. Journal of Geophysical Research, 93: 791-801.

Mast, M.A. and Drever, J.I., 1987. The effect of oxalate on the dissolution rates of oligoclase and tremolite. Geochimica et Cosmochimica Acta, 51: 2559-2568.

Murakami, T., Kogure, T., Kadohara, H. and Ohnuki, T., 1998. Formation of secondary minerals and its effect on anorthite dissolution. American Mineralogist, 83: 1209-1219.

Oelkers, E.H. and Gislason, S.R., 2001. The mechanism, rates and consequences of basaltic glass dissolution: I. An experimental study of the dissolution rates of basaltic glass as a function of aqueous Al, Si, and oxalic acid concentration at 25 ^{o}C and pH = 3 and 11. Geochimica et Cosmochimica Acta, 65(21): 3671-3681.

Oelkers, E.H. and Schott, J., 1998. Does organic acid adsorption affect alkali-feldspar dissolution rates? Chemical Geology, 151: 235-245.

Oelkers, E.H., Schott, J. and Devidal, J.L., 1994. The effect of aluminum, pH, and chemical affinity on the rates of aluminosilicate dissolution reactions. Geochimica et Cosmochimica Acta, 58: 2011-2024.

Osthols, E. and Malmstrom, M., 1995. Dissolution kinetics of ThO_2 in acids and carbonate media. Radiochimica acta, 68(2): 113-119.

Pokrovski, G.S. and Schott, J., 1998. Experimental study of the complexation of silicon and germanium with aqueous organic species: Implications for geranium and silicon transport and Ge/Si ratio in natural waters. Geochimica et Cosmochimica Acta, 62(21-22): 3413-3428.

Pokrovsky, O.S. and Schott, J., 2000. Kinetics and mechanism of forsterite dissolution at 25 degrees C and pH from 1 to 12. Geochimica et Cosmochimica Acta, 64(19): 3313-3325.

Poulson, S.R., Drever, J.I. and Stillings, L.L., 1997. Aqueous Si-oxalate complexing, oxalate adsoprtion onto quartz, and the effect of oxalate upon quartz dissolution rates. Chemical Geology, 140: 1-7.

Schecher, W.D. and McAvoy, D.C., 1992. MINEQL+ - A Software Environment for Chemical-Equilibrium Modeling. Computers Environment and Urban Systems, 16(1): 65-76.

Schnoor, J.L., 1990. Kinetics of chemical weathering: A comparison of laboratory and field weathering rates. In: W. Stumm (Editor), Aquatic chemical kinetics: Reaction rates of processes in natural waters. John Wiley and Sons, New York, pp. 475-504.

Sposito, G., 1984. The Surface Chemistry of Soils. Oxford University Press, New York, 234 pp.

Stephens, J.C. and Hering, J.G., 2002. Comparative Characterization of Volcanic Ash Soils Exposed to Decade-Long Elevated Carbon Dioxide Concentrations at Mammoth Mountain, California. Chemical Geology, 186(3-4): 289-301.

Stillings, L.L., Drever, J.I., Brantley, S.L., Sun, Y. and Oxburgh, R., 1996. Rates of feldspar dissolution at pH 3-7 with 0-8 oxalic acid. Chemical Geology, 1322: 79-89.

Stillings, L.L., Drever, J.I. and Poulson, S.R., 1998. Oxalate Adsorption at a Plagioclase (An_{47}) Surface and Models for Ligand-Promoted Dissolution. Environmental Science and Technology, 32: 2856-2864.

Stumm, W., 1992. Chemistry of the solid-water interface : processes at the mineral-water and particle-water interface in natural systems. Wiley, New York.

Stumm, W. and Furrer, G., 1987. The dissolution of oxides and aluminum silicates; examples of surface-coordination-controlled kinetics. In: W. Stumm (Editor), Aquatic Surface Chemistry - Chemical Processes at the Particle-Water Interface. John Wiley & Sons, New York, pp. 197-219.

Stumm, W., Furrer, G., Wieland, E. and Zinder, B., 1985. The effects of complex-forming ligands on the dissolution of oxides and aluminosilicates. In: J.I. Drever (Editor), The Chemistry of Weathering, pp. 55-74.

Stumm, W. and Morgan, J.J., 1996. Aquatic Chemistry, Chemical Equilibria and Rates of Natural Waters. John Wiley & Sons, Inc., New York, 1022 pp.

Sverdrup, H. and Warfvinge, P., 1993. Calculating field weathering rates using a mechanistic geochemical model PROFILE. Applied Geochemistry, 8: 273-283.

Sverdrup, H.U., 1990. The kinetics of base cation release due to chemical weathering. Lund University Press, 246 pp.

Swoboda-Colberg, N.G. and Drever, J.I., 1993. Mineral dissolution rates in plot-scale field and laboratory expeirments. Chemical Geology, 105: 51-69.

Treseder, K., 2000. University of Pennsylvania, Philadelphia, PA.

Tsapin, A., 2000. J.P.L., Pasadena, CA.

Volk, T., 1987. Feedback between weathering and atmospheric CO_2 over the last 100 million years. American Journal of Science, 287: 763-779.

Welch, S.A. and Ullman, W.J., 1993. The effect of organic acids on plagioclase dissolution rates and stoichiometry. Geochimica et Cosmochimica Acta, 57: 2725-2736.

Wogelius, R.A. and Walther, J.V., 1991. Olivine dissolution at 25^{o}C: Effects of pH, CO_2, and organic acids. Geochimica et Cosmochimica Acta, 55(4): 943-954.

Wollast, R., 1967. Kinetics of alteration of K-feldspars in buffered solutions at low temperature. Geochimica et Cosmochimica Acta, 31: 635-648.

Chapter 6

A CRITIQUE OF THE EFFECT OF CO_2 ON MINERAL WEATHERING INCORPORATED INTO THE PROFILE SOIL CHEMISTRY MODEL

6.1 Introduction

Computational modeling of soil processes has developed in recent years to integrate understanding of the many interacting processes within inherently complex soil systems. The processes involved in soil development are biological, chemical and physical (Jenny, 1980). For a given parent material in a particular climate, chemical weathering reactions and biological activity determine many aspects of soil formation while the distribution of weathering products depends upon their transport by water through the soil profile. Attempts to understand soil weathering rates and how soil weathering responds to alterations in ambient conditions based on field observations are limited by the complexity of soil systems. Much of what is currently understood about how specific factors affect soil development and mineral weathering in soils, therefore, has been derived from controlled laboratory experiments, in which interactions among different processes are minimized and the parameter of interest is isolated. Computational modeling of soils offers a way to assimilate the data derived from laboratory experiments and, in so doing, attempts to incorporate the inherent complexity of the natural soil system.

The development of computational soil models, a new direction within the classical discipline of soil science, is aimed at understanding how human-induced

environmental changes (such as acid rain, climate change and waste disposal) impact weathering and the development of soils (Wagenet and Hutson, 1994). Models attempt to predict how anthropogenic activity may affect a soil in a particular area, its associated vegetation, and the cycling of elements within that soil. The development of many of these models is motivated by the need for a scientific basis for decisions regarding soil and water acidification (Sverdrup and Warfvinge, 1995). Predictions from these models, therefore, have the potential to influence policy decisions.

All models are, by definition, simplifications of the actual system they are designed to represent, so numerous assumptions and imperfect predictions are unavoidable consequences of modeling. Model developers and users, however, have a responsibility to explain clearly all assumptions within their models and to include in their model their best interpretation of the current data and knowledge of the field. This chapter examines how the developers of one of the most widely used soil chemistry models, PROFILE, have incorporated a soil mineral weathering dependence on CO_2 (Sverdrup and Warfvinge, 1993), and presents the argument that the relationship assumed for this part of the model does not reflect the current scientific understanding reported in the literature.

This chapter will begin by explaining why the PROFILE model is unique, and therefore worthy of this analysis; among the various soil models, PROFILE is the only one that attempts to incorporate a detailed model of soil mineral weathering. A description of the PROFILE model will be followed by an explanation of the assumed

effect of CO_2 on weathering rates included in the model. A review of the current understanding of this weathering dependence on CO_2 will then be presented, followed by examples of some recent applications of the model. The chapter will conclude by presenting the argument that the inclusion of a misleading relationship within the PROFILE model may perpetuate confusion and erroneous conclusions in future model applications and should be corrected.

6.2 Chemical Weathering Within Soil Models

Essentially all soil chemistry models incorporate chemical weathering processes in some way. However, before the development of PROFILE, the detailed processes associated with weathering were considered too complex to be modeled. The most common and simplest approach to incorporating weathering in soil models assumes a single, constant rate of cation release, generally estimated from field measurements. This approach, which is used in MAGIC (Model of Acidification of Groundwater in Catchments) (Cosby et al., 1985), BIRKENES (Christofferson et al., 1982), MIDAS (Model of Ion Dynamics and Acidification of Soil) (Holmberg et al., 1989) and many others, ignores any possible dependencies of weathering rate on pH, solute concentration, or any other soil properties. Another approach, used by the ILWAS (Integrated Lake Water Acidification Study) model, includes mineral weathering as a single, first-order, pH-dependent reaction with a rate constant derived from laboratory data (Chen et al., 1982). Other models, including SMART (Simulation Model for Acidification of Regional Trends) and RESAM (Regional Soil Acidification Model), designate mineral

weathering as a user input parameter; the user, in these cases, decides how to determine a average weathering rate, either from chemical analysis of soil samples or from input-output budget data (Ball and Trudgill, 1995). PROFILE is the only model that includes a detailed, geochemical weathering sub-model, in which weathering is calculated as a function of soil mineralogy, solute composition, and other user input parameters.

6.3 General Description of the PROFILE Model

The PROFILE model is a steady-state soil chemistry model developed primarily to simulate the response of acid deposition on a regional scale (Warfvinge and Sverdrup, 1992). PROFILE is a multi-layer model; the user can input distinctly different chemical properties for each layer representing the different vertical horizons of a soil profile (Fig. 6.1). Each layer is considered to act as a continuously stirred tank reactor, i.e., all processes interact through the soil solution which is assumed to be well mixed (Jonsson et al., 1995). Within each layer, the model predicts soil solution composition using mass balance equations for acid neutralizing capacity (ANC), base cations, nitrate and ammonium and kinetic equations for nitrification and chemical weathering. These equations within the model are combined with detailed user input information on soil mineralogy, texture and geochemical properties to produce the output data which include soil solution composition, vegetation uptake rates of nitrogen and base cations (keq ha^{-1} yr^{-1}), and weathering rates based on the release of Si and base cations (Al, Ca, Mg, K, and Na) per layer, per mineral and per reaction (also in units of keq ha^{-1} yr^{-1}). PROFILE provides a prediction of the response of soil processes to a given set of conditions, but, as

a steady-state model, provides no information on the time course of such a response (Sverdrup, 1990).

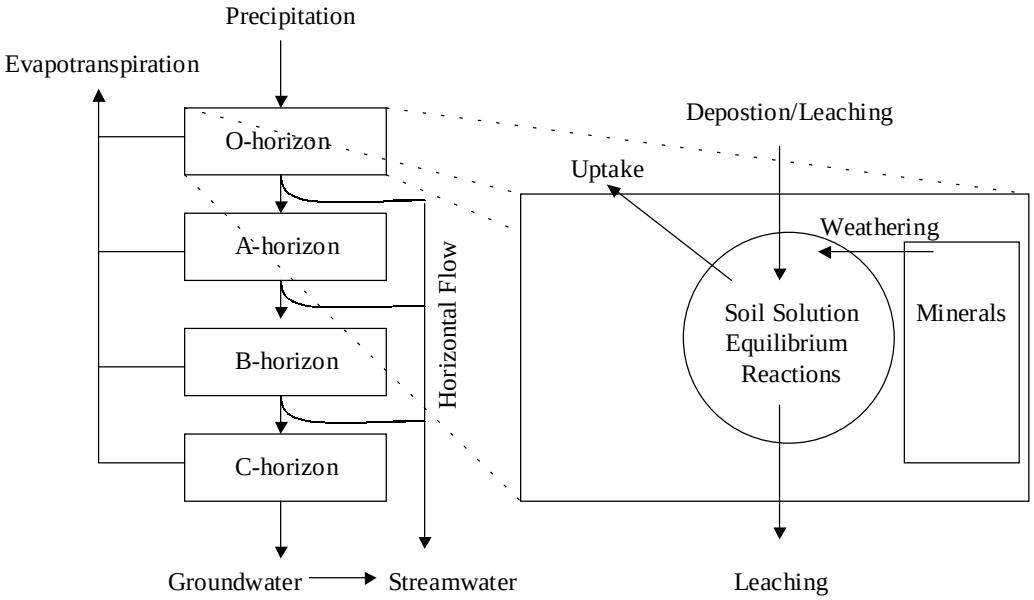

Figure 6.1 – Schematic representation of the PROFILE model.

As discussed in Section 6.2, a major difference between PROFILE and other comparable soil chemistry models is the inclusion of the weathering sub-model. The basic assumption of the weathering sub-model is that the rate equations derived from laboratory data are universally valid and can be applied to different chemical and physical environments if these environments are well defined (Sverdrup and Warfvinge, 1993). The weathering sub-model synthesizes kinetic information on mineral weathering determined from theoretical analysis of laboratory data and is dependent on the mineral composition of the soil. Input data required for the model must be obtained for a specific

site (and soil type) and include site properties such as precipitation rate, runoff rate, average soil temperature, litter fall, and vegetation uptake, and properties of each soil layer such as soil layer height, moisture content, soil density, exposed surface area, P_{CO_2}, percent of percolation entering and leaving the layer, DOC (dissolved organic carbon), and mineralogical composition.

An extensive review of datasets on mineral dissolution kinetics from the literature (dating from 1938 to 1987) was undertaken to develop the weathering sub-model within the PROFILE model (Sverdrup, 1990). Information from 217 published and unpublished studies on mineral dissolution kinetics were evaluated. Results from experiments with undefined conditions or insufficient mineral characterization were discarded, while steady-state rates from well-designed studies were compiled. To fill gaps that became apparent during the review of these dissolution studies, the developers conducted their own experimental work and also derived some kinetic information by comparing rates reported in the literature under different conditions. The later approach, involving the estimation of kinetic coefficients from different independent datasets, is associated with substantial uncertainty and potential for error, because poor reproducibility of rates determined in different laboratories has been well documented (Blum and Stillings, 1995). The kinetic information of the assumed dissolution reaction involving CO_2 included in PROFILE was derived in this manner and will be discussed in more detail in Section 6.4.

The total weathering rate (expressed as release of Si, Al, Ca, Mg, K, and Na) of the entire soil column is calculated as the sum of the weathering rate of each soil layer. The rate of each soil layer is the sum of the rate of each mineral times the exposed surface area of the mineral fraction, the soil moisture saturation, and the depth of the soil layer:

$$R_w = \sum_{j=1}^{\text{minerals}} r_j \cdot A_w \cdot x_j \cdot \theta \cdot z\,, \qquad (1)$$

where

R_w = the bulk weathering rate of a soil horizon ($mol \cdot m_{soil}^{-2} \cdot s^{-1}$)

r_j = the dissolution rate of mineral j adjusted to take into account both the temperature of the soil and the chemistry of the bulk solution ($mol \cdot m_{mineral}^{-2} \cdot s^{-1}$)

A_w = the exposed surface area of the mineral fraction ($m_{mineral}^{2} \cdot m_{soil}^{-3}$)

x_j = the fraction of the total mineral surface area contributed by mineral j

θ = soil moisture saturation ($m^3 \cdot m_{soil}^{-3}$) (mineral surfaces are assumed to weather only when wet)

Z = soil horizon thickness (m).

Of these five parameters, r_j and θ are calculated by the model from constants and user inputs, while the other terms, A_w, x_j, and Z are input directly by the user.

The soil moisture saturation factor, θ, reflects that reactions within the PROFILE model are assumed to take place only on wetted surfaces, and that the degree of surface wetting is considered proportional to the soil moisture saturation (Sverdrup and Warfvinge, 1995). These assumptions imply that the dissolution reactions are not transport controlled, a questionable implication for actual soil systems. Soil moisture

saturation, θ, is calculated by combining the densities of the phases present with the volumetric water content using this expression:

$$\theta = \frac{\rho_{mineral} \cdot \Theta}{\rho_{mineral} + 1000 \cdot \Theta - \rho_{bulk}} \ , \qquad (2)$$

where $\rho_{mineral}$ is the mineral density (kg m^{-3}) defined within the model for each mineral, while ρ_{bulk}, the bulk soil density (kg m^{-3}) and Θ, the soil water content ($m^3 \cdot m_{soil}^{-3}$), are user input parameters for each soil layer (Sverdrup and Warfvinge, 1995).

Weathering rates of each mineral are calculated from the compiled kinetic data for fourteen of the most common soil minerals (Table 6.1). For each mineral, the overall rate of cation release is equal to the sum of the release rates associated with the reaction between the mineral and H^+, H_2O, CO_2, and organics, represented in this kinetic expression:

$$r_j = k_{H^+} \cdot \frac{[H^+]^{n_H}}{f_H} + \frac{k_{H_2O}}{f_{H_{2O}}} + \frac{k_{CO_2} \cdot P_{CO_2}^{n_{CO_2}}}{f_{CO_2}} + k_R \cdot \frac{[R]^{n_R}}{f_R} \ , \qquad (3)$$

where

r_j = dissolution rate of mineral j (kmol m^{-2} s^{-1})
k_{H+} = rate coefficient for the reaction with H^+ (m s^{-1})
k_{H2O} = rate coefficient for the reaction with H_2O (kmol m^{-2} s^{-1})
k_{CO2} = rate coefficient for the reaction with CO_2 (kmol atm^{-1} m^{-2} s^{-1})
k_R = rate coefficient for the reaction with DOC (m s^{-1})
n_H = reaction orders for the reaction with H^+

n_{CO2} = 0.5, reaction order for the reaction with CO_2 assumed for all minerals

n_R = 0.5, reaction order for the reaction with organic acids assumed for all minerals

P_{CO2} = partial pressure of CO_2 in the soil solution (atm)

[R] = concentration of organic acids in the soil solution (kmol m^{-3})

f_H, f_{H2O}, f_{CO2}, and f_R = rate retardation factors for product inhibition.

The rate retardation factors, f_H, f_{H2O}, $f_{CO2,}$ and f_R, account for inhibition due to high soil solution concentrations of base cations and aluminum that may be close to saturation with respect to the parent mineral. These expressions are represented by:

$$f_H = \left(1+\left(\frac{[BC]}{k_{BC}}\right)^{X_{BC}}\right)\cdot\left(1+\left(\frac{[Al^{3+}]}{k_{Al}}\right)^{X_{Al}}\right) \quad (4)$$

$$f_{H_2O} = \left(1+\left(\frac{[BC]}{k_{BC}}\right)^{Z_{BC}}\right)\cdot\left(1+\left(\frac{[Al^{3+}]}{k_{Al}}\right)^{Z_{Al}}\right) \quad (5)$$

$$f_{CO_2} = 1 \quad (6)$$

$$f_R = 1+\left(\frac{[R^-]}{k_R}\right)^{0.5}, \quad (7)$$

where

[BC], $[Al^{3+}]$ = concentration of base cations or aluminum in soil solution (kmol m^{-3})

$k_{Al,}$ k_{BC} = saturation coefficients for dissolution reduction (keq m^{-3})

k_R = organic acid half-rate saturation constant (keq m^{-3})

X_{Al}, X_{BC}, Z_{Al}, Z_{BC} = reaction orders.

Table 6.1

Minerals with their associated rate coefficents, reactions orders and saturation coefficients included in PROFILE[abcd]

Mineral	pk_H	n_H	pk_{H2O}	pk_{CO2}	n_{CO2}	pk_R	n_R	k_{Al}	x_{Al}	z_{Al}	k_{BC}	x_{BC}	z_{BC}	k_R
K-feldspar	16.0	0.5	17.2	17.2	0.6	15.8	0.5	$1 \cdot 10^{-5}$	0.4	0.14	$5 \cdot 10^{-4}$	0.15	0.15	$5 \cdot 10^{-5}$
Oligoclase	15.9	0.5	17.0	15.8	0.6	14.7	0.5	$2 \cdot 10^{-5}$	0.4	0.14	$1 \cdot 10^{-5}$	0.2	0.15	$5 \cdot 10^{-5}$
Albite	15.4	0.5	17.0	15.9	0.6	14.7	0.5	$1 \cdot 10^{-5}$	0.4	0.14	$5 \cdot 10^{-4}$	0.2	0.15	$5 \cdot 10^{-5}$
Hornblende	15.4	0.7	17.0	15.9	0.6	14.3	0.5	$5 \cdot 10^{-5}$	0.3	0.3	$2.5 \cdot 10^{-3}$	0.3	0.3	$1 \cdot 10^{-4}$
Pyroxene	13.8	0.7	17.5	15.8	0.6	14.4	0.5	$5 \cdot 10^{-4}$	0.2	0.1	$2.5 \cdot 10^{-2}$	0.3	0.3	$5 \cdot 10^{-5}$
Epidote	12.6	0.8	16.8	15.8	0.6	14.4	0.5	$5 \cdot 10^{-4}$	0.3	0.2	$2.5 \cdot 10^{-2}$	0.2	0.2	$1 \cdot 10^{-4}$
Garnet	12.4	1.0	16.9	15.8	0.6	14.7	0.5	$1 \cdot 10^{-3}$	0.4	0.2	$5 \cdot 10^{-2}$	0.2	0.2	$5 \cdot 10^{-5}$
Biotite	15.3	0.6	17.6	15.8	0.5	14.8	0.5	$1 \cdot 10^{-5}$	0.3	2	$5 \cdot 10^{-4}$	0.2	0.2	$1 \cdot 10^{-4}$
Muscovite	15.2	0.5	17.5	16.5	0.5	15.3	0.5	$1 \cdot 10^{-6}$	0.4	0.2	$5 \cdot 10^{-5}$	0.1	0.1	$1 \cdot 10^{-4}$
Chlorite	15.3	0.7	16.7	15.8	0.5	14.5	0.5	$5 \cdot 10^{-5}$	0.2	0.1	$2.5 \cdot 10^{-3}$	0.2	0.1	$1 \cdot 10^{-4}$
Vermiculite	14.8	0.6	17.6	16.5	0.5	15.2	0.5	$1 \cdot 10^{-6}$	0.4	0.1	$5 \cdot 10^{-5}$	0.2	0.1	$5 \cdot 10^{-5}$
Apatite	12.8	0.7	15.8	-	-	-	-	-	-	-	$3 \cdot 10^{-4}$	0.4	0.2	-

[a] Rate coefficients expressed as the flux of base cations related to a total rate expressed as keq $m^{-2} s^{-1}$ at 8°C

[b] First seven columns relate to equation 3, while the last seven columns are for equations 4 through 7

c The difference between the total sum of all minerals entered and 100 is assumed to be quartz, whose dissolution is assumed negligible.

d Minerals and coefficients listed in Sverdrup & Warfvinge (1993). Current international version 4.2 also includes calcite and kaolinite, but reference for their rate coefficients were not found. The German and Swiss versions include additional minerals.

Explanation on the derivation of these expressions was not found in the PROFILE literature, so it is not clear how the saturation coefficients, k_{Al}, K_{BC}, and K_R, are estimated.

The influence of soil temperature on weathering rates is incorporated using an Arrhenius relationship. In the compilation of kinetic data from the literature, rate coefficients were standardized to 8°C, so the following equation is used to adjust the coefficients to the ambient soil temperature:

$$\ln\left(\frac{k_T}{k_{8^oC}}\right) = \frac{E_A}{R} \cdot \left(\frac{1}{281} - \frac{1}{T}\right), \qquad (8)$$

where E_A is the activation energy (kJ kmol^{-1}), R is the universal gas constant (kJ kmol^{-1} K^{-1}) and T is the absolute temperature (K). The activation energies incorporated into the model were compiled from experimental data from the literature and were assumed to be equal for laboratory and field conditions (Table 6.2).

6.4 Effect of CO_2 on Mineral Weathering

Sverdrup and Warfvinge, the developers of PROFILE, assumed in their model that the reaction with carbon dioxide and a given mineral results in an activated complex which promotes mineral dissolution at all pH ranges (Sverdrup, 1990). They have, therefore, included in their model an explicit CO_2-mineral reaction that contributes to the overall weathering rate (see eq. 3 in Sec. 6.3). When the PROFILE model was being developed in 1989, very few papers had been published on the effect of CO_2 on mineral weathering, so by including this explicit reaction, the model developers made an

Table 6.2

PROFILE model activation energies (E_A/R) used to calculate the weathering rate coefficient from 8°C to actual soil temperaure for the reactions with each mineral and H^+, H_2O, CO_2, and organics (R). Adapted from Sverdrup and Warfvinge, 1993.

	Formula	E_A/R			
		H	H_2O	CO_2	R
K-feldspar	$KAlSi_3O_8$	3500	2000	1700	3000
Oligoclase	$(NaCa)(Al,Si)AlSi2O_8$	4200	2500	1700	3000
Albite	$NaAlSi_3O_8$	3800	2500	1700	3000
Hornblende	$(Na,Ca)_2(Mg,Fe,Al)_5(S,Al)_8O_{22}(OH)_2$	4300	3800	1700	3000
Pyroxene	$XY(Si, Al)_2O_6$	2700	3800	1700	3000
Epidote	$Ca_2(Al, Fe)_3(SiO_4)_3(OH)$	2500	3800	1700	3000
Garnet	$X_3Y_2(SiO_4)_3$	2500	3500	1700	3000
Biotite	$K(Mg,Fe)_3Si_3(Al,Fe)O_{10}(OH,F)_2$	4500	3800	1700	3000
Muscovite	$KAl_2(AlSi_3O_{10})(F,OH)_2$	4500	3800	1700	3000
Chlorite	$(Fe, Mg, Al)_6(Si, Al)_4O_{10}(OH)_8$	4500	3800	1700	3000
Vermiculite	$(Mg,Fe,Al)_3(Al,Si)_4O_{10}(OH)_2 \cdot 4H_2O$	4300	3800	1700	3000
Apatite	$Ca_5(PO_4)_3(OH,F,Cl)$	3500	4000	1700	3000

important assumption and derived rate coefficients using somewhat unorthodox approaches.

The only study reporting enhancement of dissolution rates by CO_2 examined feldspar dissolution at 100-200^oC with P_{CO2} values of 0, 2, 6 and 20 atm at drifting pH values ranging from 3-5 (Lagache, 1965; Lagache, 1976). The observations of apparent CO_2 enhancement of dissolution rates have been interpreted by some as a pH effect only indirectly related to CO_2 (Helgeson et al., 1984), since the pH was not well controlled and may have been lower in the experiments with high P_{CO2}. Another study on feldspar dissolution reported rates at 25^oC and 1 atm P_{CO2}; however, this study did not make a comparison to rates under ambient P_{CO2} (Busenberg and Clemency, 1976). A study on bronzite ($(Mg,Fe)_2Si_2O_2$) dissolution reported no significant difference between rates under ambient and 1 atm P_{CO2} in the pH range from 1-4.5 at 22^oC (Grandstaff, 1977), and the same result, no dependence on CO_2, was observed in dissolution experiments with anorthite in the presence of elevated P_{CO2} (Amrhein and Suarez, 1988).

Using the data of Lagache (1965) and Busenberg and Clemency (1976), Sverdrup and Warfvinge estimated the rate of the reaction between feldspars and CO_2 by comparing rate coefficients derived from other experiments without CO_2 (Chou and Wollast, 1985; Holdren and Berner, 1979; Manley and Evans, 1986) using the following relationship:

$$k_{CO_2} \cdot P_{CO_2}^n = r - k_{H^+}[H^+]^n - k_w \qquad (9)$$

Then by plotting the logarithm of the various P_{CO2} values of Lagache versus the logarithm of the rate, both reaction order and the rate coefficient were approximated:

$$\ln k_{CO_2} \cdot P_{CO_2}^{n} = n \cdot \ln P_{CO_2} + \ln k_{CO_2} \qquad (10)$$

The kinetic coefficients derived in this manner were assumed in the model to represent the effect of CO_2 on all minerals.

Since the PROFILE model was developed, several laboratory studies designed specifically to observe the possible effect of CO_2 on dissolution rates (including the dissolution of whole soils discussed in Chapter 5), have shown that, at ambient pressures and temperatures, the presence of CO_2 does not enhance dissolution rates under acidic conditions (Brady and Carroll, 1994; Knauss et al., 1993; Wogelius and Walther, 1991). A CO_2 dependence in the basic pH range has been observed and is attributed to the formation of carbonate surface complexes (Berg and Banwart, 2000; Bruno et al., 1992; Osthols and Malmstrom, 1995), but such complexes would be less likely to form at low pH (and corresponding low carbonate concentrations). Thus, the inclusion of a pH-independent CO_2 effect in the PROFILE model appears to be erroneous and misleading. The potential implications for modeling are discussed in section 6.6.

Why, one might ask, were the developers of the PROFILE model not more critical in their assumption that CO_2 has a direct effect on mineral weathering?

CO_2 is often included explicitly in weathering reactions to represent the fact that interactions between water and CO_2 (and other weak acids) are responsible for the dissociation of water to form H^+, which is the constituent that is actually promoting the dissolution reaction.

$$CaSiO_{3(s)} + 2CO_2 + 3H_2O = H_4SiO_4 + 2HCO_3^- + Ca^{2+} \quad (11)$$

By substituting the products of the reaction of CO_2 and water from reaction 12 below, reaction 11 can be rewritten (reaction 13) without CO_2:

$$H_2O + CO_2 = H^+ + HCO_3^- \quad (12)$$

$$CaSiO_{3(s)} + 2H^+ + H_2O = H_4SiO_4 + Ca^{2+} \quad (13)$$

The assumption that CO_2, a weak acid, enhances mineral weathering, is, therefore, reasonable in the context of specific acid catalysis. If the rate of a reaction depends on the H^+ concentration, that reaction exhibits specific acid catalysis. Acids other than H^+ that may be present contribute to the reaction rate only through their contribution to pH determination, because under these conditions the rate-determining step does not involve proton transfer (Lowry and Richardson, 1987). In contrast, general acid catalysis refers

to reactions where each individual acid present in the system can act as a proton donor in the rate determining step. In mineral dissolution reactions, the rate determining step is generally assumed to be the detachment of the surface complex, so general acid catalysis is unlikely. General acid catalysis is assumed for CO_2 within the PROFILE model despite minimal evidence supporting a mechanism.

The same erroneous assumption, that increased CO_2 accelerates weathering rates directly, has been made by other model developers (Marshall et al., 1988; Volk, 1987). In the geochemical carbon cycle modeling study by Marshall et al. (1988), the same interpretation of the data from Lagache (1965) was used, although these modelers acknowledged the speculative nature of this relationship:

> *The rate of silicate dissolution presumably depends directly on carbon dioxide partial pressure as well as indirectly through temperature and runoff. There are no field observations to bear on this question, however; the discussion that follows is tentative and preliminary; the derived direct dependence of weathering rate on carbon dioxide partial pressure is speculative.* (Marshall et al., 1988).

Other modelers of the global carbon cycle have been more conservative and, in the absence of evidence for a direct CO_2 effect, have neglected the possible direct dependence of silicate dissolution rates on P_{CO2} (Berner et al., 1983). Sverdrup and Warfvinge's decision to include this direct dependence of weathering rate on CO_2 may be perpetuating confusion on this issue.

6.5 Applications of the PROFILE Model

The PROFILE model has been described in the scientific literature by its developers (Sverdrup, 1996; Sverdrup and Warfvinge, 1993; Sverdrup and Warfvinge, 1995; Warfvinge and Sverdrup, 1992), and is available free of charge for other researchers to use. A comparison of weathering rates calculated by field-based methods, including input-output mass budgets and depletion of elements relative to a conservative element, show that the rates calculated by PROFILE are on the order of ± 20% compared to these other estimations (Sverdrup and Warfvinge, 1993). Due to the heterogeneity of soil properties over large geographic areas, the detailed user input parameters necessary to run the PROFILE model limit its application to regional-scale applications. Since no other model attempts to calculate weathering rates with this level of detail, however, the PROFILE model is used for mapping regional weathering rates in at least 27 countries around the world (Sverdrup, 1996).

Recent applications of the PROFILE model include a study of weathering rates on the Norwegian-Russian border (Koptsik et al., 1999), a comparison weathering rates of two contrasting regions in Switzerland (Eggenberger and Kurz, 2000), and an assessment of regional variation in weathering rates of loess and clay soils in the Netherlands (van der Salm, 2001). Another study adapted the PROFILE model to include volcanic glass, the major primary mineral in volcanic ash soils (Fumoto et al., 2001).

Several applications of PROFILE have illustrated limitations of the model. For example, PROFILE predicted higher weathering rates in older soils than younger soils, while estimates made by empirical and depletion methods exhibit a decrease in

weathering rates as soils age (Hodson and Langan, 1999). Although the older soils in this study had lower concentrations of reactive minerals, PROFILE calculated higher weathering rates due to the model sensitivity to soil density and surface area, parameters with larger values in the old soils compared to the younger soils. Other users of the model have also found that weathering rates predicted by PROFILE are highly sensitive to the specific surface area input by the user (Hodson and Langan, 1999; Jonsson et al., 1995). Surface area is a recurring problem in weathering rate studies for several reasons: the assumption that the total mineral surface area is reacting is not always valid (Hodson, 1999), surface area changes as the soils weather (see discussion in Chapter 4), and the two common methods of determining surface area, the B.E.T. method using N_2 adsorption and the geometric approximation method, often give different values (Blum and Stillings, 1995). In addition, the PROFILE model requires determination of a bulk surface area as well as an estimation of the contribution to the bulk surface area of each soil mineral (the user must input mineral composition as % of total surface area). Despite the limitations associated with model sensitivity and surface area, an uncertainty analysis of the PROFILE model performed by Monte Carlo analysis, in which input parameter errors were varied individually and simultaneously, shows that PROFILE does calculate weathering rates with high precision if the errors in input parameters are within the range generally reported in the literature (Jonsson et al., 1995).

6.6 Illustration of the CO_2 Dependence

Typical concentrations of soil CO_2, produced primarily from root and microbial respiration, range from 10 to 100 times atmospheric concentrations, which corresponds to a P_{CO2} of ~0.003 - 0.03 atm (Castelle and Galloway, 1990; Holland et al., 1986). Under these typical conditions, the CO_2-weathering relationship included in the PROFILE model does not have a noticeable influence on predicted overall weathering rates in the acidic pH range because proton-promoted dissolution dominates (Jonsson et al., 1995). However, if the PROFILE model were to be used to predict weathering rates for a soil with anomalously high CO_2 concentrations the weathering rates would increase substantially as soil CO_2 increased.

To illustrate this, weathering rates predicted by PROFILE from a series of model calculations with varying soil CO_2 values are plotted in Figure 6.2. All input parameters

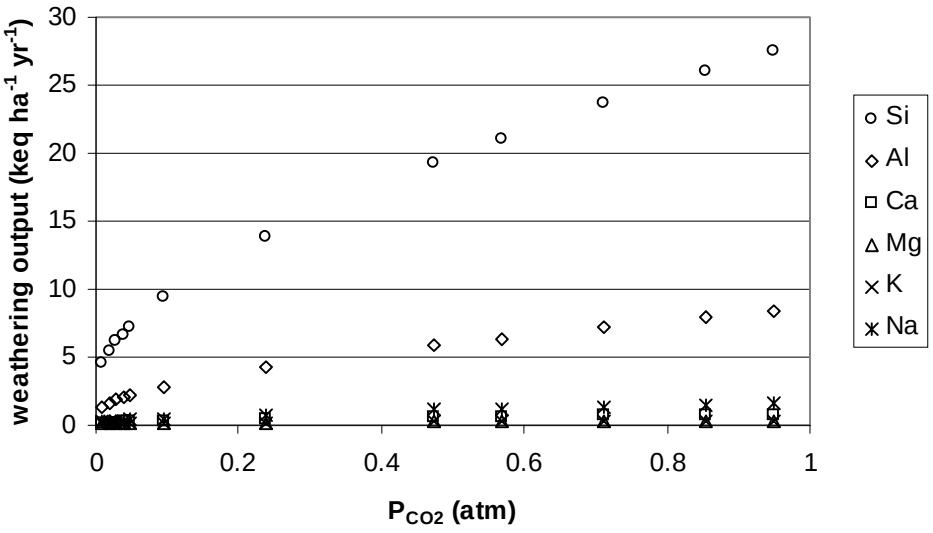

Figure 6.2 – Illustration of dependence of weathering output calculated by the PROFILE mode on the P_{CO2} value input by the user.

are those of the default values listed in Table 6.3 (default "typical" values are present in the model before a user enters site-specific details), except for the soil CO_2 concentration.

Table 6.3
Default input data for the PROFILE model for four soil layers

Parameter	Unit	1	2	3	4
Soil layer thickness	m	0.04	0.06	0.23	0.35
Soil water content	%	0.15	0.2	0.25	0.35
Soil bulk density	kg m^{-3}	200	880	610	1250
Specific surface area	m^2 m^{-3} * 10^{-6}	5.5 x 10^5	1.34 x 10^6	1.4 x 10^6	1.18 x 10^6
CO_2 pressure	times ambient	1	10	20	30
Dissolved organic carbon	$kmol^2$ m^{-3}	34	36	8	6
Inflow	% of precipitation	100	50	46	42
Percolation	% of precipitation	50	46	42	42
Mg+Ca+K uptake	% of total max	30	30	30	10
N uptake	% of total max	50	40	10	0
Mineralogy (%)	K-feldspar	15	15	18	13
	Plagiocalse	14	14	12	16
	Albite	0	0	0	0
	Horblende	0.1	0.5	1.5	1.5
	Pyroxene	0	0	0	0
	Epidote	0	0.1	1	1.5
	Garnet	0	0	0.1	0.1
	Biotite	0	0.1	0.5	0.5
	Muscovite	0	0	0	0
	Fe-Chlorite	0	0.4	0.5	0.4
	Mg-Vermiculite	0	0	5	0
	Apatite	0	0.1	0.2	0.2
Soil Temperature (^oC)	7.5				
Precipitation Rate (m)	0.9				
Runoff Rate (m)	0.38				

The extremely high soil CO_2 conditions input in this series of calculations may appear unrealistic; however, scenarios exist where researchers may be interested in calculating weathering rates under such conditions. Recent U.S. Department of Energy sponsorship of carbon sequestration research has resulted in numerous researchers assessing environmental implications of injecting CO_2 into underground storage reservoirs. An associated risk is CO_2 leakage from the reservoir through the soil back into the atmosphere, a scenario that could produce anomalously high soil CO_2 concentrations. Currently a naturally occurring CO_2 degassing phenomena similar to that described above is taking place on the flanks of Mammoth Mountain, California; a magmatic CO_2 reservoir at depth is leaking CO_2 to the atmosphere (see Chapters 2 and 3). In the soils where the CO_2 is seeping through, 30-90% of the soil gas has been measured as CO_2. Applications of the current PROFILE model in these high-CO_2 scenarios would result in an enormous overcalculation of the actual weathering rate.

6.7 Conclusions

Although the PROFILE model has been widely used within the soil modeling community and weathering rate calculations from the model confirm other estimates, the parameters associated with the dependence of the weathering rate on soil CO_2 are not well founded and should be revisited. When the model was developed over ten years ago, the assumption of a CO_2 dependence may have been reasonable; however, given the numerous recent studies that have been unable to substantiate any CO_2 effect on dissolution under acidic conditions and the lack of a mechanism to explain such an effect,

it would be prudent for the PROFILE developers to remove this relationship from their model. The inclusion of this CO_2 dependence in the PROFILE model may result in erroneous conclusions in future applications and may perpetuate confusion on this issue.

6.8 References

Amrhein, C. and Suarez, D.L., 1988. The use of a surface complexation model to describe the kinetics of ligand-promoted dissolution of anorthite. Geochim. Cosmochim. Acta, 52: 2785-2793.

Ball, J. and Trudgill, S., 1995. Overview of Solute Modelling. In: S.T. Trudgill (Editor), Solute Modelling in Catchment Systems. John Wiley & Sons Ltd., Chichester, pp. 3-56.

Berg, A. and Banwart, S.A., 2000. Carbon dioxide mediated dissolution of Ca-feldspar: implications for silicate weathering. Chemical Geology, 163(1-4): 25-42.

Berner, R.A., Lasaga, A.C. and Garrels, R.M., 1983. The carbonate-silicate geochemical cycle ad its effects on atmospheric carbon dioxide over the past 100 million years. American Journal of Science, 283: 641-683.

Blum, A.E. and Stillings, L.L., 1995. Feldspar dissolution kinetics. In: A.F. White and S.L. Brantley (Editors), Chemical Weathering Rates of Silicate Minerals. Reviews in Mineralogy. Mineralogical Society of America, Washington D.C., pp. 291-351.

Brady, P.V. and Carroll, S.A., 1994. Direct effects of CO_2 and temperature on silicate weathering: Possible implications for climate control. Geochimica et Cosmochimica Acta, 58(8): 1853-1856.

Bruno, J., Stumm, W., Wersin, P. and Brandberg, F., 1992. On the influence of carbonate in mineral dissolution: I. The thermodynamics and kinetics of hematite dissolution in bicarbonate solutions at T=25^{o}C. Geochim. Cosmochim. Acta, 56: 1139-1147.

Busenberg, E. and Clemency, C.V., 1976. The dissolution kinetics of feldspars at 25^{o}C and 1 atm CO_2 partial pressure. Geochimica et Cosmochimica Acta, 40: 41-49.

Castelle, A.J. and Galloway, J.N., 1990. Carbon dioxide dynamics in acid forest soils in Shenandoah National Park, Virginia. Soil Science Society of America Journal, 54(1): 252-257.

Chen, C.W., Dean, J.D., Gherini, S.A. and Goldstein, R.A., 1982. Acid rain model: hydrologic model. Journal of Environmental Engineering - ASCE, 108: 455-472.

Chou, L. and Wollast, R., 1985. Steady-state kinetics and dissolution mechanisms of albite. American Journal of Science, 285: 963-993.

Christofferson, N., Seip, H. and Wright, R., 1982. A model for stream and water chemistry at Birkenes, Norway. Water Resources Research, 18: 977-996.

Cosby, B., Wright, R.F., Hornberger, G. and Galloway, J., 1985. Modeling the effects of acid deposition: Assessment of a lumped parameter model for soil water and stream water chemistry. Water Resources Research, 21: 51-63.

Eggenberger, U. and Kurz, D., 2000. A soil acidification study using the PROFILE model on two contracting regions in Switzerland. Chemical Geology, 170: 243-257.

Fumoto, T., Shindo, J., Oura, N. and Sverdrup, H., 2001. Adapting the PROFILE model to calculate the critical loads for east Asian soils by including volcanic glass weathering and alternative aluminum solubilit system. Water, Air, and Soil Pollution, 130: 1247-1252.

Grandstaff, D.E., 1977. Some kinetics of bronzite orthopyroxene dissolution. Geochimica et Cosmochimica Acta, 41: 1097-1103.

Helgeson, H.C., Murphy, W.M. and Aagaard, P., 1984. Thermodynamic and kinetic constraints on reaction rates among minerals and aqueous solutions. II. Rate constants, effective surface area, and the hydrolysis of feldspar. Geochimica et Cosmochimica Acta, 58: 2405-2432.

Hodson, M.E., 1999. Micropore surface area variation with grain size in unweathered alkali feldspars: Implications for surface roughness and dissolution studies. Geochimica et Cosmochimica Acta, 62(21/22): 3429-3435.

Hodson, M.E. and Langan, S.J., 1999. The influence of soil age on calculated mineral weathering rates. Applied Geochemistry, 14: 387-394.

Holdren, G.R.J. and Berner, R.A., 1979. Mechanism of feldspar weathering - I. Experimental studies. Geochimica et Cosmochimica Acta, 43: 1161-1171.

Holland, H.D., Lazar, B. and McCaffrey, M., 1986. Evolution of atmospheres and oceans. Nature, 320: 27-33.

Holmberg, M., Hari, P. and Nissinen, A., 1989. Model of ion dynamics and acidification of soil: Application to historical soil chemistry data of Sweden. In: J. Kamari, D.F. Brakke, A. Jenkins, S.A. Norton and R.F. Wright (Editors), Regional Acidification Models: Geographical Extent and Time Development. Kluwer Academic Publishers, Dordrecht, Netherlands, pp. 229-240.

Jenny, H., 1980. Factors of Soil Formation. McGraw-Hill, New York, 239 pp.

Jonsson, C., Warfvinge, P. and Sverdrup, H., 1995. Uncertainty in predicting weathering rate and environmental stress factors with the PROFILE model. Water, Air and Soil Pollution, 81: 1-23.

Knauss, K.G., Nguyen, S.N. and Weed, H.C., 1993. Diopside dissolution kinetics as a function of pH, CO_2, temperature, and time. Geochimica et Cosmochimica Acta, 57: 285-294.

Koptsik, G., Teveldal, S., Aamlid, D. and Venn, K., 1999. Calculations of weathering rate and soil solution chemistry for forest soils in the Norwegian-Russian border area with the PROFILE model. Applied Geochemistry, 14: 1999.

Lagache, M., 1965. Contribution a l'etude de l'alteration des feldspaths, dans l'eau, entre 100 et 200 C, sous diverses pressions de CO_2, et application a la synthese des mineraux argileux. Bull. Soc. Franc. Miner. Crist, 88: 223-253.

Lagache, M., 1976. New data on the kinetics of the dissolution of alkali feldspars at 200^{o}C in CO_2 charged water. Geochimica et Cosmochimica Acta, 40: 157-161.

Lowry, T.H. and Richardson, K.S., 1987. Mechanism and Theory in Organic Chemistry. Harper & Row, New York, 1090 pp.

Manley, E.P. and Evans, L.J., 1986. Dissolution of feldspars by low-molecular-weight aliphatic and aromatic acids. Soil Science, 141(2): 106-112.

Marshall, H.G., Walker, J.C.G. and Kuhn, W.R., 1988. Long-term climate change and the geochemical cycle of carbon. Journal of Geophysical Research, 93: 791-801.

Osthols, E. and Malmstrom, M., 1995. Dissolution kinetics of ThO_2 in acids and carbonate media. Radiochimica acta, 68(2): 113-119.

Sverdrup, H., 1996. Geochemistry, the key to understanding environmental chemistry. The Science of the Total Environment, 183: 67-87.

Sverdrup, H. and Warfvinge, P., 1993. Calculating field weathering rates using a mechanistic geochemical model PROFILE. Applied Geochemistry, 8: 273-283.

Sverdrup, H. and Warfvinge, P., 1995. Estimating field weathering rates using laboratory kinetics. In: A.F. White and S.L. Brantley (Editors), Chemical weathering rates of silicate minerals. Reviews in Mineralogy. Mineralogical Society of America, Washington DC, pp. 485-541.

Sverdrup, H.U., 1990. The kinetics of base cation release due to chemical weathering. Lund University Press, 246 pp.

van der Salm, C., 2001. Assessment of the regional variation in weathering rates of loess and clay soils in the Netherlands. Water, Air, and Soil Pollution, 131: 217-243.

Volk, T., 1987. Feedback between weathering and atmospheric CO_2 over the last 100 million years. American Journal of Science, 287: 763-779.

Wagenet, R.J. and Hutson, J.L., 1994. Modeling Water and Chemical Fluxes as Driving Forces of Pedogenesis. In: R.B. Bryant and R.W. Arnold (Editors), Quantitative Modeling of Soil Forming Processes. Soil Science Society of America, Madison, WI, pp. 17-35.

Warfvinge, P. and Sverdrup, H., 1992. Calculating critical loads of acid deposition with PROFILE - a steady-state soil chemistry model. Water, Air, and Soil Pollution, 63: 119-143.

Wogelius, R.A. and Walther, J.V., 1991. Olivine dissolution at 25^{o}C: Effects of pH, CO_2, and organic acids. Geochimica et Cosmochimica Acta, 55(4): 943-954.

Chapter 7

CONCLUSIONS

7.1 Summary

This research provides confirming evidence that CO_2 does not directly influence dissolution rates under acidic conditions, while indirect effects of elevated CO_2, including decreasing pH and changes in organic acid composition, may alter soil weathering rates. The identification of chemical and mineralogical differences between the soil exposed to high levels of CO_2 and the unexposed soil on the flanks of Mammoth Mountain suggests that decade-long exposure to elevated CO_2 concentrations has altered soil dissolution rates. Although a comparison of dissolution rates determined in the laboratory on samples from within and outside the high-CO_2 area did not confirm a difference in weathering history, dissolution experiments on a single soil under varying conditions demonstrated the sensitivity of the dissolution rate of these soils to changes in pH and organic acid concentrations. A decrease in surface area during the dissolution experiments demonstrates the importance of measuring surface area before and after experiments in order to decide what value of surface area should be used in the normalization of dissolution rates.

Although some researchers have assumed the total rate of dissolution is the sum of the proton-promoted, ligand-promoted, and CO_2-promoted rates:

$$R_T = R_H + R_L + R_{CO_2} \quad (1)$$

the work presented herein demonstrates that under acidic conditions, the R_{CO2} term should be disregarded, because CO_2 does not have a direct effect on dissolution rate. The indirect effects of CO_2 are incorporated into the R_H and R_L terms, so reaction 1 should be rewritten as:

$$R_T = R_H + R_L \qquad (2)$$

7.2 Environmental Implications

Three different scales of environmental implications can be derived from the conclusions of this work: (1) at the global scale, this research contributes to the understanding of geochemical cycling associated with the mineral weathering of volcanic ash soils, (2) at the local scale, the focus on the site at Mammoth Mountain provides insight into how leaks from an underground reservoir of CO_2 may alter processes at the surface, and (3) at the laboratory scale, this work demonstrates the significance of surface area changes during dissolution experiments and also illustrates uncertainties in weathering rates at all scales associated with specific surface area.

The weathering of volcanic ash soil is generally faster than the weathering of other soils, so it has been suggested that its weathering may represent a disproportionate sink for CO_2 (Gaillardet et al., 1999). So, although volcanic ash soils make up less than 1% of the earth surface (Shoji et al., 1993), this study on factors affecting the weathering rates of volcanic ash soils may be a critical component of improving our comprehension

of the global carbon cycle and how natural systems are responding to the currently rising atmospheric CO_2 concentrations.

The evidence suggesting that decade-long exposure to elevated CO_2 concentrations have altered soil dissolution rates at Mammoth Mountain has implications for current efforts to understand risks associated with injection of CO_2 into underground reservoirs. The primary mechanism proposed for sequestering CO_2 underground, known as hydrodynamic trapping, involves trapping the CO_2 as a gas or a supercritical liquid under a low-permeability caprock, similar to the way natural gas is stored (Department of Energy, 1999). This type of storage would not be permanent, so leaks would be expected at some point. In addition to killing vegetation, CO_2 leaking from an underground reservoir could indirectly enhance mineral dissolution, affecting soil development and altering the natural cycling of elements and organic material.

In addition to the above mentioned environmental implications, this research illustrates the dependence of all approaches of calculating mineral weathering rates on specific surface area; laboratory dissolution experiments, field-based estimations, and computational modeling are all highly sensitive to specific surface area. Consideration must be given in the comparison of reported weathering rates to what measure of speicifc surface area is being used in normalization of the rate. In laboratory dissolution experiments, pre- and post-dissolution measurements of specific surface area should always be made and the dissolution rates should be adjusted appropriately. Hopefully, this work along with the work of others who have reported changes in their dissolution rates based on changes in specific surface area occurring during dissolution experiments

(Burch et al., 1993; Stillings and Brantley, 1995), will convince researchers that the convention of calculating dissolution rates based upon the measurements of initial specific surface area is likely to be a major oversimplification leading to the reporting of erroneous rates of mineral dissolution.

7.3 Suggestions for Future Research

Although this research offers some insight into how the soils at Mammoth Mountain are responding to the anomalous conditions, there is much more to be investigated at this unique site. A more detailed assessment, including spatial and temporal variability, of the concentrations of low-molecular-weight organic acids within and outside the anomalous site would provide a better understanding of the role of organic acids in altering the mineral weathering regime. Characterizing the microbial populations living in these extreme, high-CO_2 conditions could reveal previously unidentified species and would also contribute to the understanding of interactions between the inorganic and organic fractions of the soil.

This work is one of only a few studies assessing dissolution rates of whole soils, so more research on the kinetics of whole soil dissolution using different types of soils would expand the current understanding of the kinetics of soil mineral weathering. Experiments designed to assess synergistic or antagonistic relationships among different factors affecting dissolution rates would be useful. Oxalate has been used extensively as a proxy for a host of LMW organic acids commonly found in soils, but different acids have been shown to have very different effects on dissolution rates of pure minerals, so

whole soil dissolution experiments assessing the variable effects of different acids would improve our understanding of the role of LMW organic acids in mineral dissolution in natural settings.

7.4 References

Burch, T.E., Nagy, K.L. and Lasaga, A.C., 1993. Free energy dependence of albite dissolution kinetics at 80^{o}C and pH 8.8. Chemical Geology, 105: 137-162.

Department of Energy, U.S., 1999. Carbon Sequestration - Research and Development.

Gaillardet, J., Dupre, B., Louvat, P. and Allegre, C.J., 1999. Global silicate weathering and CO_2 consumption rates deduced from the chemistry of large rivers. Chemical Geology, 159: 3-30.

Shoji, S., Dahlgren, R. and Nanzyo, M., 1993. Terminology, concepts and geographic distribution of volcanic ash soils. In: S. Shoji, M. Nanzyo and R.A. Dahlgren (Editors), Volcanic Ash Soils, Genesis, Properties and Utilization. Developments in soil science 21. Elsevier, Amsterdam, pp. 288.

Stillings, L.S. and Brantley, S.L., 1995. Feldspar dissolution at 25^{o}C and pH 3: Reaction stoichiometry and the effect of cations. Geochimica et Cosmochimica Acta, 59(8): 1483-1496.

Appendix A

DETAILS OF SOIL MINERALOGICAL ANALYSIS

A.1 X-ray Diffraction

X-ray diffraction analysis, the most widely used method of identifying minerals, was conducted to characterize the different mineral phases present in the soils. This method uses the unique and characteristic distance between planes of atoms in different mineral phases for identification; when an X-ray beam of wavelength λ diffracts off the various planes within a crystalline phase, a characteristic pattern is produced whenever the Bragg law, $n\lambda = 2d \sin\theta$, is satisfied. During the XRD analysis, θ, the angle of incidence, is varied producing peaks in a pattern that correspond to d values, the characteristic plane spacing.

A.1.1 Methods

Powder X-ray diffraction (XRD) analysis was performed on whole soil samples and clay-size fraction samples using a Scintag Pad V X-ray Powder Diffractometer with Cu K-α radiation generated by a 40 kV accelerating potential and 35 mA tube current. Samples were step scanned for 2 s at a rate of 0.01 ^{o}/min at a 0.01^{o} 2θ step. Diffractograms were obtained for samples treated following standard methods, including Mg and K saturation, glycolation, and heating to 550^{o}C to differentiate among different minerals that exhibit different peaks under the different preparations (Whittig and Allardice, 1986).

A.1.2 Results

The high percentage of non-crystalline material present in these soils results in low intensity and poor signal-to-noise ratios (Fig. A.1), severely limiting the interpretation of the XRD results. Figure A.1 is a representative diffractogram, which shows that despite the noise, several characteristic peaks are apparent and were used to qualitatively identify the presence of several mineral phases.

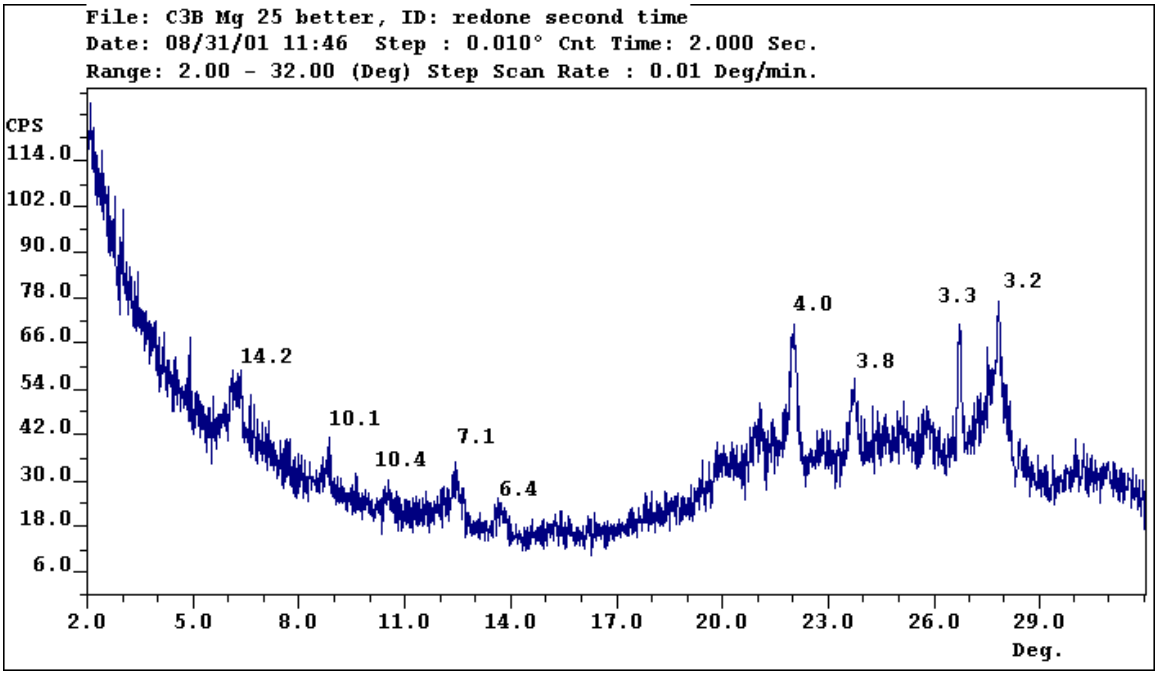

Figure A.1 - This diffractogram is from a sample that has been saturated with Mg. The peak at 14.2 angstroms (A)[1] represents the presence of either smectite, vermiculite or chlorite, the 10.1 peak suggests either mica or halloysite, the 7.1 peak indicates kaolinite or serpentine, the 4.0 peak cristobalite, the 3.8 peak gypsum, the 3.3 peak is quartz, and the 3.2 peak is either K-feldspar or hornblende.

[1] The diffraction spacing is often reported as nm, i.e. the first peak represents a spacing of 1.4 nm. The software used here, however, reported the peaks as angstroms, Å, 10^{-10}m.

The clay size mineralogy is dominated by smectite as indicated by the shift of the 14.2-Å peak in the Mg-saturated treatment to ~18 Å peak following glycol treatment. The small 14.2 Å peak that remains following glycol treatment collapses upon K saturation indicating the presence of vermiculite.

A.2 Petrographic Microscope

Thin sections of the bulk (< 2 mm) size fraction soil were prepared and examined under a petrographic microscope. A minimum of 400 points of a grid on each slide were counted and characterized as either volcanic glass or other (some of the other phases, including hornblende with its characteristic green color, were also identifiable, however quantification of these other phases was not attempted). The results of this counting provided the estimate that the soils are predominantly composed of volcanic glass (50-60%). Figure A.2 shows an image of the view from the petrographic microscope. In this image hornblende is the dark green mineral and the volcanic glass is the striated material in the upper-right corner

A.3 Transmission Electron Microscope (TEM)

Clay samples of both the control and high-CO_2 soils were analyzed by transmission electron microscope (TEM). A Philips EM430 TEM at an accelerating voltage of 300kV was used to examine samples of the < 2 μm fraction for the presence of allophane, imogolite or ferrihydrite. These mineral phases are commonly found in

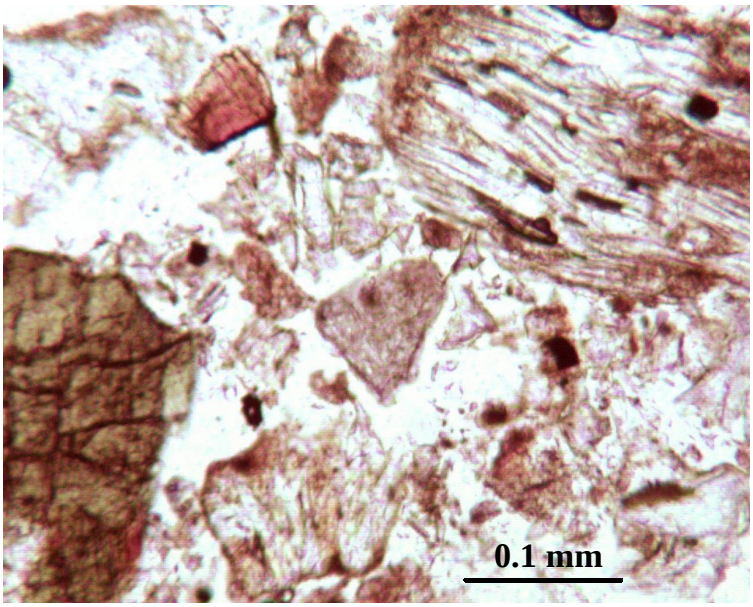

Figure A.2 - An image of the soil thin-section viewed through the petrographic microscope. Hornblende is the dark green mineral on the left side and the volcanic glass is the striated material in the upper-right corner.

volcanic ash soils, and although these minerals are essentially X-ray amorphous, order in their structure can be detected using TEM.

Allophane, imogolite, and ferrihydrite are short-range order minerals that are commonly associated with volcanic-ash soils (Parfitt et al., 1980; Wada, 1977). Whether or not these minerals are present in the Mammoth Mountain soils gives some information about the weathering stage of these soils. Imogolite ($SiO_2 \cdot Al_2O_3.3.5H_2O(+)$) has a smooth, curved thread-like morphology and the electron diffraction pattern gives a series of ring reflection at 0.14, 0.21, 0.23, 0.33, 0.37, 0.41, 0.57, 0.78, 1.18, and 2.1 to 2.3 nm (Wada and Yoshinaga, 1969). Allophane is made up of fine, rounded particles that form irregular aggregates and gives two broad ring reflections with intensity maxima at 0.33 and 0.225 nm (Wada, 1977). Ferrihydrite characteristically has 4 broad bands at 1.4, 2.5,

2.21, and 1.72 nm. A synthesized imogolite sample was used as a standard to ensure the detection of the rings reported in the literature.

Neither allophane nor immogolite was identified in either the control or high-CO_2 clay samples. The only mineral phase positively identified using TEM in the soils was ferrihydrite (Fig. A.3).

Figure A.3 – A selected area electron diffraction pattern representing ferrihydrite in the soils. The radii of the four broad rings correspond to the d-spacing characteristic of ferrihydrite using the relationship $d = \frac{\lambda\ L}{R}$, where R = radius of rings, L = camera length (1054 nm) and λ = wavelength (.00197 nm).

A.4 References

Parfitt, R.L., Furkert, R.J. and Henmi, T., 1980. Identification and structure of two types of allophane from volcanic ash soils and tephra. Clays and Clay Mineralogy, 28(5): 328-334.

Wada, K., 1977. Allophane and Imogolite. In: J.B. Dixon and S.B. Weed (Editors), Minerals in Soil Environments. Soil Science Society of America, Madison, WI.

Wada, K. and Yoshinaga, N., 1969. The structure of "imogolite". The American Mineralogist, 54: 50-71.

Whittig, L.D. and Allardice, W.R., 1986. X-ray diffraction techniques. In: A. Klute (Editor), Methods of soil analysis. Part 1. ASA and SSSA, Madison, WI, pp. 331-362.

Appendix B

ADDITIONAL EXPERIMENTAL DATA

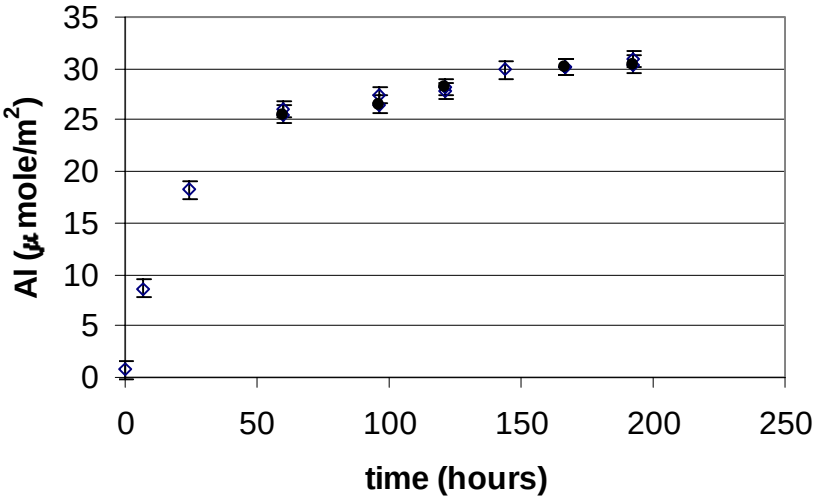

Figure B.1 - A comparison of Al measurements of samples passed through a 0.2 μm cellulose acetate filter (solid circles) and the 0.02 μm aluminum oxide membrane filter (open circles) obtained from a pH-stat batch experiment dissolving soil from control site 3 at pH 2.78. The measured Al concentrations are similar and within the reproducibility error associated with the ICPMS measurement, so the use of the aluminum oxide filter is not altering the Al measurements.

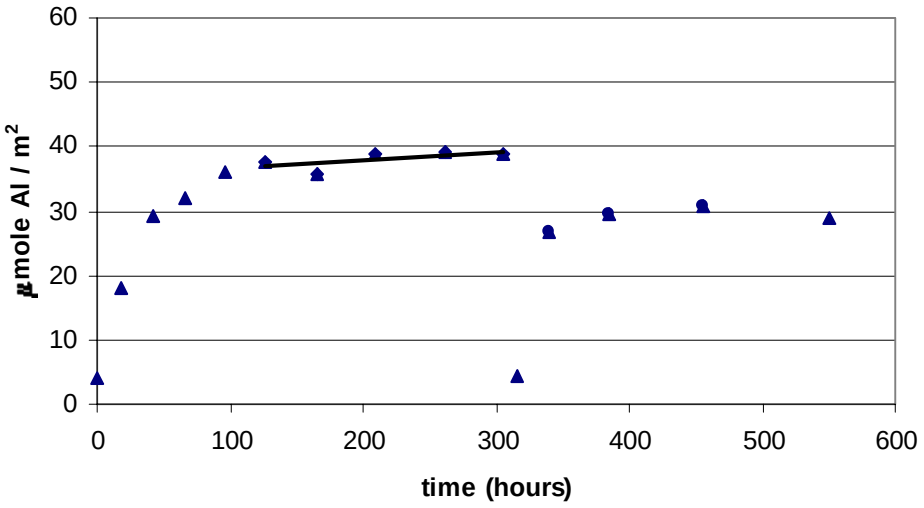

Figure B.2 - Release of Al before and after re-suspension of control site 3 soil sample in fresh solution at pH 2.78 normalized to pre-dissolution surface area. The data representing the samples taken after the re-suspension prohibit the calculation of an Al release rate.